NASA CR-191172

AN INVESTIGATION OF CONDUCTED AND RADIATED EMISSIONS FROM A HOLLOW-CATHODE PLASMA CONTACTOR

Prepared for

LEWIS RESEARCH CENTER

NATIONAL AERONAUTICS AND SPACE ADMINISTRATION

Grant NAG 3-776

Annual Report

July 1993

By

Brett W. Buchholtz

Approved by

Paul J. Wilbur
Department of Mechanical Engineering
Colorado State University
Fort Collins, Colorado 80523

NASA
National Aeronautics and Space Administration

Report Documentation Page

1. Report No.	2. Government Accession No.	3. Recipient's Catalog No.
CR 191172		

4. Title and Subtitle
An Investigation of Conducted and Radiated Emissions From a Hollow-Cathode Plasma Contactor (PLASMA CONTACTOR RESEARCH - 1992)

5. Report Date
July 1993

6. Performing Organization Code

7. Author(s)
Brett W. Buchholtz
Paul J. Wilbur

8. Performing Organization Report No.

10. Work Unit No.

9. Performing Organization Name and Address
Department of Mechanical Engineering
Colorado State University
Fort Collins, CO 80523

11. Contract or Grant No.
NAG 3-776

13. Type of Report and Period Covered
Annual:
Jan. 1, 1992 - Jan. 1,1993

12. Sponsoring Agency Name and Address
National Aeronautics and Space Administration
Washington, D.C. 20546

14. Sponsoring Agency Code

15. Supplementary Notes
Grant Monitor - Joel T. Galofaro
NASA Lewis Research Center
Cleveland, OH 44135

16. Abstract

An investigation conducted on the electrical interference induced by the operation of a hollow-cathode plasma contactor in a ground-based facility is described. The types of electrical interference, or noise, which are important to Space Station Freedom designers are classified as either conducted or radiated emissions. This report examines the procedures required to perform conducted and radiated emission measurements on a plasma contactor. The experimental data obtained are typically examined in the frequency domain (i.e. amplitudes of the noise fluctuations versus frequency). Results presented indicate the conducted emissions, which are the current fluctuations from the contactor into the space station wiring, are affected by operating parameters such as expellant flow rate and discharge current. The radiated emissions, which are the electromagnetic waves induced and emitted by the contactor, appear to be influenced by the contactor emission current. Other experimental results suggest possible sources which are responsible for the observed noise. For example, the influence of the plasma environment downstream from the contactor on noise emission levels is described. In addition, a brief discussion is given on the correlation between conducted and radiated emissions and the mechanisms through which both are influenced by the plasma downstream of the contactor.

17. Key Words (Suggested by Author(s))	18. Distribution Statement
Plasma Contactor Conducted Emissions Radiated Emissions	Unclassified - Unlimited

19. Security Classif. (of this report)	20. Security Classif. (of this page)	21. No of pages	22. Price*
Unclassified	Unclassified	93	

NASA FORM 1626 OCT 86

*For sale by the National Technical Information Service, Springfield, Virginia 22161

TABLE OF CONTENTS

LIST OF FIGURES

LIST OF TABLES

I. INTRODUCTION

In order to control natural and forced electrical charging events on-board Space Station Freedom, it has been proposed that a hollow-cathode-based plasma contactor be incorporated into the design. A plasma contactor is an active charge-control device which ionizes an expellant, such as xenon gas, and can either collect or emit electrons to another plasma, such as the ionosphere. The plasma contactor for Space Station Freedom (SSF) must satisfy several design requirements in order to ensure adequate and reliable charge control. For example, the plasma contactor should be able to emit substantial currents (but less than 10 A) for long periods of time (between 3 to 5 years) [1,2]. Another requirement, and the focus of this paper, is that the device be electrically compatible with other systems on-board SSF. Specifically, normal plasma contactor operation should not induce electrical interference with other equipment associated with SSF such as that required for communications and various science experiments. The two types of electrical interference, or noise emissions, that are created by the contactor and are of concern to SSF designers are categorized as conducted and radiated emissions [3]. Conducted emissions (CE) are defined as the electrical noises produced by normal contactor operation which are transmitted to other systems on SSF through the electrical wiring. On the other hand, radiated emissions (RE) are defined as the electromagnetic radiation produced by the plasma contactor and emitted to space. The measured levels of these noise emissions should be sufficiently low (Ref. [4] describes the exact levels) to ensure electrical compatibility between the plasma contactor and other equipment.

Ultimately, contactor operation in space will reveal the true nature of noise produced in that environment, however, ground-based experiments provide useful insight into the noise levels created and given off by a hollow-cathode plasma contactor. Results obtained on the ground can then serve as a useful guide to the plasma contactor design in order to reduce or control the observed noise levels. This report describes ground-based investigations of the conducted and radiated emissions caused by the operation of a plasma contactor housed inside a vacuum tank.

As the space station orbits the earth in the ionosphere, natural charging events can occur which are typically induced by the bombardment of electrons on the exposed surfaces of SSF. This collection of electrons will consequently cause SSF structure to be charged negative to the point where the less mobile ions in the ionosphere are attracted at a current equal to that associated with the electrons. A significant portion of the exposed surfaces on SSF consists of the photovoltaic solar arrays which are to provide power to the station. The proposed solar arrays will produce ~160 V potential drop which will establish itself relative to the space plasma potential in a manner which depends on how the arrays are connected to SSF. If the negative side of the array is connected to SSF structure, electron collection on the positive regions of the exposed solar array surfaces must balance the ion collection on the station structure as pictured in Fig. 1a. If these collection currents are not controlled with a plasma contactor, they will induce potentials with respect to the space plasma potential as illustrated by the natural charging case in Fig. 1c. Operating under this condition, ions in the space plasma can be accelerated through a large potential difference (i.e. -140 V as pictured in Fig. 1c) and will, as a result, induce substantial surface erosion of the station structure.

If a plasma contactor is installed, then the electron current collected on the

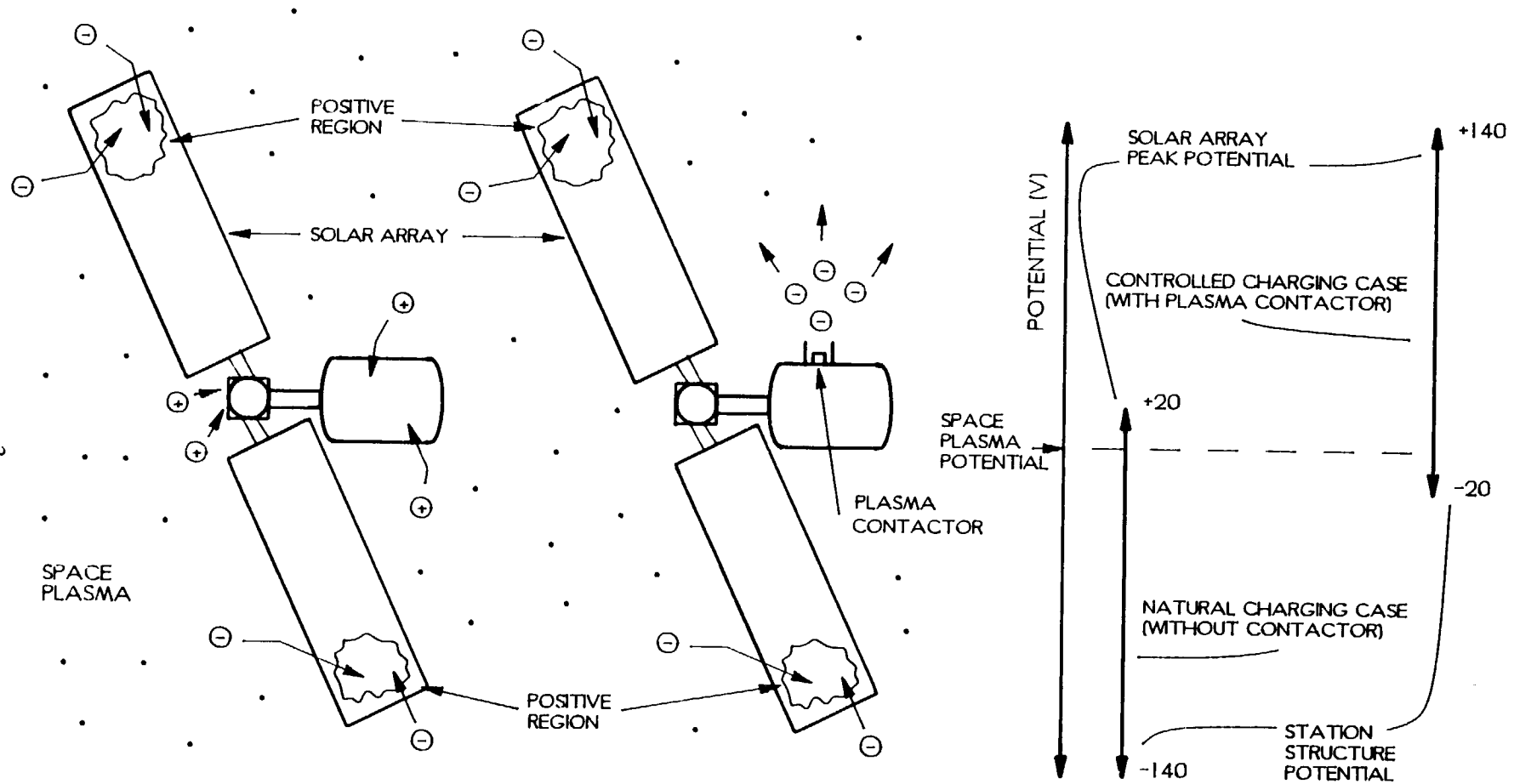

a) Natural Charging Case b) Controlled Charging Case c) Potentials

Fig. 1 Plasma Environment Schematic for a Space Station

exposed solar arrays is balanced by the electrons emitted from the contactor (Fig. 1b) and the potentials establish themselves as shown in the controlled charging case in Fig. 1c. In this case, the potential of the station structure is maintained within about –20 V relative to the surrounding space plasma. Under this condition, computer models [1,2] suggest that the ions which strike the SSF will have insufficient energies to cause significant surface erosion. In order for the contactor to maintain the station potential at -20 V, the same computer models have estimated it should typically emit about 1 A of electrons [2]. However, to handle unforseen charging events, the plasma contactor will be designed to emit up to 10 A [2]. Therefore, the typical contactor emission current levels presented in this report will be between 0 and 10 A. In general, plasma contactors can also be used to collect electrons for other spacecraft such as the electrodynamic tether mission [5], however, experiments associated with this operating condition will not be examined.

In order to determine the noise emissions caused by normal contactor operation, various measurement techniques can be implemented. For example, conducted emissions can be measured with a current monitor which senses the fluctuations in current to the plasma contactor. Radiated emissions can be detected with devices such as an antenna or various Langmuir probes which can sense electric field or plasma density fluctuations downstream from the contactor (in the plume). Each of these methods are described in this report. Typically, the output of these instruments is in the form of voltage fluctuations which directly correspond to the noise emissions. Useful information can be extracted from these voltage fluctuations by examining their spectral composition (i.e. amplitudes v. frequency).

By examining the conducted and radiated emissions in the frequency domain, dominant amplitudes and/or harmonics can be recognized. With this information it

should then be possible to determine the sources of the measured noise and then take the precautions necessary to reduce undesirable noise levels. For example, a careful examination of spectral data might reveal the harmonics of a certain power supply are one source of unacceptable noise emissions. This power supply could then be replaced with a more "electrically quiet" supply in hopes of reducing the observed noise. Also, conducted- or radiated-emission spectral data will be compared against predetermined emission specifications [4] to determine if they are acceptable for SSF design. These specifications describe the tolerable levels of conducted and radiated emissions a component, such as the contactor, can produce before significant interference could be induced in other electrical hardware on SSF.

For the data presented in this paper, conducted and radiated emission spectral data were obtained using one of two possible methods. The first method is to analyze emission data recorded on an oscilloscope with a fast-Fourier-transform (FFT) computer algorithm. The FFT routine is a mathematical technique which transforms a time-varying signal into its amplitudes as a function of frequency (Appendix A provides an in-depth description of this technique). An example of this method could be the analysis of the current being emitted by the plasma contactor which fluctuates in time about a mean value. These current fluctuations, or CE, can be sensed with a current monitor, recorded on an oscilloscope, and then transformed into the frequency domain using FFT analysis. The second method, and a more direct approach, is to use a spectrum analyzer instead of an oscilloscope. The spectrum analyzer detects the amplitudes of a signal as a function of frequency, thus eliminating the need for FFT analysis. For either method, the frequency response of the instrumentation becomes important and must be determined before accurate frequency data can be obtained. Appendix B describes the procedures used to determine the frequency response of the

various instruments utilized for noise emission measurements in this investigation.

This report examines 1) the procedures required to perform conducted- and radiated-emission measurements on the plasma contactor in a ground-based facility, 2) the effects of various contactor operating parameters on the noise levels, and 3) the correlation between the conducted and radiated emissions. A detailed description of the instrumentation and measurement techniques used to determine noise emissions is presented. In addition, experimental results which illustrate the general nature of noise emission levels are presented and discussed. Finally, the relationship between CE and RE is addressed. For comparison purposes, SSF specifications for noise emissions [4] are presented whenever possible.

II. EXPERIMENTAL APPARATUS

Noise emissions were examined while a hollow-cathode-type plasma contactor emitted electrons to an ambient plasma in the 5.3 m long by 1.2 m diameter cylindrical vacuum tank shown schematically in Fig. 2. The plasma contactor was mounted at one end of the vacuum tank and it could emit electrons to the simulator and the vacuum tank walls via the ambient plasma. The ambient plasma was generated in part by the simulator shown at a location near the middle of the vacuum tank. The simulator is used to qualitatively "simulate" a space plasma environment by providing ions and electrons. Plasma properties could be measured at various locations downstream from the contactor using the spherical Langmuir and emissive probes attached to either a probe support rod or the cart positioner (Fig. 2).

The plasma contactor used for the noise emission experiments is similar in construction to ones used in previous contactor performance and noise investigations [5,6,7,8]. This contactor, which is shown schematically in Fig. 3a, consists of an anode and cathode, separated by ~4 mm, between which an electrical discharge could be sustained. The cathode was constructed of a 0.6 cm diameter tantalum tube capped by a thoriated-tungsten plate with a 1.0 mm diameter orifice. Located inside the tube is a cylindrical tantalum-foil insert coated with low work-function materials ($BaCO_3$ and $SrCO_3$) which served to provide electrons at modest temperatures. The anode consists of a 1.3 cm I.D by 12 cm O.D. stainless steel plate with a 3 mm I.D. by 5 mm O.D. tantalum loop at its center (Fig. 3a). The loop is made of refractory metal so it can withstand the high temperatures induced in this region of the anode under high

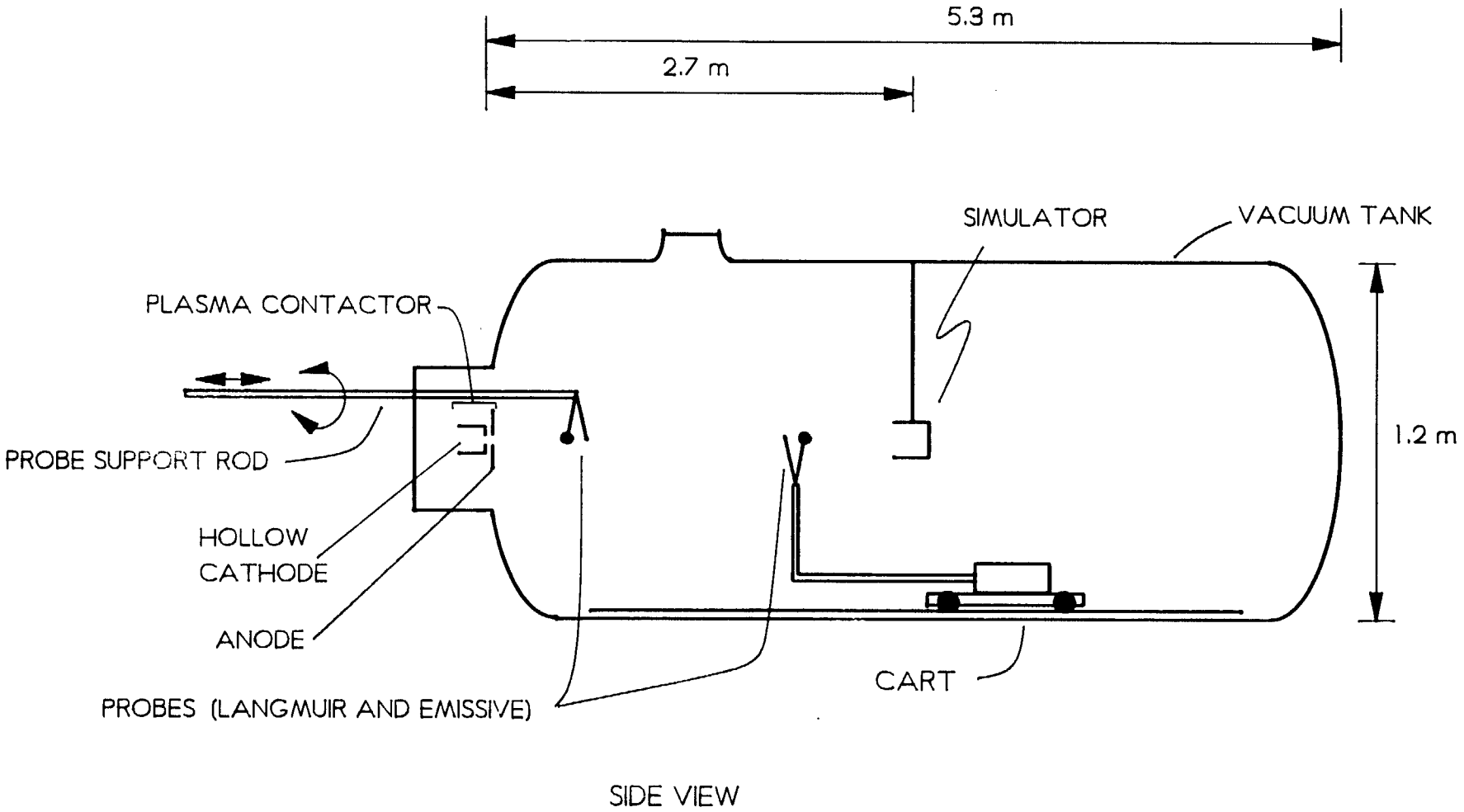

Fig. 2 Mechanical Diagram Schematic

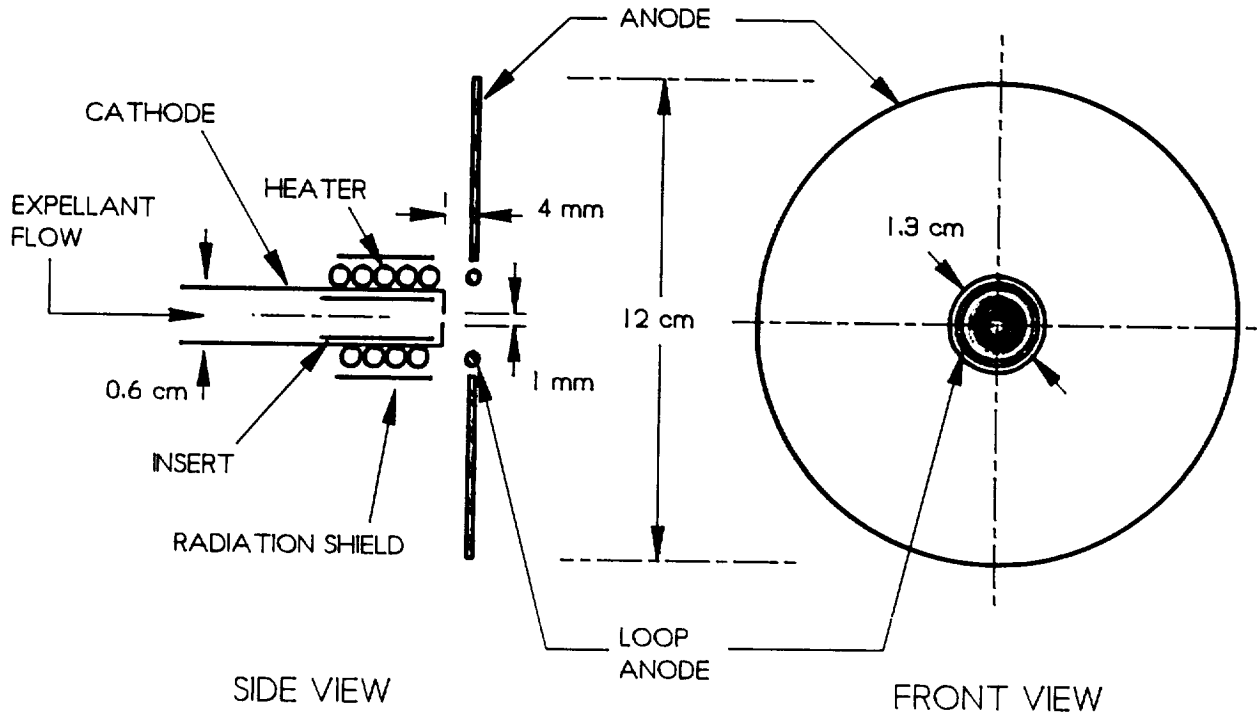

a) Hollow Cathode Plasma Contactor Schematic

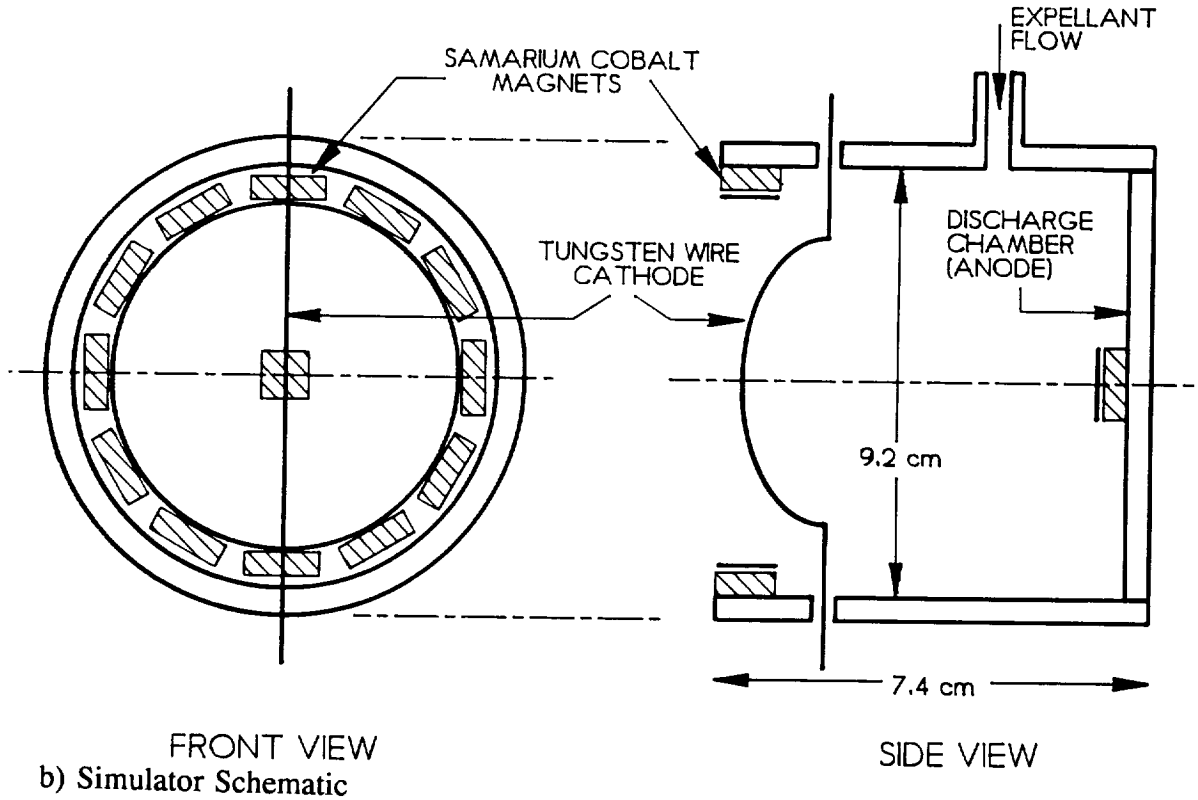

b) Simulator Schematic

Fig. 3 Plasma Contactor and Simulator Schematics

discharge-current operating conditions. A more detailed description of hollow-cathode operation can be found in Refs. [6] and [7].

The simulator, which is shown schematically in Fig. 3b, consists of a mild-steel, cylindrical discharge chamber (inner diameter of 9.2 cm and length of 7.4 cm) which houses a filament cathode and several magnets. The cathode is fabricated from 0.25 mm diameter tungsten wire and emits electrons thermionically when it is heated by passing a current through it. The magnets are made of samarium-cobalt and are placed on the discharge chamber (Fig. 3b) so they will induce a magnetic field which impedes direct flow of electrons from the cathode to the anode. This impedance allows the electrons to have more opportunities for ionizing collisions with the atoms supplied to the chamber and thus maintain the production level of ions required to sustain the ambient plasma. Both the contactor and simulator used xenon gas as expellants.

For the noise emission experiments, the plasma contactor, simulator, and vacuum tank were connected in the electrical configuration shown schematically in Fig. 4. The discharge power supplies for the contactor and simulator are depicted in Fig. 4 as squares. Each has a current and voltage meter (circles) which are labeled, respectively, J_{CD} (discharge current) and V_{CD} (discharge voltage) for the contactor. Likewise, these meters are labeled J_{SD} and V_{SD} for the simulator discharge current and voltage, respectively. Another power supply, shown as the heater supply, is used to heat the insert of the cathode to the point where it will emit a significant electron current [6,7]. The bias power supply is used to force the contactor negative with respect to the vacuum tank walls and simulator anode, thus causing the electrons produced near the contactor to be emitted from it. This electron emission current, at a particular bias voltage (V_b), is referred to as the contactor emission current (J_{CE}).

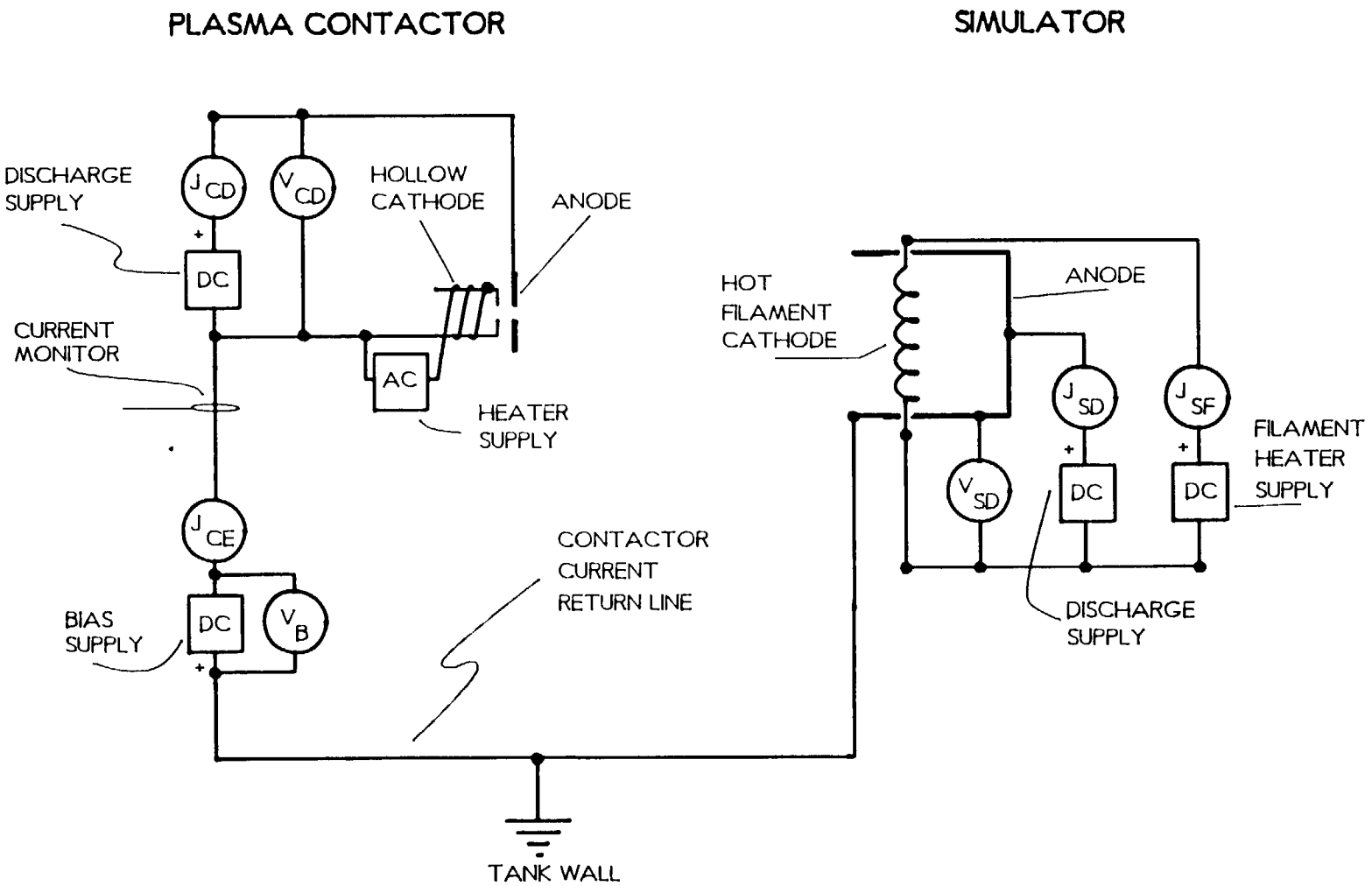

Fig. 4 Electrical Schematic

Typical operating conditions and plasma properties measured 1 m downstream of the contactor are listed below in Table 1.

	Contactor	Simulator
Discharge Voltage	V_{CD} = 7 to 13 V	V_{SD} = 34 V
Discharge Current	J_{CD} = 0.6 A	J_{SD} = 0.45 A
Expellant Flow Rate	$\dot{m}_c$ = 4.0 sccm (Xe)	$\dot{m}_s$ = 3.0 sccm (Xe)
Typical Plasma Properties and Anticipated Instability Frequencies 1 m downstream (J_{CE} = 1 A)		
Parameter	**Symbol**	**Quantity**
Electron Density	n_e	$3x10^6$ cm^{-3}
Plasma Potential	V_p	21 V
Electron Temperature	T_e	3.5 eV
Plasma Frequency	f_p	16 MHz
Ion Acoustic Frequency	f_i	~32 kHz
Frequency of Beam-Plasma Instability	-	~16 MHz
Frequency of Two-Stream Instability	-	~100 kHz

Table 1. Typical Operating Conditions and Plasma Properties

Typical noise emissions expected when a plasma contactor is operated in a vacuum test facility might be associated with power supplies, extraneous electrical equipment, and/or the plasma environment downstream from the contactor. Figure 5 is a schematic which illustrates how an electrical disturbance, depicted as a small-amplitude wave, in the wiring of the contactor might propagate through the ambient

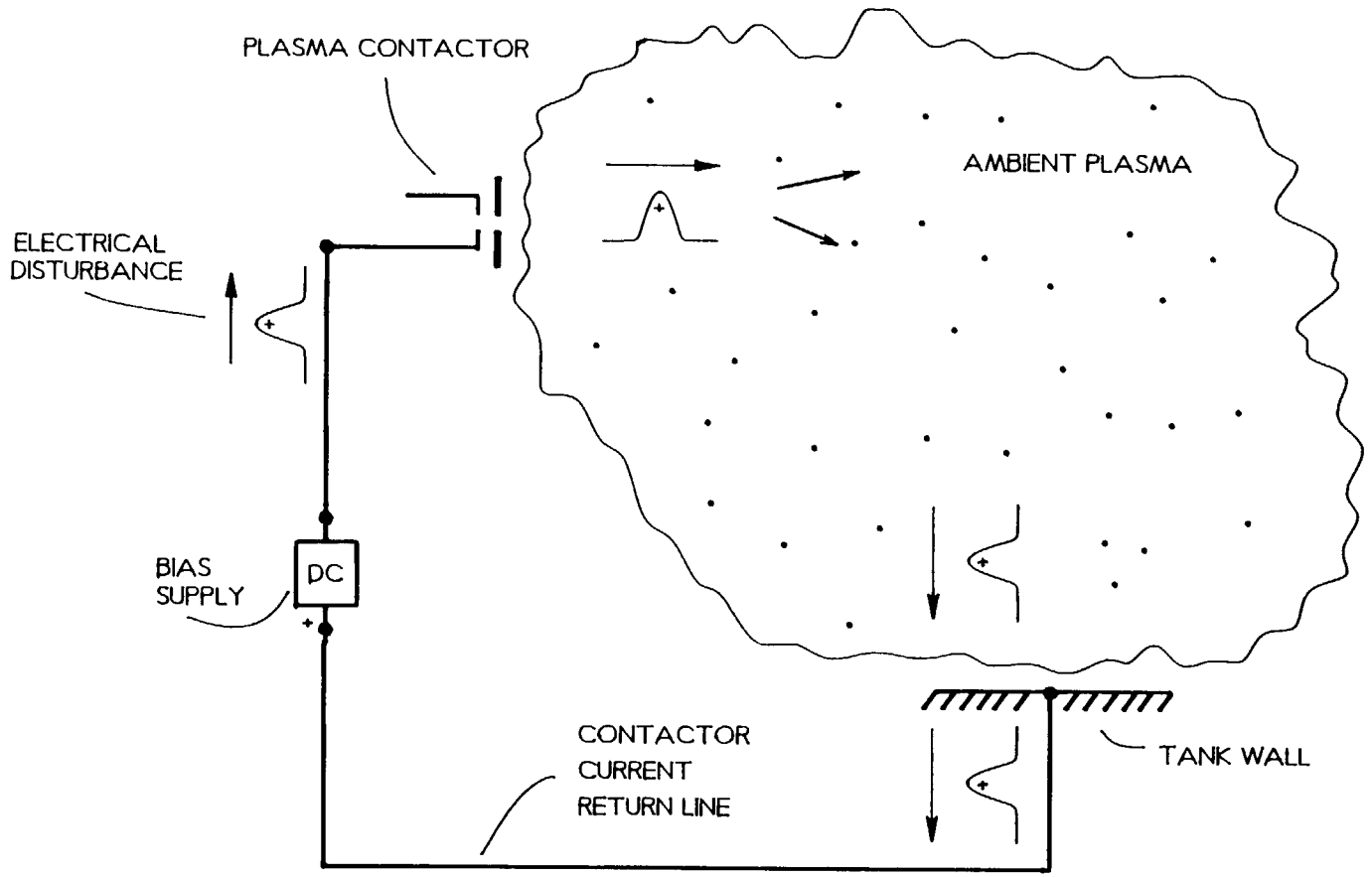

Fig. 5 Diagram of Conducted and Radiated Emissions

plasma and circuit. Accumulated electrical disturbances in the wiring (conducted emissions) represent a fluctuation about a mean, or steady, current which must also exist in the plasma as a consequence of current continuity. Such electrical disturbances might, for example, be induced by the bias power supply and reflect its particular characteristics [9].

Downstream from the plasma contactor, the mean and fluctuating emission currents can drive several types of plasma instabilities in the vicinity of the hollow cathode which, in turn, produce waves in the ambient plasma (i.e. plasma waves). The term plasma wave can refer to 1) oscillations in either the mean electron or ion densities and/or plasma potentials, 2) fluctuations about mean electric and/or magnetic fields due, for example, to electromagnetic radiation (photons), or 3) combinations of the first two [10,11]. Some of the types of plasma instabilities which might be observed in the plume downstream from a contactor include 1) *ion acoustic waves*, which are spatial perturbations about the mean ion density that propagate at the ion acoustic velocity, 2) *beam-plasma instabilities*, which occur when the distribution function describing the electrons has a high-energy hump in addition to a Maxwellian-like, low-energy hump, and 3) *two-stream instabilities*, which are present when two species with different charges are counter-flowing [10,11,12]. A more complete description of each of these noise sources can be found in Refs. [10] and [11]. The frequencies at which these three might be expected in the plasma environment downstream from the contactor are listed in Table 1.

The resulting plasma waves from these instabilities continuously influence the nature of collisions in and radiation from a plasma and they therefore affect energy dissipation in the plasma (i.e. the impedance of the plasma) which, in turn, can affect the output of the bias power supply. In addition, plasma waves that interact with

vacuum tank walls can influence electrical disturbances in the contactor-current-return line. The combined effect of the current fluctuations in the contactor-current-return line inducing plasma waves that may, in turn, re-influence the current fluctuations is illustrated in Fig. 5. As a result of this coupling, the bias power supply and the plasma environment can affect each other. The degree of this influence must be examined in order to determine which effects observed in a ground-based test facility will be observed in space.

Plasma waves might induce other effects observed in ground-based experiments that will not be present in space. For example, plasma waves created near the contactor will propagate into the ambient plasma and might be detected as either fluctuations in electric field, electron density, and/or ion density. When these fluctuations are sensed in the plasma they are referred to as radiated emissions. Such waves continue to propagate until they either interact with other waves or encounter vacuum tank walls where part of the waves might reflect. If a reflected wave returns to its origin just as another wave is created, resonance effects might be observed. Also, because of the coupling between the bias power supply and the plasma, transitions that cause the character of the noise emissions to change might be observed. For example, if the plasma contactor operating conditions are varied slightly, this may drastically affect plasma wave production (e.g. more waves may be created at specific emission current levels). This would in turn influence the measured conducted and radiated emissions. Therefore, resonance and/or transition effects, may be observed in a test facility but they would not occur in space.

Other types of noise emissions that could be observed might be induced by processes associated with hollow-cathode operation. For example, conducted and/or radiated emissions might depend upon the expellant flow rate or discharge current of the plasma contactor because operating parameters such as these dictate the ease with which the contactor is able to emit electrons to another plasma [5].

III. EXPERIMENTAL PROCEDURES

For either conducted- or radiated-emission measurements, care was exercised to ensure that the overall frequency response of the instrumentation was well behaved within the range of frequencies being investigated. Appendix B describes how the frequency response of the various instruments was determined and also presents results from assorted frequency calibration tests. Also, regardless of type of noise measurement conducted, the output of the various sensors were measured on the same data acquisition system which consisted of either an oscilloscope/filter or a spectrum analyzer connected to a computer. The oscilloscope/filter arrangement is described in Appendix A. It was determined that data acquired with the oscilloscope and spectrum analyzer were similar (see Appendix A) and therefore distinction between data collected with either instrument will not be given.

Conducted Emission Measurements

The conducted emissions induced by normal contactor operation were measured by placing a current monitor in the contactor-current-return line as depicted in Fig. 4. The current monitor itself, illustrated schematically in Fig. 6a, was designed to handle 10 A and consisted of ~50 wraps of a fine wire around a steel core through which the contactor-current-return line was wrapped once around. Similar to a transformer, current fluctuations in the return line induce magnetic field fluctuations in the steel core of the current monitor. These magnetic field fluctuations create current fluctuations in the fine wire which can then be detected with an oscilloscope. A resistor (~5.5 Ω) and capacitor (~100 pF) are connected in such away to establish a

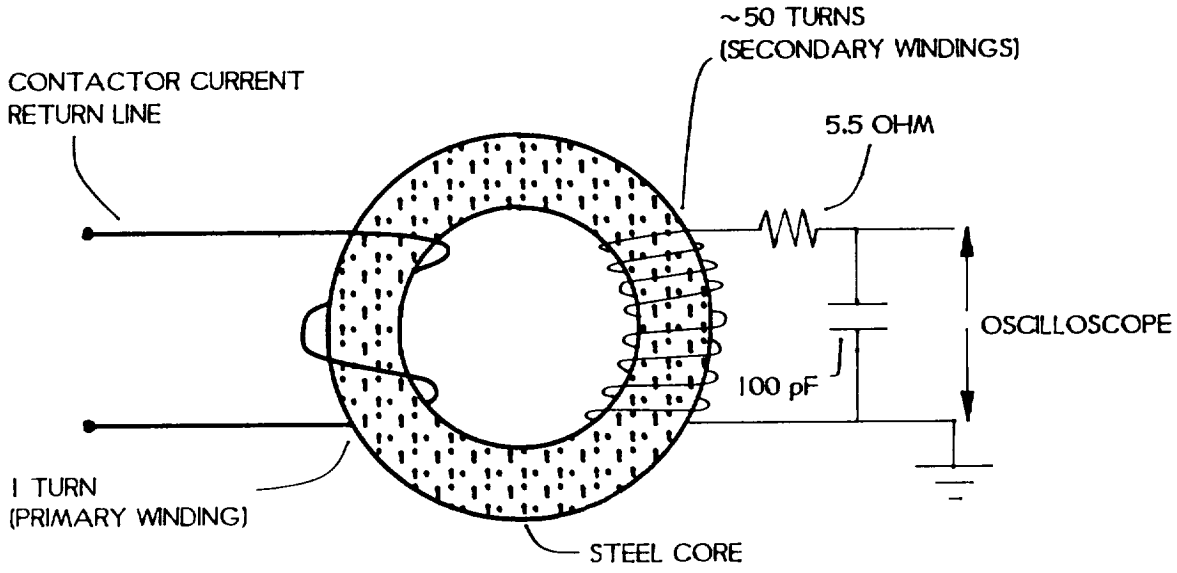

a) Current Monitor

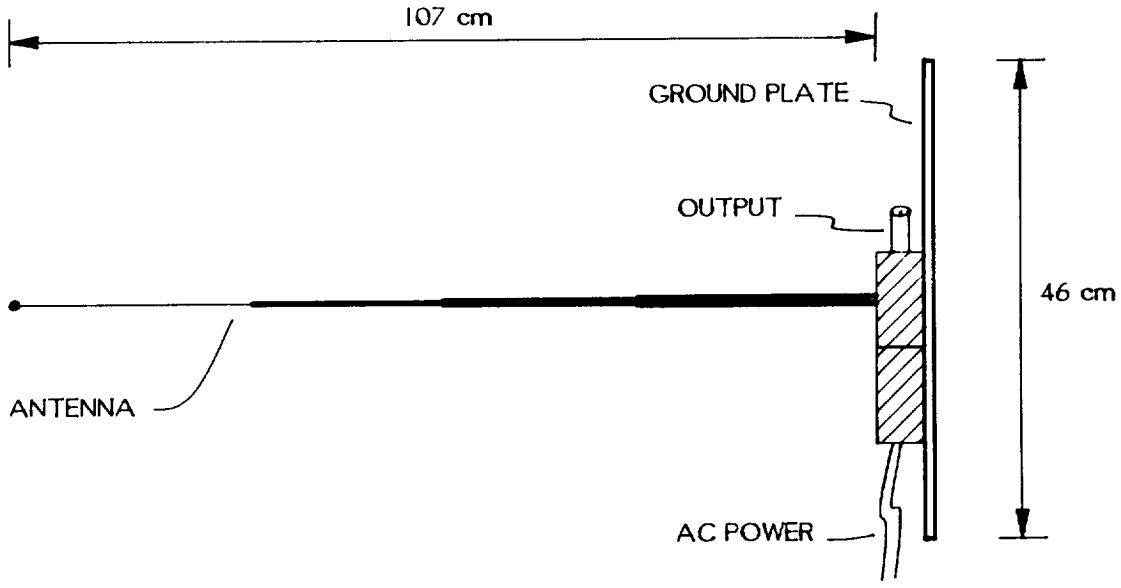

b) Mono-pole Antenna

Fig. 6 Instrumentation Schematics

natural cutoff frequency of ~ 290 MHz for the device in order to reduce aliasing. The frequency response characteristics and calibration tests conducted on the device are described in Appendix B.

Typical conducted emission measurements were performed while the contactor was operating at standard conditions and had been biased to emit electrons. Any fluctuations of this current (J_{CE}) were sensed by the current monitor, recorded with an oscilloscope, and then analyzed with the FFT algorithm to compute emission current amplitudes as a function of frequency. Conducted emissions are usually measured using narrowband emission guidelines described in Ref. [3] and Appendix A which suggest a particular resolution bandwidth to be used for a given frequency range. Conducted emission data are usually plotted as narrowband emissions (dB [μA/A] v. frequency) where the amplitudes of the signal are divided by 1 A of mean current. Recall, the decibel unit is defined as $10\ \mathrm{Log}_{10}(P_1/P_2)$ where P_1/P_2 is a ratio of power [13]. For narrowband emissions, the power is defined as the current squared multiplied by a resistance and therefore dB[μA/A] is equivalent to $10\ \mathrm{Log}_{10}\ (\mu A^2/A^2) = 20\ \mathrm{Log}_{10}\ (\mu A/A)$. Data, representative of those obtained when the contactor was emitting 1 A (J_{CE} = 1 A) are plotted in Fig. 7a (dB [μA/A] v. frequency) where these data indicate distinct signals at 120 Hz, 240 Hz, and ~ 2 MHz. The Space Station Freedom specifications for CE are reproduced from Ref. [4] to show how the contactor CE compare with these requirements. This specification, plotted in Fig. 7a, reflects the typical decay in amplitude with frequency observed with "1/f noise" [9]. It appears from the data in Fig. 7a, the contactor satisfies the SSF specification for most frequencies except in the range around 2 MHz.

Another approach for examining the CE was to compute the power spectral density (PSD) of the current fluctuations which could then be integrated within a given

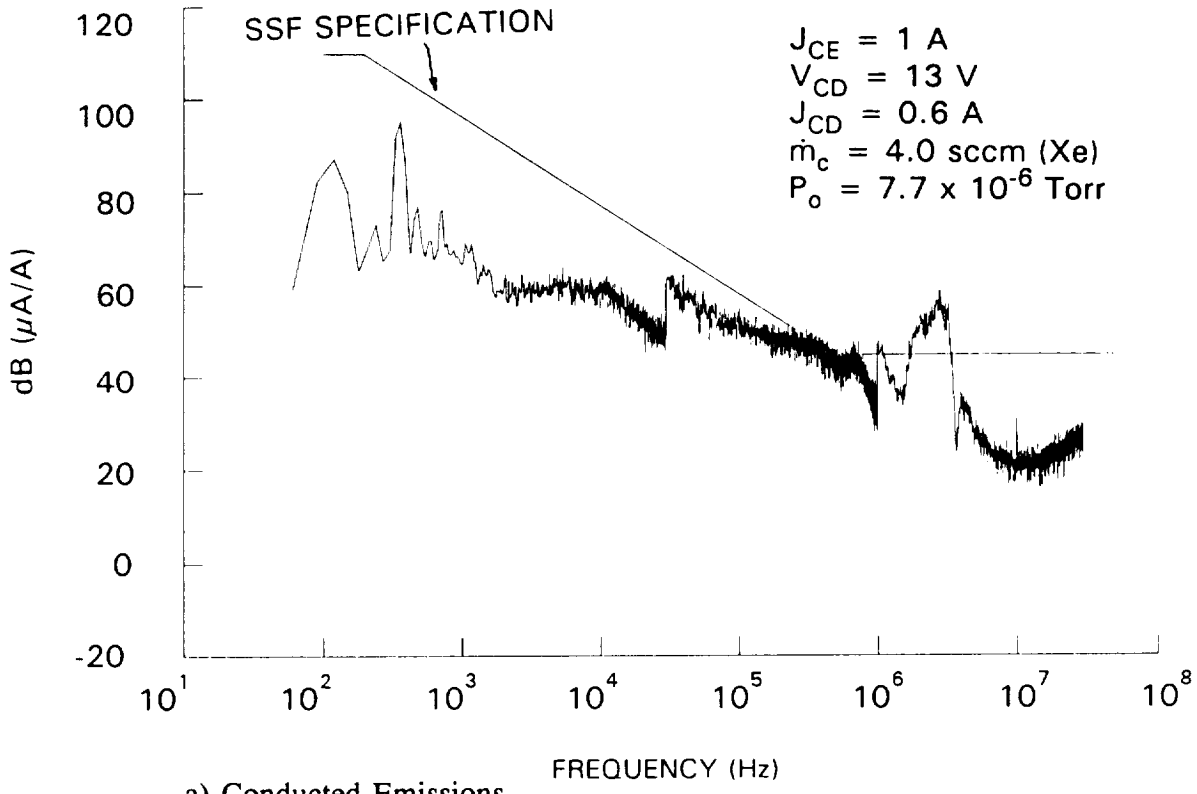

a) Conducted Emissions

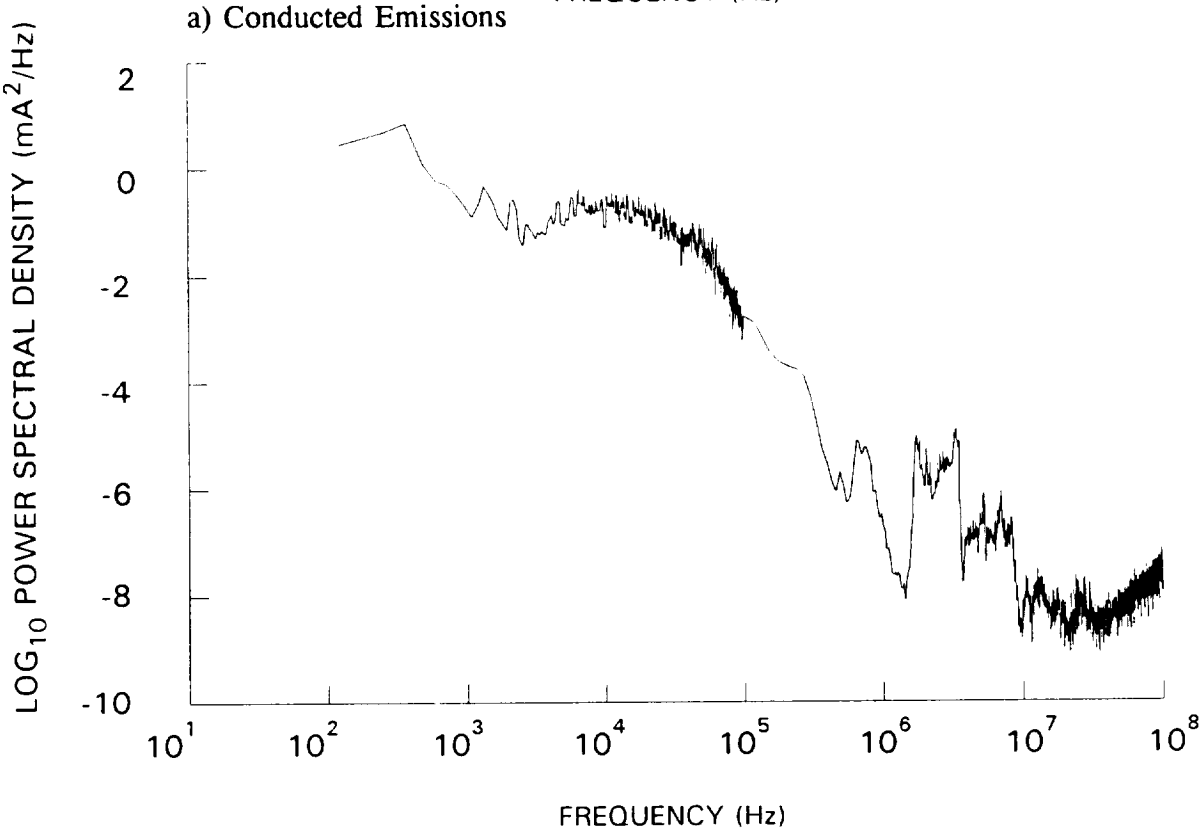

b) Power Spectrum

Fig. 7 Typical Current-Fluctuation Spectra

frequency range to obtain mean-squared values of the fluctuations (see Appendix A). By taking the square root of these mean-squared values, the root-mean-square of the current fluctuations (ΔJ_{rms}) can be determined. For example, a typical power spectral density plot associated with the current fluctuations in the return line to the contactor emitting 1 A (J_{CE} = 1 A) is plotted in Fig. 7b where the logarithm of the PSD is plotted against frequency (i.e. Log_{10} [mA^2/Hz] v. frequency). When these PSD data are integrated between the frequency ranges 0.1 to 100 kHz and 0.1 to 100 MHz, the root-mean-square values of the current fluctuations (ΔJ_{rms}) were determined to be 83 mA and 11 mA, respectively. This result indicates that more power of the current fluctuations resides in the lower frequency range. By examining the variations in ΔJ_{rms} induced by such effects as changes in the emission current, for example, can assist in determining the degree of influence these effects may have on the conducted emissions [8].

Radiated Emission Measurements

It can be a difficult task to determine the electromagnetic radiation produced by the contactor in a plasma environment because of the coexistence of electromagnetic fields and charged particles. It is easy to describe the plasma environment as a dynamic soup containing charged particles and electromagnetic radiation but it is a challenge to measure the radiation without the influence of the particles. For these experiments, three instruments were utilized in pursuit of a first-order description of the environmental changes in the plasma plume produced downstream of the contactor.

One of these instruments is an active, mono-pole antenna which was collapsible, extended to 1.1 m for normal operation, and is illustrated schematically in Fig. 6b. The antenna was connected to an active-amplifying circuit attached to a

square, aluminum ground plate (46 cm x 46 cm). This antenna-circuit arrangement was then mounted to the probe positioning cart, illustrated schematically in Fig. 8, so that the antenna was aligned parallel along the contactor-vacuum tank centerline. As depicted in Fig. 8, a cover, which was constructed of plexiglas, could be placed over the antenna to shield it from direct exposure to the plasma. Power to the antenna was provided by a 120 V, 60 Hz power line which was connected to a feed-through on the vacuum tank. The frequency response of the antenna is described in Appendix B.

The antenna detects electric-field fluctuations by sensing the induced potential differences between the antenna and the ground plate. These voltage fluctuations are then amplified and transmitted out of the vacuum tank via coaxial cable where they can be detected with an oscilloscope (or spectrum analyzer). The voltage fluctuations (μV) are converted to electric field fluctuations (μV/m) by dividing them by a factor (i.e. antenna length combined with amplifier gain) as provided by the manufacturer of the antenna. The procedures for RE measurements are described in Ref. [3] and for most of the measurements, these guidelines, which mainly suggest the appropriate resolution bandwidth required for a particular frequency range, were followed. Recall, the resolution bandwidth is smallest frequency detectable using an oscilloscope or spectrum analyzer (see Appendix A).

Typical electric field fluctuation data sensed by the antenna and measured with a spectrum analyzer while the contactor was emitting 1 A of electrons are plotted in Fig. 9 as broadband emissions (dB [μV/m/MHz] v. frequency). These data correspond to the power associated with electric-field-amplitude fluctuations within the resolution bandwidth used to make the measurement (i.e. power spectral density). The data are divided by this resolution bandwidth (BW), in MHz, and the power definition for the decibel unit is used (i.e. dB [μV/m/MHz] =

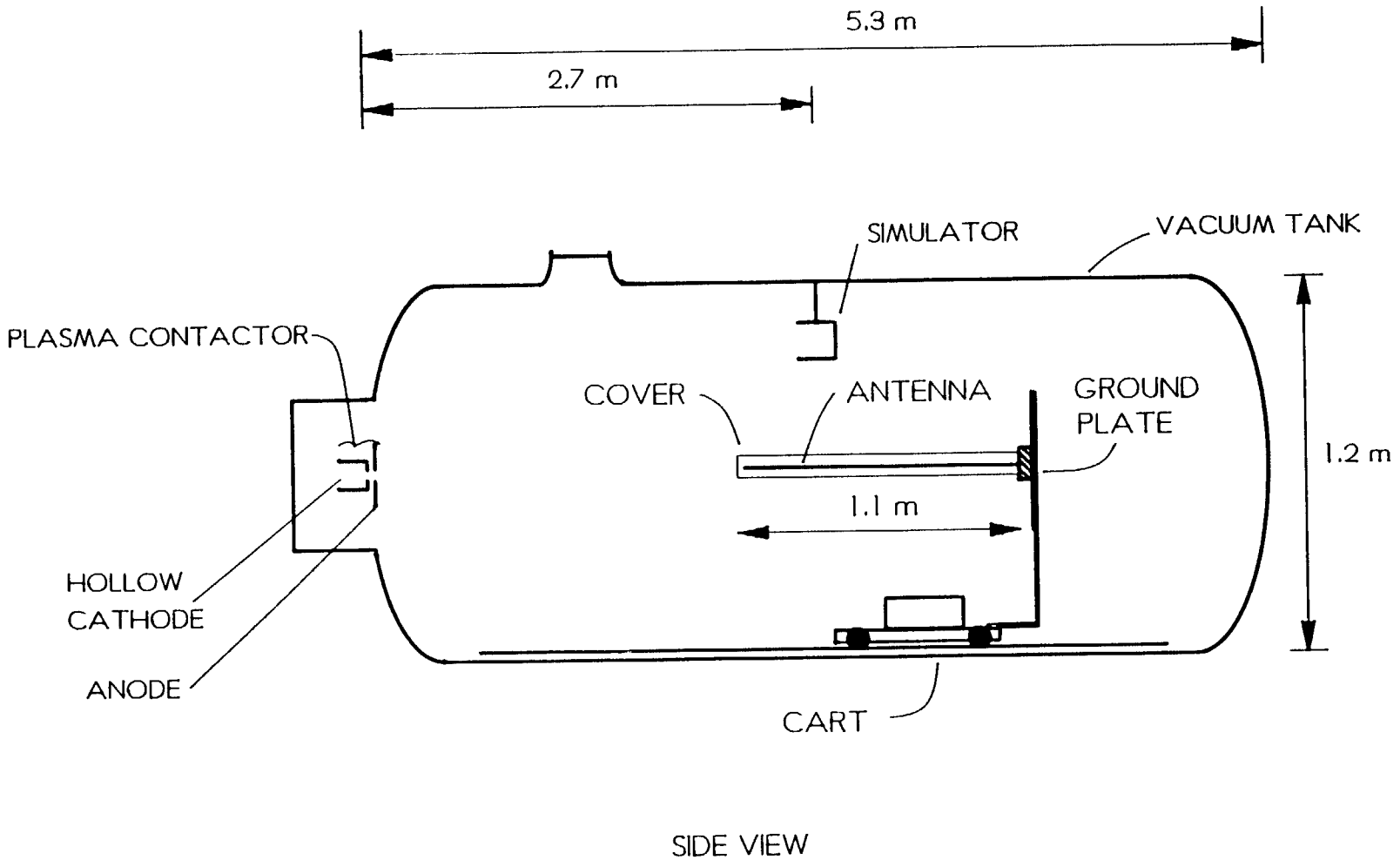

Fig. 8 Horizontal Antenna Configuration

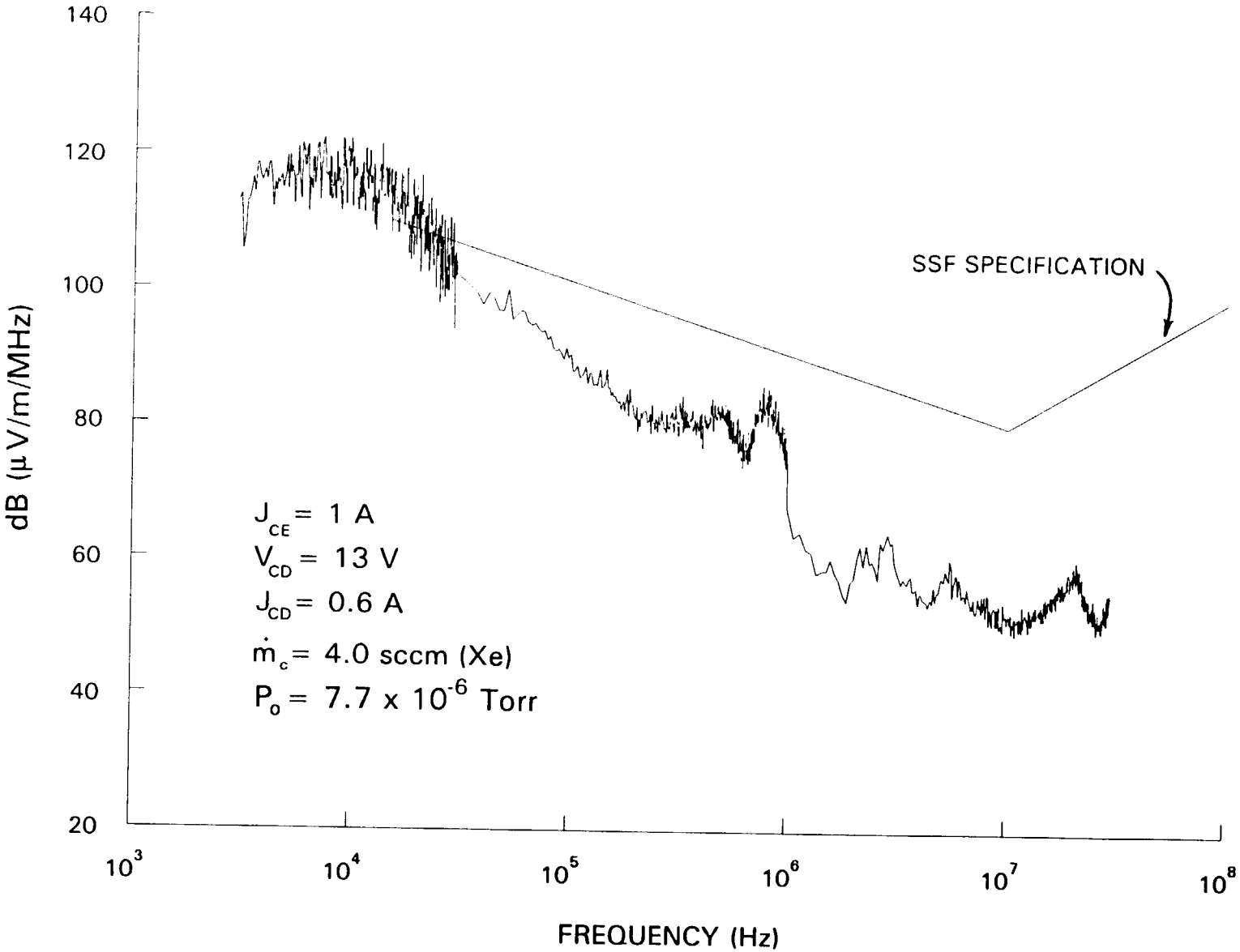

Fig. 9 Typical Radiated Emissions Spectral Data

$10\ \mathrm{Log}_{10}\ [(\mu V/m)^2/MHz] = 20\ \mathrm{Log}_{10}[\mu V/m] - 10\ \mathrm{Log}_{10}[BW\ in\ MHz]$). Three frequency ranges and corresponding resolution bandwidths were selected for this particular measurement and are discussed in Appendix A. In addition, the data in Fig. 9 were taken with the tip of the horizontal antenna positioned 100 cm downstream from the plasma contactor and unless otherwise stated, other RE data presented in this report were also taken at this location. Also plotted in Fig. 9 is the line which represents the upper limit on the allowable RE for the space station [4]. A comparison between the data in Fig. 9 and the line indicates the particular contactor used in this study produces RE that exceed the specifications between 15 and 30 kHz.

Initial measurements of fluctuations in plasma density and potential, also referred to as "plasma noise", were made using a spherical Langmuir probe placed downstream from the plasma contactor. The Langmuir probe (LP) was constructed from a 3.2-mm-diameter stainless steel ball and was biased to local plasma potential with a power supply in the manner suggested in Fig. 10a. The power supply consisted of several 1.5 V DC batteries which could be connected in series to match the plasma potential. Fluctuations in plasma density and/or potential were then sensed as current fluctuations to the LP. These current fluctuations, detected as voltage fluctuations across a 1 kΩ resistor, were filtered to pass only the amplitudes in a frequency range of interest before they were recorded by an oscilloscope (Fig. 10a). Typical power spectral density results from current fluctuations to a LP placed 18 cm downstream while the contactor was operating at standard conditions (J_{CE} = 1A) are plotted in Fig. 11a. This graph (PSD v. frequency on a Log-Log scale) indicates that most of the power resides in the plasma at frequencies below ~100 kHz.

A problem with the conventional Langmuir probe was its poor response to high frequency oscillations (greater than 1 MHz). The frequency response of the probe

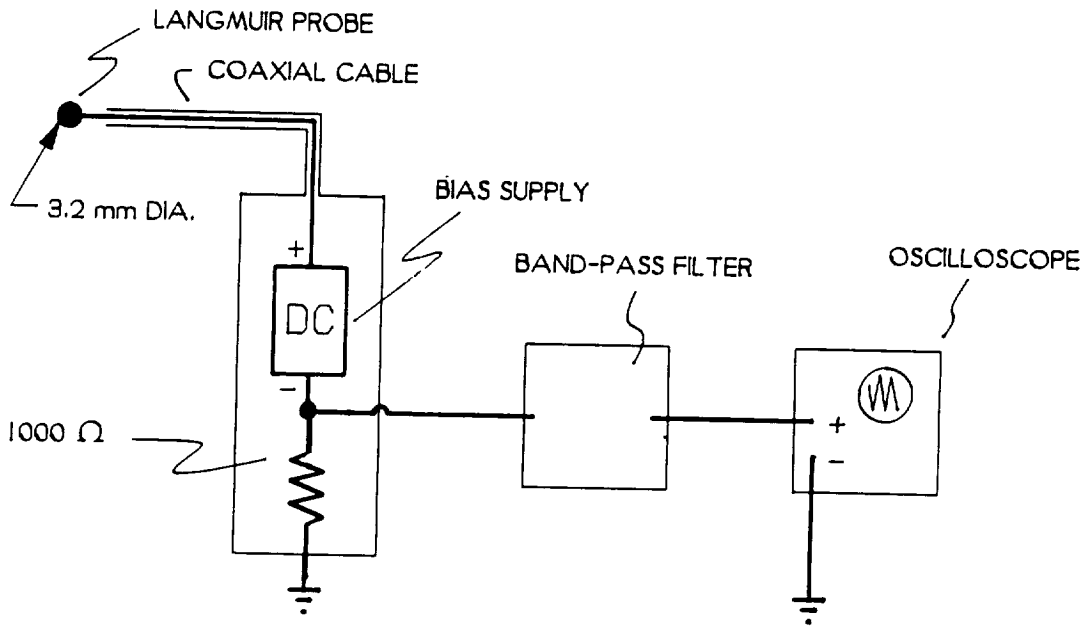

a) Langmuir Probe

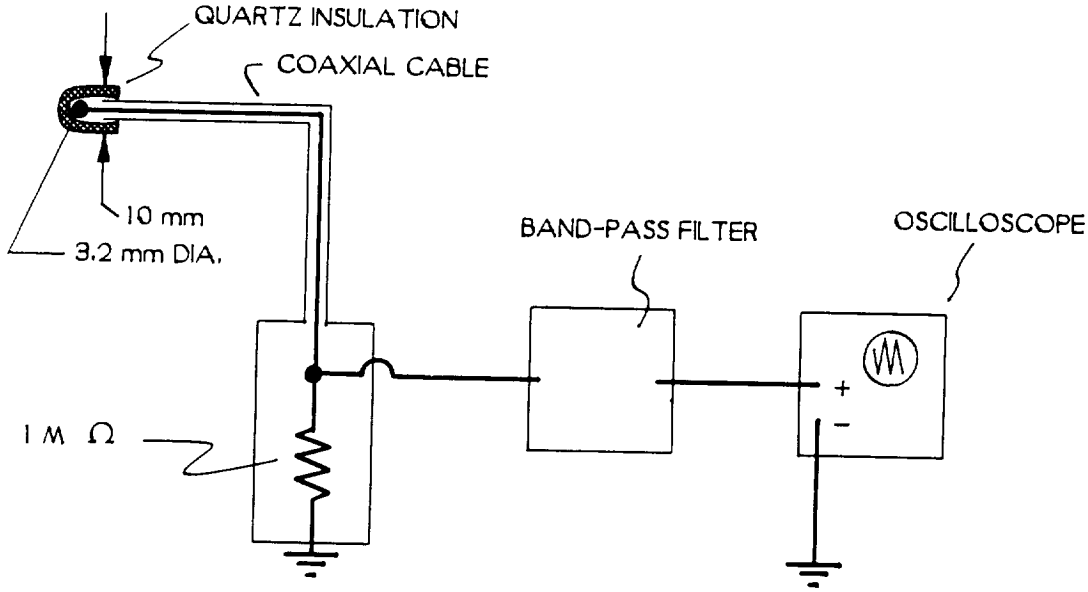

b) Capacitive Langmuir Probe

Fig. 10 Instrumentation Schematics

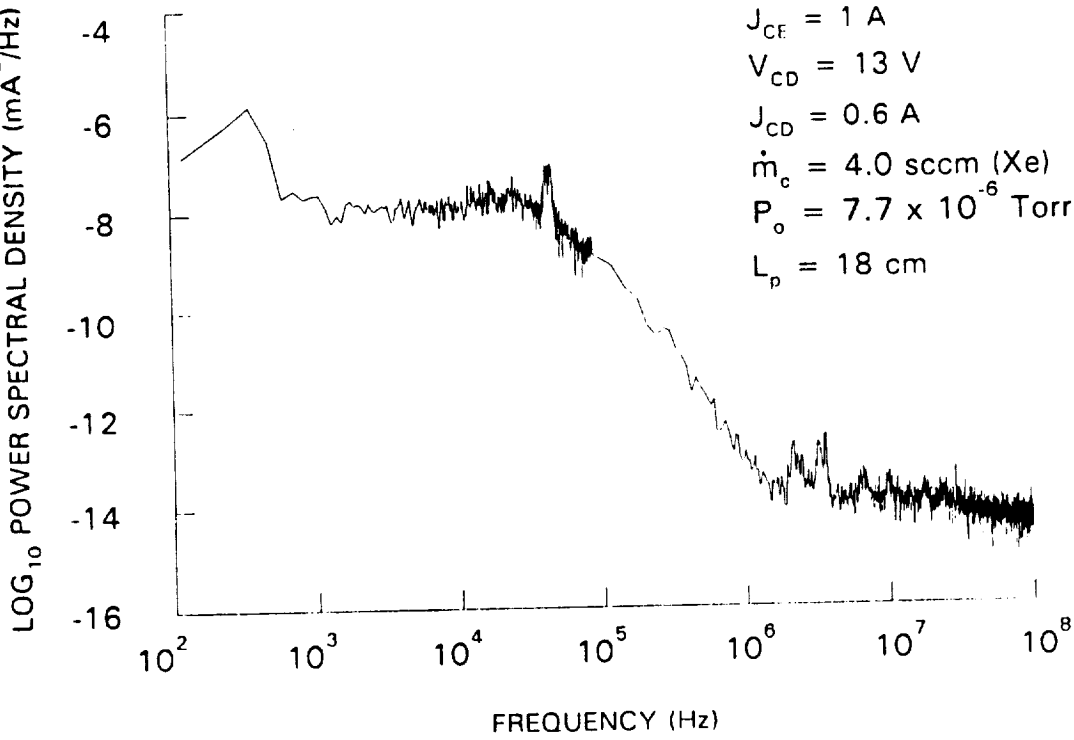

a) Obtained with the Langmuir Probe

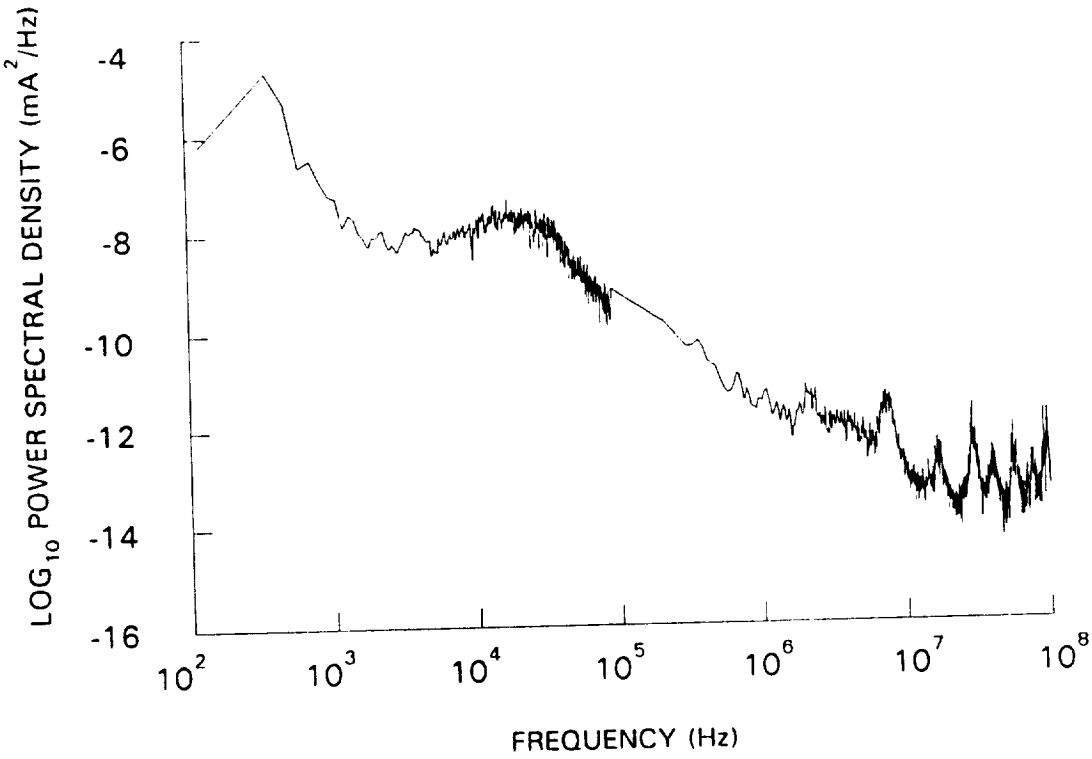

b) Obtained with the Capacitive Langmuir Probe

Fig. 11 Typical Plasma-Oscillation Spectra

arrangement in Fig. 10a was determined to be adequate for frequencies less than 1 MHz as described in Ref. [8]. However, for frequencies greater than 1 MHz where natural plasma frequency resonances are expected, the sheath associated with this type of probe changes its frequency response and can cause spurious signals to occur [14]. These spurious signals can affect spectral data at high frequencies. As a result, another method for measuring plasma noise was pursued so that data collection over the full frequency range (100 Hz to 100 MHz) could be examined.

Some experimentalists use capacitive Langmuir probes to detect oscillations in plasma density and potential [15,16]. A capacitive Langmuir probe (CLP), as illustrated schematically in Fig. 10b, consists of a standard spherical Langmuir probe which is covered with a thin layer of quartz insulation to shield it from direct contact with the plasma. When this probe is placed in a plasma, the high energy electrons from the plasma contactor or ions in the ambient plasma which strike the quartz knock off secondary electrons [15]. As more secondary electrons leave the probe surface, the quartz becomes positively charged until it reaches plasma potential. As a consequence of this phenomenon, the interior electrode tends to float close to local plasma potential [16]. Therefore, plasma density and/or potential oscillations can be observed by measuring the potential fluctuations of the interior electrode. These fluctuations were sensed across a 1 MΩ resistor, filtered, and then detected using the oscilloscope as illustrated in Fig. 10b.

Before measurements were conducted using the CLP, its frequency response was determined and is described in Appendix B. It is believed that the CLP should follow high-frequency fluctuations in plasma density and potential more rapidly than the conventional LP because the inductance associated with the bias power supply is not present. It was necessary to calibrate the CLP because this probe cannot sense

plasma density directly. This calibration was done by shifting power spectral density data from the CLP in the frequency range 0.1 to 100 kHz to approximately match data obtained from the LP in the same frequency range. Typical power spectral data obtained with the probe at the same location and plasma conditions when plasma noise data were taken with the LP (Fig. 11a) are plotted in Fig. 11b. A comparison between these data illustrate the CLP and LP detect similar but shifted spectrum at frequencies below 100 kHz. However, for frequencies above 100 kHz it appears the CLP detects additional signals.

IV. EXPERIMENTAL RESULTS

The emphasis of this research was on the radiated emissions because the conducted emissions were believed to be more controllable. Radiated emissions, on the other hand, are influenced by the plasma environment and can have an equally adverse effect on other SSF equipment. Results from preliminary investigations into the noise emissions [8] suggest the conducted emissions were fairly repeatable (± 3 dB) between various experiments provided the operating conditions were the same. Likewise, during the course of this investigation it was observed that variations in the measured radiated emissions are also repeatable (± 4 dB) between experiments. The most significant changes in either type of measurement were produced by differences in the operating conditions of the plasma contactor, such as contactor emission current (J_{CE}).

Conducted Emissions

The investigation of CE focused on the effects of several variables which were expected to influence these emissions. These included power-supply influence, the plasma environment downstream, and the contactor flow rate, discharge and emission currents. The noise signature of the bias power supply was investigated by comparing the CE induced with a resistive load against those induced by the plasma contactor "load". With a resistive load connected across the power supply, its CE were measured with the current monitor when 1 A was being supplied at the same voltage drop observed with the contactor operating at this current. The resulting narrowband spectral data are plotted in Fig. 12 as the dashed line. For comparison purposes,

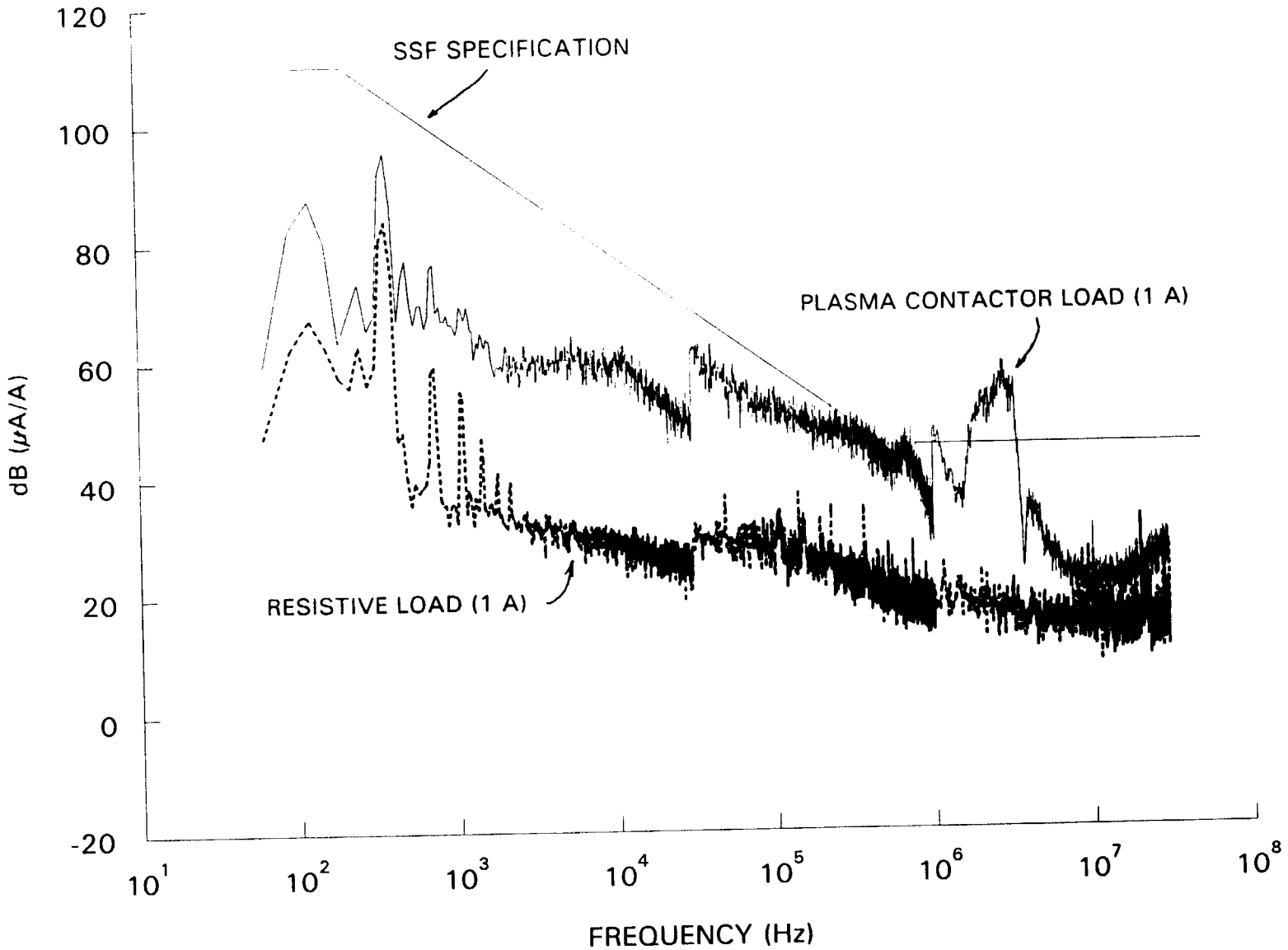

Fig. 12 A Comparison of the Conducted Emissions From the Bias Power Supply

corresponding CE data associated with the contactor are also plotted in Fig. 12 (solid line). It is evident that the bias power supply influences the contactor CE at frequencies of 60 Hz harmonics (i.e. 120,180, 240 Hz etc.) but not at frequencies greater than ~2 kHz. As a result, it appears the bias power supply is responsible for some of the low-frequency noise emissions.

The effect of the ambient plasma environment on the CE of the contactor was investigated by changing the simulator operating conditions. First, the CE were measured when the simulator was operated at standard conditions (on) and then, when it was shut down (off) while the contactor emission current was held constant at 1 A (J_{CE} = 1 A). The resulting CE data are plotted in Fig. 13 as the solid and dashed lines which correspond to the simulator on and off respectively. It appears that simulator operation decreases the conducted emissions in the frequency range 240 Hz to ~ 200 kHz. This result suggests that those conducted emissions, which are driven by the contactor and couple to the return-line current via the ambient plasma, are affected by plasma damping effects. With the simulator on, the ambient plasma density and dissapative effects increase. The results of Fig. 13 are consistent with the fact that plasma oscillations are dissipated at frequencies below the plasma frequency [11].

Two other parameters which might influence the conducted emission levels, are the contactor flow rate ($\dot{m}_c$) and discharge current (J_{CD}). The relative effect of $\dot{m}_c$ on the CE was examined by adjusting the flow rate incrementally and measuring the CE. The results corresponding to $\dot{m}_c$ = 1.4, 2.7, and 4.0 sccm, which are plotted in Fig. 14, indicate that CE generally increase with reductions in the flow rate from 4.0 sccm. The effects of discharge current (J_{CD}) on CE were examined and the results obtained at J_{CD} = 0.1, 0.3, and 0.6 A are plotted in Fig. 15. These data suggest that the CE levels

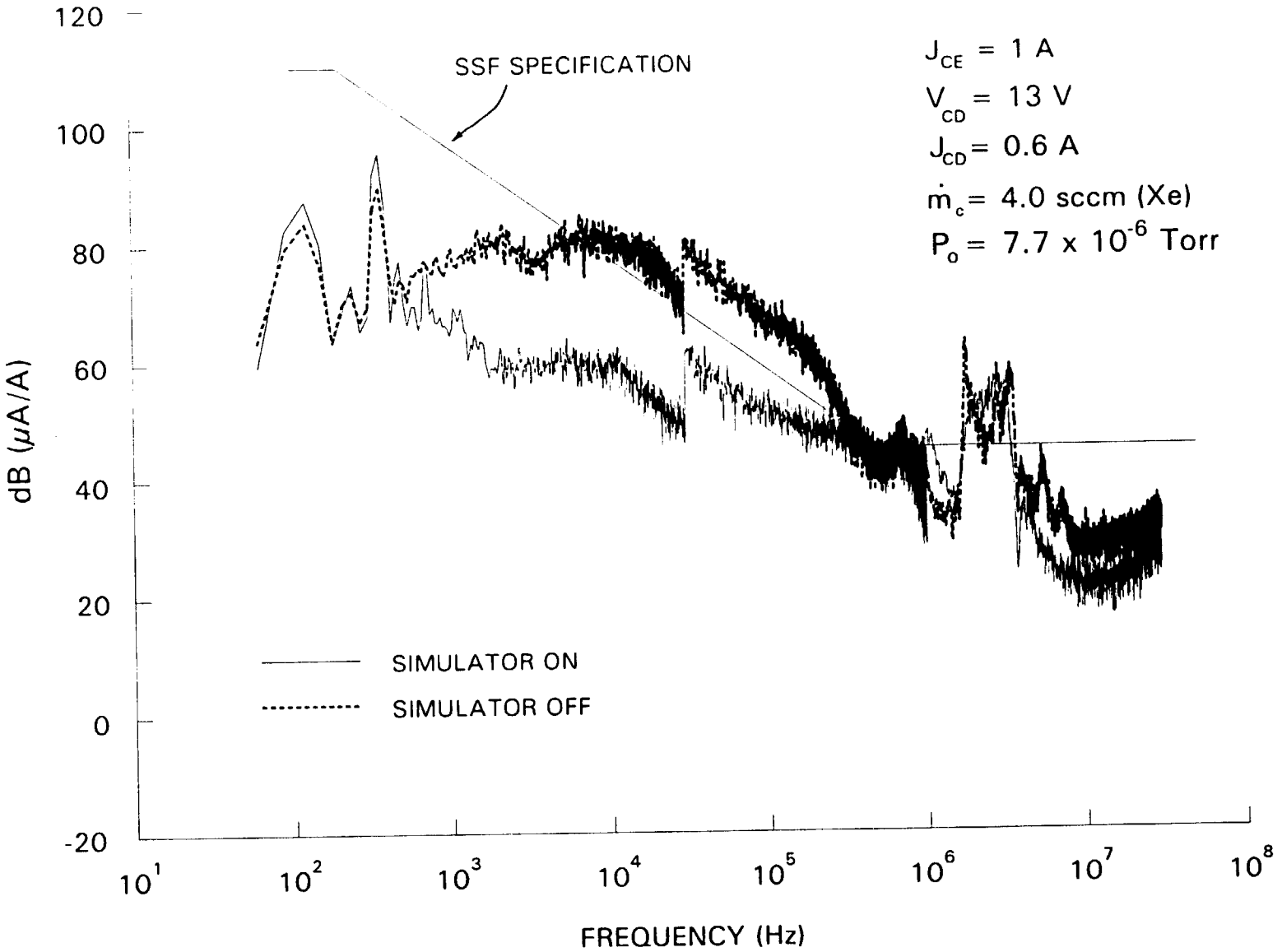

Fig. 13 The Effect of Simulator Operation on the Conducted Emissions

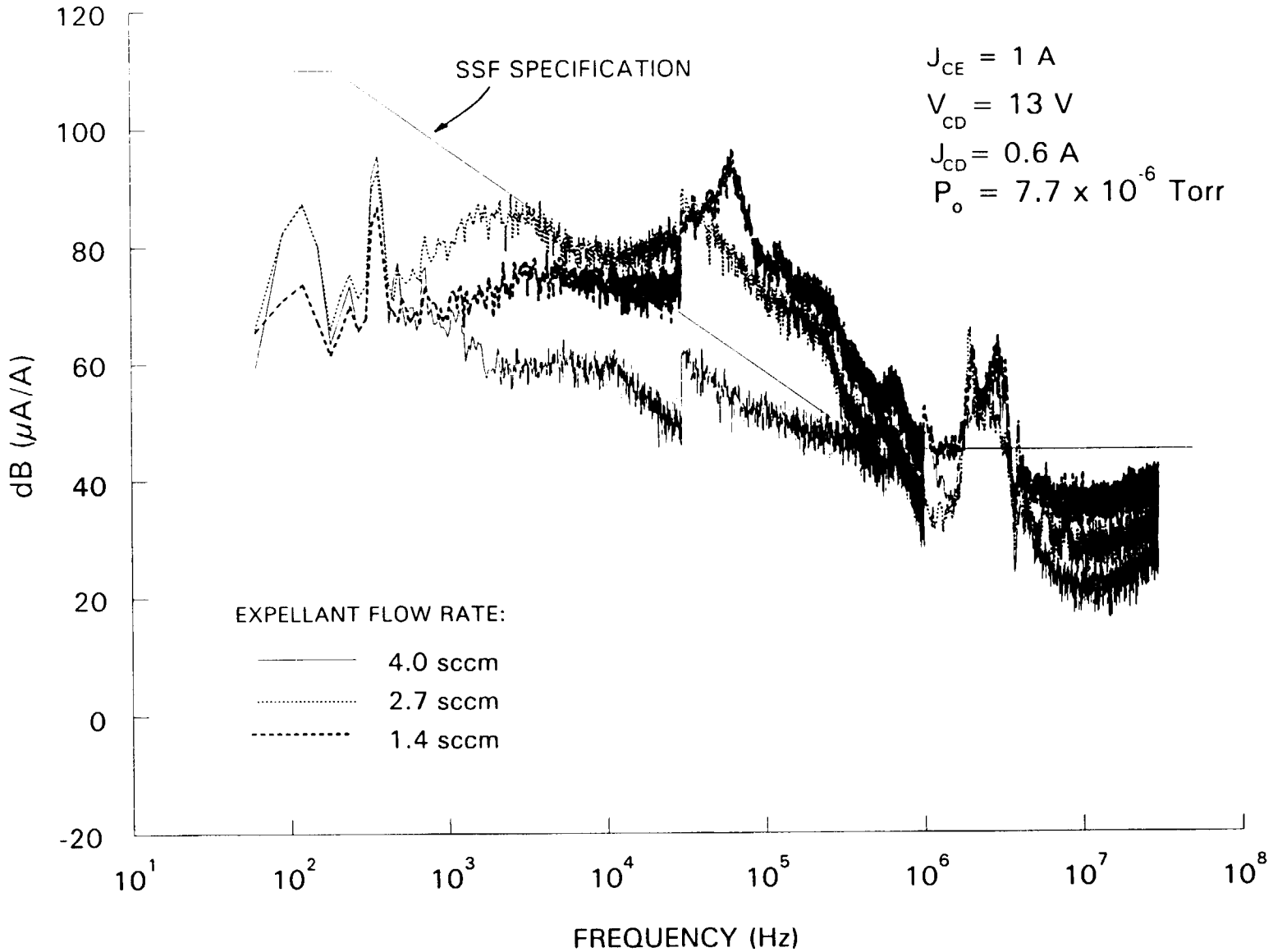

Fig. 14 The Effect of $\dot{m}_c$ on the Conducted Emissions

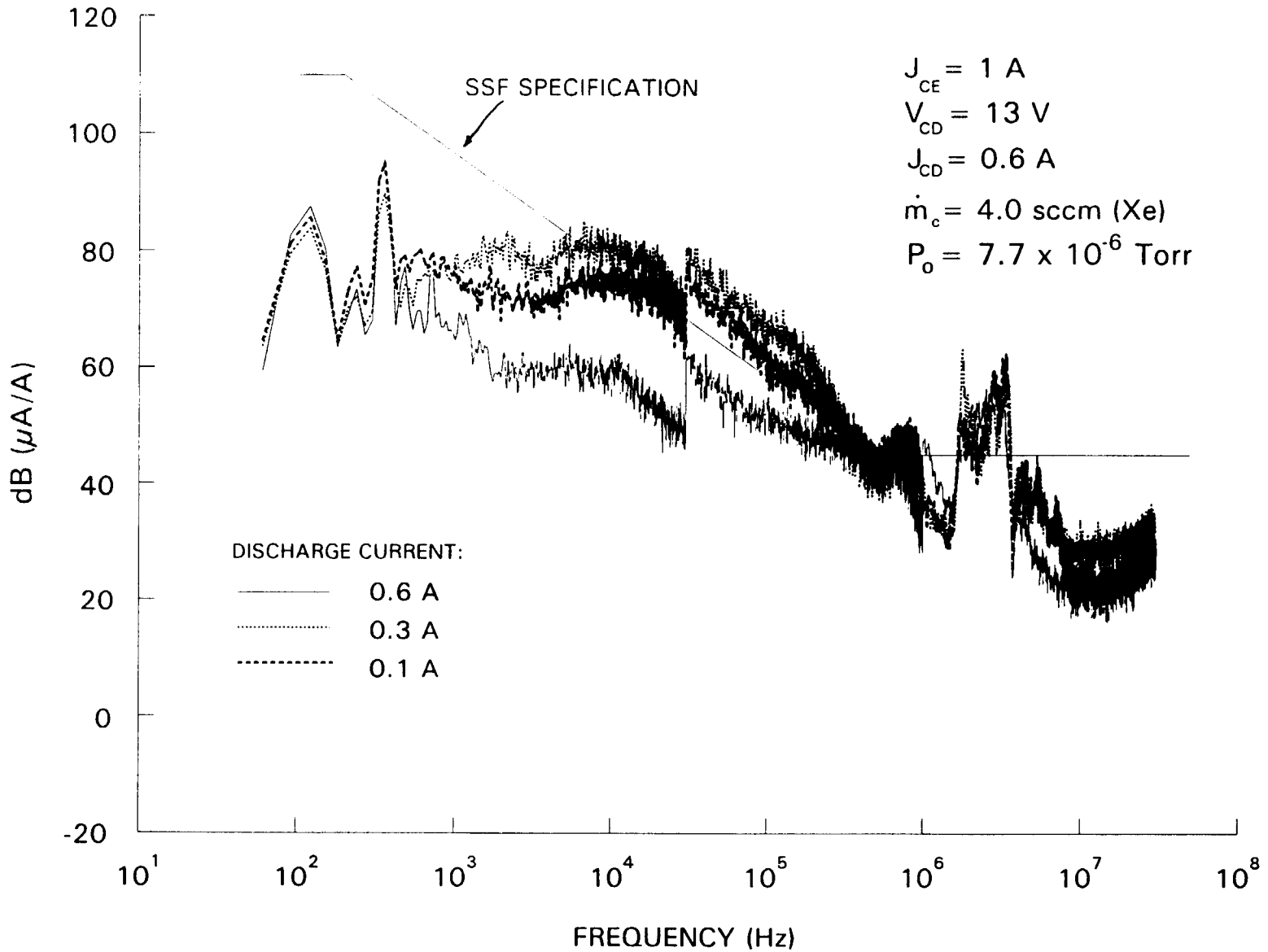

Fig. 15 The Effect of J_{CD} on the Conducted Emissions

generally increase as discharge current is decreased from 0.6 A. From Figs. 14 and 15 it appears that the conducted emissions are decreased by operating the plasma contactor at a selected flow rate ($\dot{m}_c$ = 4.0 sccm) and discharge current (J_{CD} = 0.6 A).

The effect of contactor emission current (J_{CE}) on the CE are plotted in Fig. 16 for three values (J_{CE} = 1, 5, and 10 A) which cover the designed operating range for the space station. These spectral data indicate that signals from the power supply in addition to signals around 2 MHz are present regardless of the emission current. It might appear from the data in Fig. 16 that the amplitudes of the current fluctuations decrease as J_{CE} is increased. Actually, these amplitudes remain approximately constant and the decrease in the conducted emission levels results from dividing by the mean emission current.

The effect of J_{CE} can be further understood by examining the root-mean-square of the current fluctuations (ΔJ_{rms}) at various mean emission currents (J_{CE}). Values of ΔJ_{rms} were determined by integrating power-spectral-density data, obtained at different contactor emission current levels, for two frequency ranges (i.e. 0.1 to 100 kHz and 0.1 to 100 MHz) and the results are plotted against J_{CE} in Fig. 17. These results indicate the greatest current fluctuation levels, which are slightly over 10% of the mean current, develop at J_{CE} = 1 A and 6 A. A comparison of the data in the two frequency ranges clearly illustrates that the noise levels are greater in the lower frequency range (upper plot). Also, the data in both frequency ranges do not follow a particular trend which indicate that transitions in the character of the conducted emissions are present.

Initial Investigation of the Radiated Emissions

Before the radiated emissions created by normal plasma contactor operation

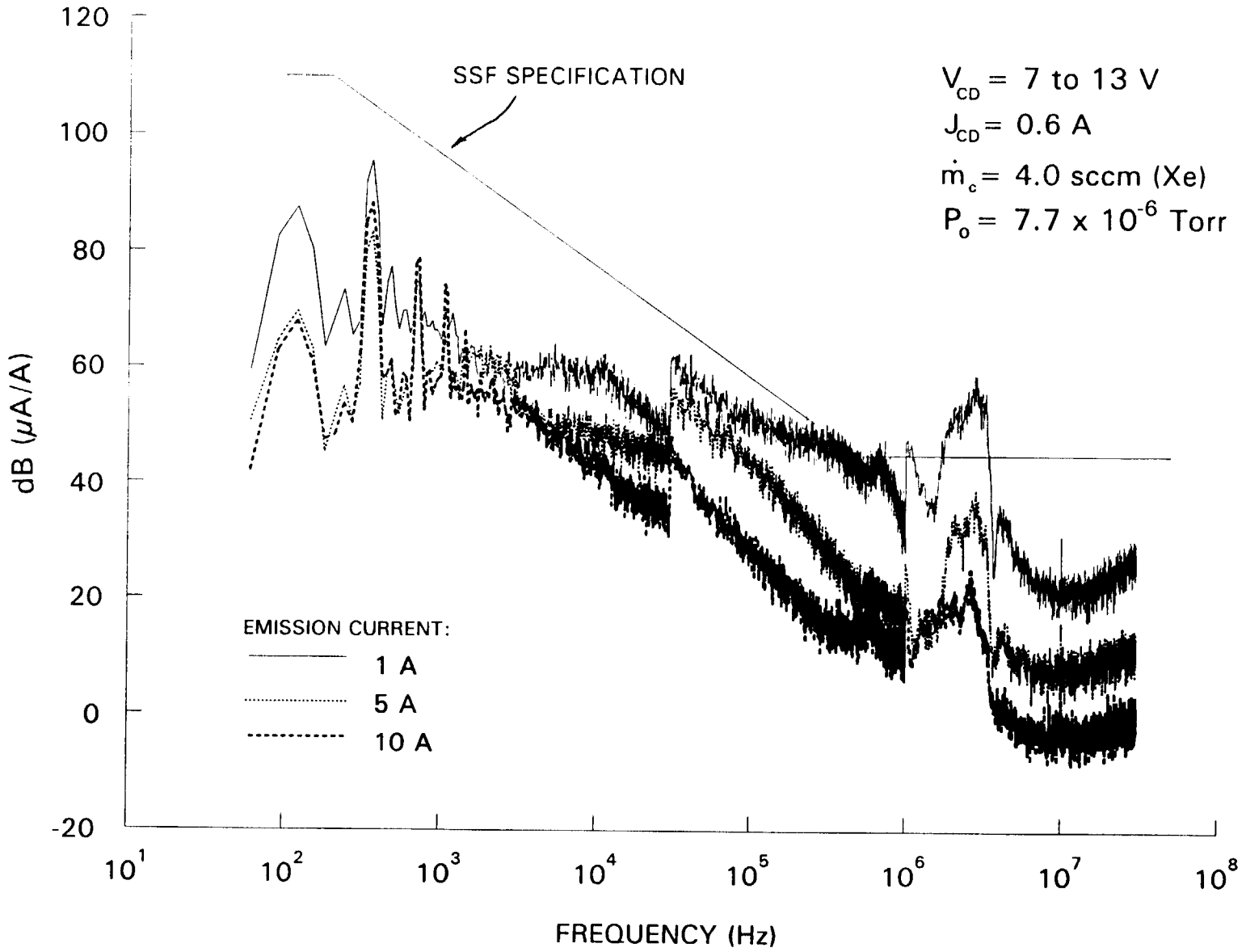

Fig. 16 The Effect of J_{CE} on the Conducted Emissions

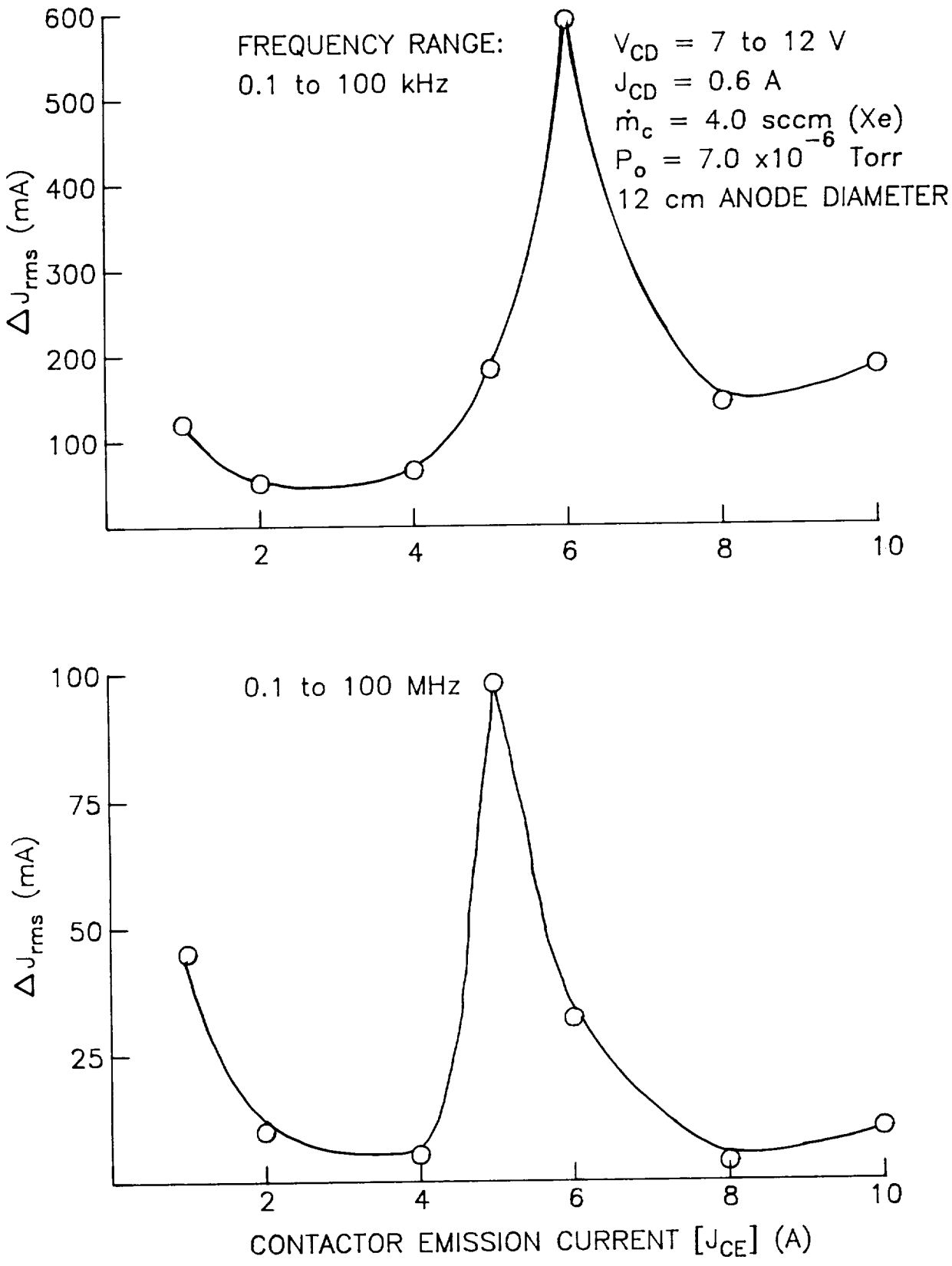

Fig. 17 Current Fluctuations as a Function of Contactor Emission Current

were determined, the appropriate antenna configuration (i.e. in contact with or isolated from the ambient plasma) had to be selected. As a prerequisite to this, the background radiation levels, present with both the contactor and simulator off, were sensed with the antenna for the cases where the plexiglas cover, used to isolate the antenna from the plasma, was in-place (with cover) or removed (without cover). These background radiation levels are plotted in Fig. 18 as broadband emissions (dB[μV/m/MHz] v. frequency) and they suggest the cover does not have a significant effect on the measured noise levels. This background radiation was observed to be caused by the electromagnetic interference induced from computer equipment, lights, and other electrical devices in the laboratory which are picked up on, and re-radiated from the various wires which enter the vacuum tank. As the data in Fig. 18 indicate, these background RE levels are far below the space-station specifications.

The next step was to determine the RE caused by the plasma contactor when its discharge was ignited and not while it emitted electrons. Specifically, radiated emission measurements were made while the discharge current between the anode and cathode of the contactor was set to 0.6 A (Jcd = 0.6 A), the contactor was not biased to emit electrons (V_b = 0 V and J_{CE} = 0 A), and the simulator was turned off (Jsd = 0 A). The resulting RE detected by the antenna with and without the plexiglas cover are plotted in Fig. 19 and these results again suggest the cover does not significantly affect the measured noise levels. As expected, these RE data are substantially greater than the observed background levels (Fig. 18). However, the data in Fig. 19 indicate the plasma contactor is able to satisfy the SSF specifications except in the frequency range 0.1 to 3 MHz.

Next, the radiated emissions were measured when the simulator was operating (Jsd = 0.45 A) and the contactor was shut down (J_{CE} = Jcd = 0 A). The RE

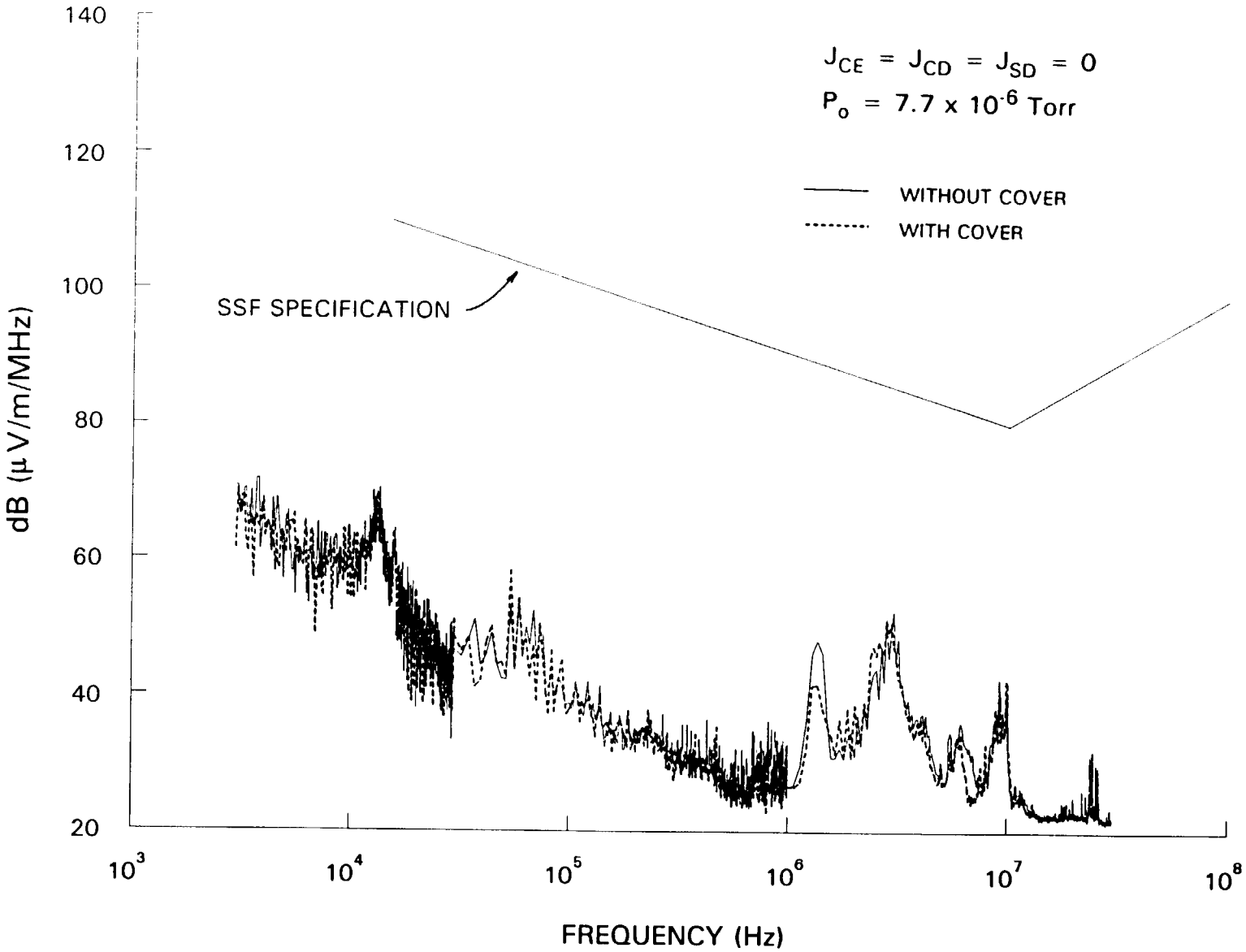

Fig. 18 Background Radiated Emissions

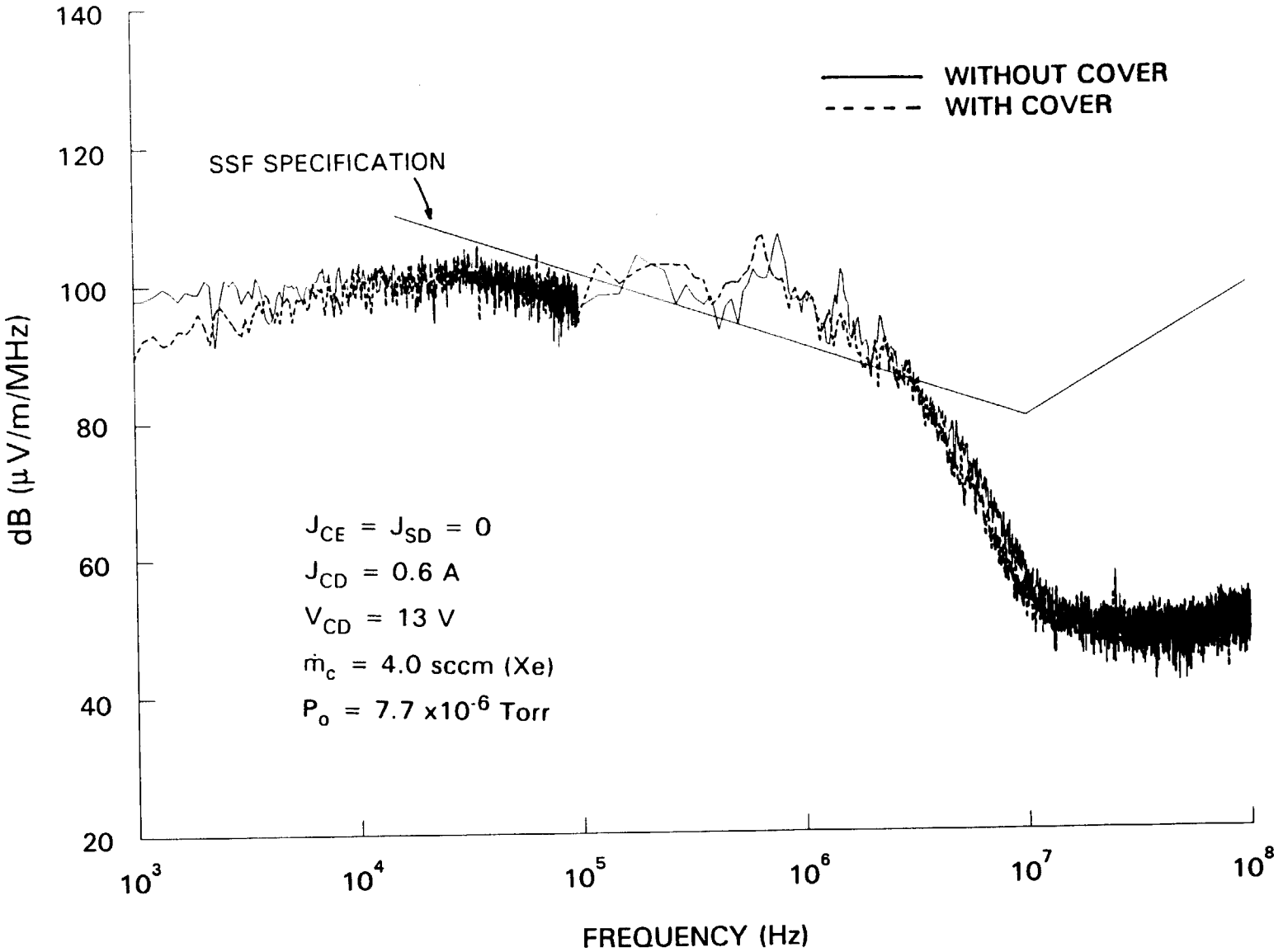

Fig. 19 Typical Radiated Emissions When Just the Contactor is Operated

spectral data for this test are graphed in Fig. 20 where there appears to be a significant difference between the electric fields detected by the antenna with and without a cover. For both cases, however, the RE from the simulator are lower than those observed when the contactor was operating alone (Fig. 19) and they are below the SSF specification.

Before addressing the difference in spectral data taken with and without the cover, it is beneficial to consider the results of another test conducted in which the plasma contactor and simulator were operating at standard conditions (i.e. Jcd = 0.6 A and Jsd = 0.45 A). In this test, the contactor was biased to emit 1 A (J_{CE} = 1 A) and the resulting RE spectrum sensed with the antenna is plotted in Fig. 21. Again, the observed spectrum depends on whether or not the plexiglas cover is used to shield the antenna from direct contact with the plasma. As a result of these tests and before other variables which could influence the RE are investigated, it must be determined which antenna configuration (i.e. with or without a cover) should be used to make the measurements.

The experimental results in Figs. 19 - 21 can be understood by considering the mechanism by which an antenna detects fluctuating electric fields. A mono-pole antenna detects electric fields by measuring the potential difference induced between the antenna and a reference, or ground, plate (Fig. 6b) [17]. If a low-impedance electrical connection between the antenna and the ground plate develops, potential differences induced between the antenna and the ground plate will be perturbed and the antenna will not function properly. This effect is illustrated by the data plotted in Fig. 22 which were taken with the antenna exposed to typical radiated noise in the laboratory (e.g. lights, computers, etc.). First, the antenna was allowed to operate normally and the spectral data corresponding to an "open circuit" were measured

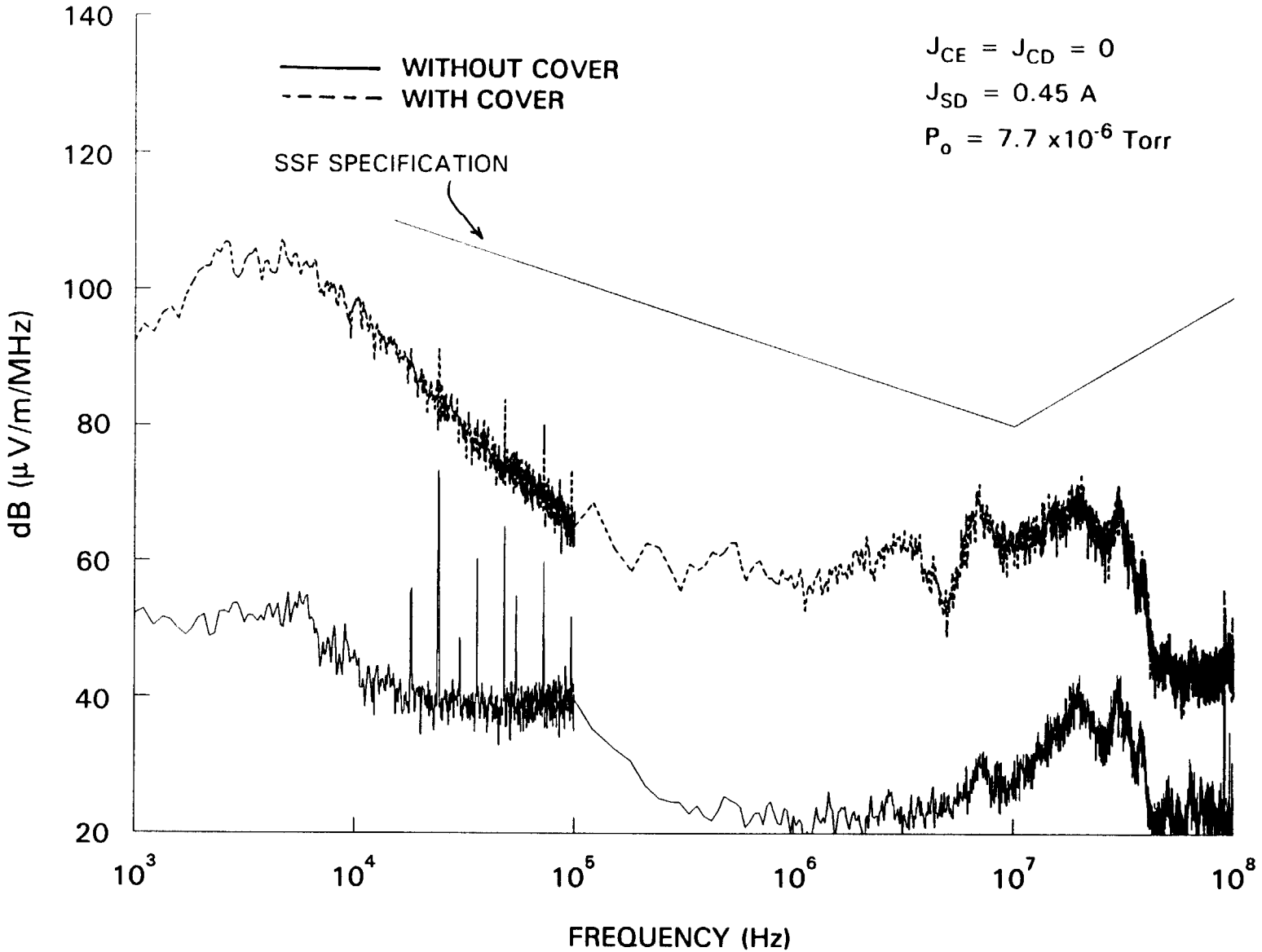

Fig. 20 Typical Radiated Emissions When Just the Simulator is Operated

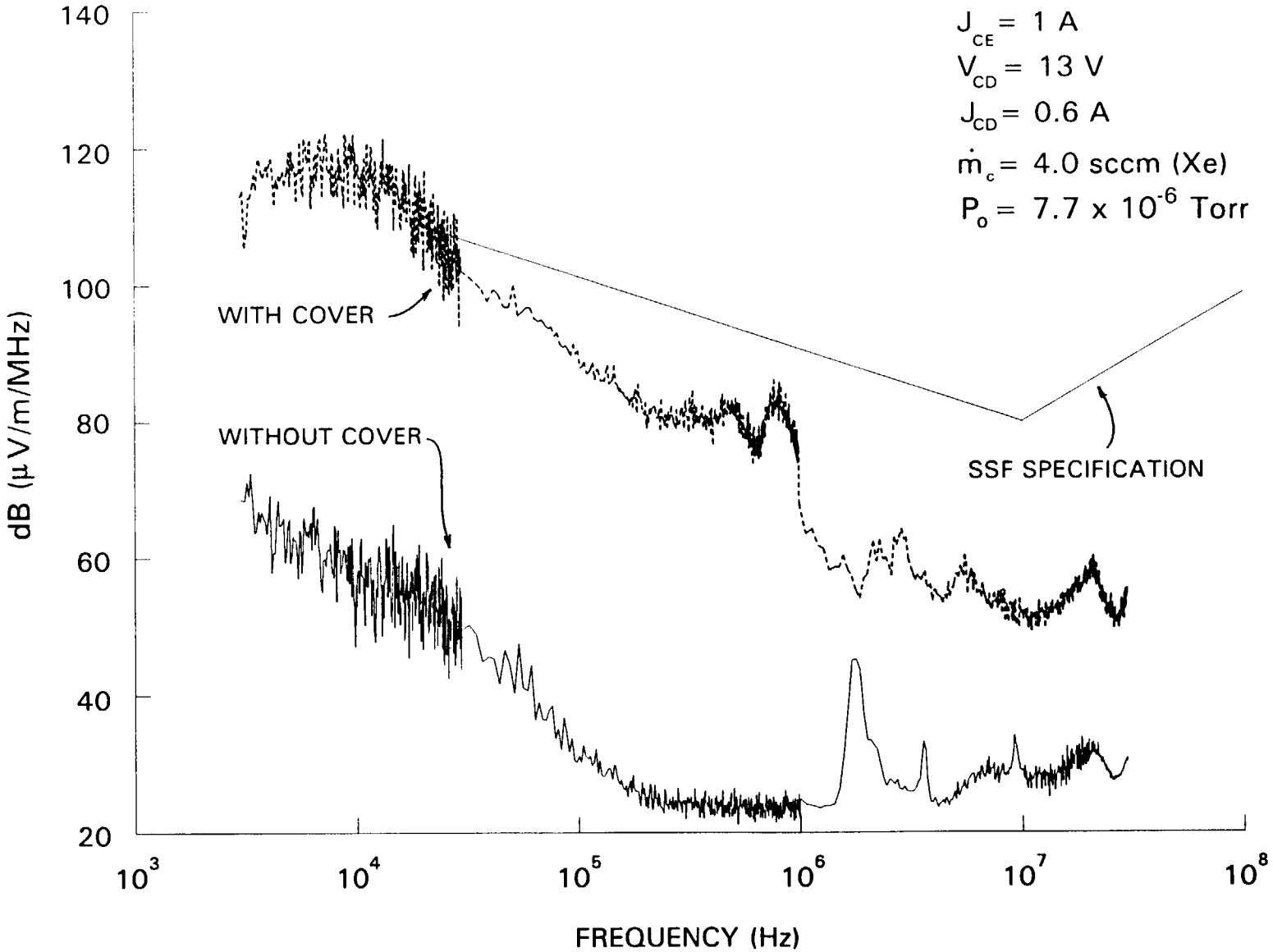

Fig. 21 The Effect of the Cover on Typical Radiated Emissions

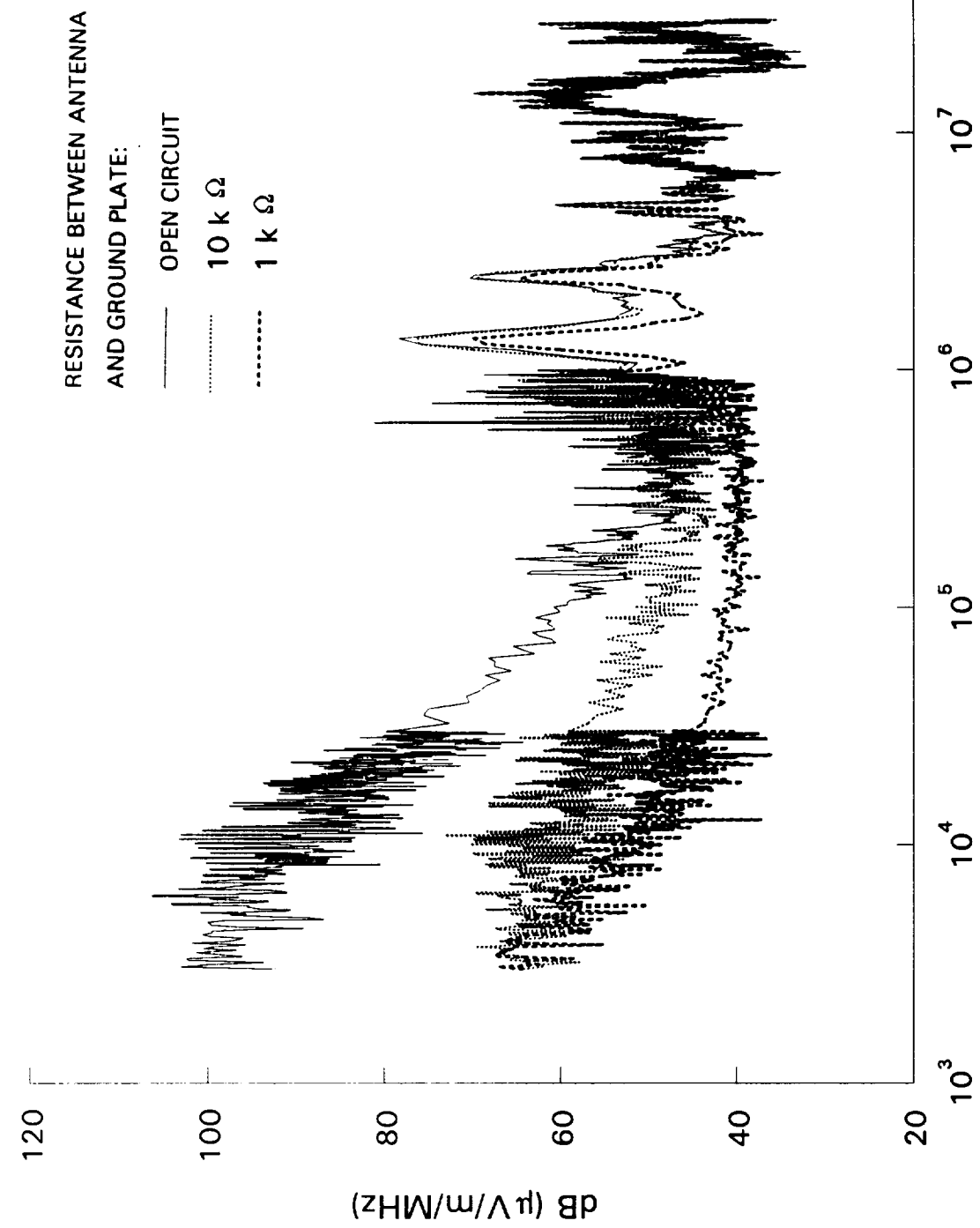

Fig. 22 The Effect of an Electrical Connection Between the Antenna and its Ground Plate

(solid line in Fig. 22). Next, two resistors (1 and 10 kΩ) were connected one after the other between the antenna and the ground plate. The resulting spectra are plotted in Fig. 22 as the dashed and dotted lines corresponding to the 1 and 10 kΩ resistors, respectively. Clearly the data in Fig. 22 indicate that any electrical connection between the antenna and its ground plate causes low-frequency noise to be attenuated. It is suggested, therefore, a plasma in contact with an antenna will provide an electrical connection between the antenna and the ground plate and thereby cause the attenuation observed in the data presented in Figs. 20 and 21. Additionally, if there is plasma between the noise source and the antenna, the radiated signals which pass through this plasma are attenuated for frequencies below plasma frequency (f_p ~ 16 MHz). Using this information, it is now possible to understand the different effects of the plexiglas cover shown in Figs. 19 and 20.

In Fig. 19, where only the plasma contactor was operating and the antenna was far downstream of it, the same radiated emissions were detected with and without the cover. In this case it is argued that the impedance of the plasma is sufficiently high, because of the low density plasma brought on by $J_{SD} = J_{CE} = 0$ A, that the current flow between the antenna and ground plate through the ambient plasma is not significant. Hence, the data in Fig. 19 are not influenced by the cover. On the other hand, the simulator produces a modest plasma when it is operating alone (Fig. 20), and this plasma does provide a low-impedance connection between the antenna and the ground plate thus attenuating the output signals from the antenna.

On the basis of these preliminary tests, it has been concluded that the RE induced by the contactor are more accurately detected if the antenna is shielded from direct exposure to the plasma. Therefore, unless otherwise stated, the RE data that follow were measured with the plexiglas cover placed over the antenna. In addition,

these data were obtained with the simulator operating under the normal conditions in Table 1.

Typical Radiated Emissions from a Hollow Cathode Plasma Contactor

Now that the effects of antenna configuration (i.e. with or without a cover) have been addressed it is desirable to understand how the variation of contactor operating parameters, such as J_{CE}, $\dot{m}_c$, and J_{CD}, influence the radiated emissions. Also, it is of interest to determine the effects of antenna location and orientation on RE because measurements in a vacuum tank are susceptible to plasma wave attenuation and reflection effects. In order to understand these effects, several experiments were conducted to determine their impact on radiated emissions.

The effect of contactor emission current (J_{CE}) on RE were measured with the contactor biased to yield the same current levels considered for the examination of the CE (i.e. J_{CE} = 1, 5, or 10 A). The electric-field fluctuations sensed by the antenna at each emission current are presented in standard broadband data format in Fig. 23. These spectra are different for frequencies greater than 30 kHz for these currents. As J_{CE} is increased from 1 to 5 A the RE levels increase in the 30 kHz to 1 MHz range and decrease in the 1 MHz to 30 MHz range. When J_{CE} is increased further from 5 to 10 A, this particular trend is not apparent. This unpredictable behavior might be induced by the same transition effects as those observed in experiments on the CE. Also, depending upon the current levels, the data in Fig. 23 indicate the SSF specifications are not exceeded for most frequencies. The apparent discontinuity in all the spectra of Fig. 23 at 1 MHz is a result of changing the resolution bandwidth for the measurement (see Appendix A).

An examination of the effect of flow rate ($\dot{m}_c$) and discharge current (J_{CD}) on the RE was studied by first biasing the plasma contactor to emit 1 A (J_{CE} = 1 A) and

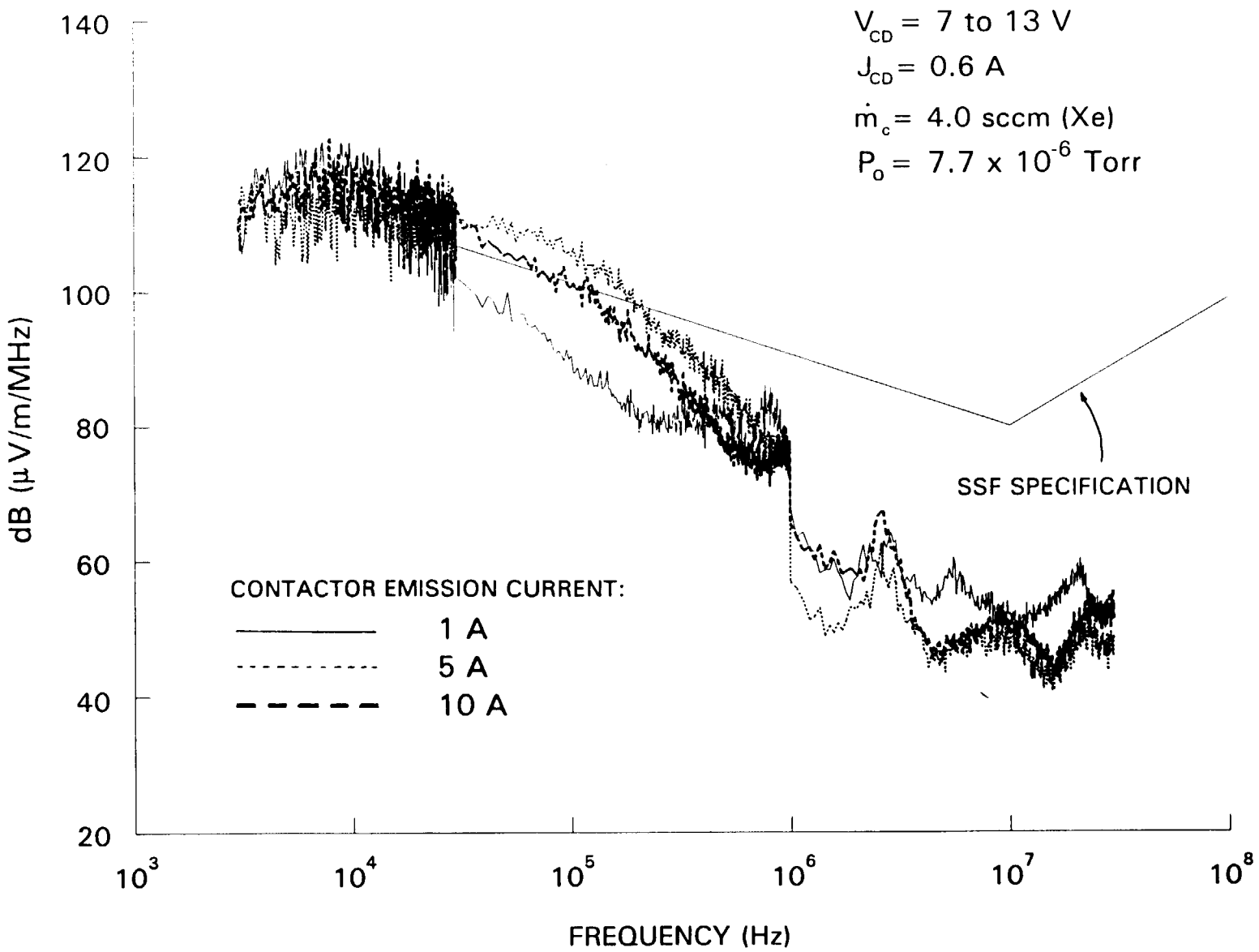

Fig. 23 The Effect of J_{CE} on the Radiated Emissions

then measuring the RE as either $\dot{m}_c$ or J_{CD} were varied incrementally. The results for the variation in expellant flow rate ($\dot{m}_c$ = 1.4, 2.7, and 4.0 sccm) are illustrated in Fig. 24 where slight but insignificant changes in the RE are apparent. Similarly, the results obtained when the contactor discharge current was varied (J_{CD} = 0.1, 0.3, and 0.6 A) are plotted in Fig. 25. Again, the RE are essentially the same at these selected currents. The data acquired from these tests (Figs. 23, 24, and 25) suggest that RE are mainly influenced, however not very dramatically, by emission current and not by flow rate and discharge current.

Next, the antenna was placed at three locations downstream from the contactor (i.e. the tip of the antenna was placed 12, 100 and 190 cm from the contactor) in order to determine the attenuation of the RE with distance from the contactor. After the contactor had been biased to emit 1 A (J_{CE} = 1 A) the RE were measured at each antenna position. The results, which are plotted in Fig. 26, reveal the radiated emission levels are attenuated in the frequency range 30 kHz to 1 MHz as the antenna is moved further away from the plasma contactor. This attenuation can be attributed to the intensity of the plasma waves produced close to the contactor. The current fluctuations from the plasma contactor which drive electric field fluctuations are localized near the contactor and then decrease with increasing distance from the contactor. As a result, radiated emissions levels are larger near the contactor when compared with those further downstream. In addition, electric field fluctuations can also be attenuated if their frequency of oscillation is lower than the plasma frequency (f_p ~ 16 MHz). Therefore, when the antenna was close to the contactor, the electric field oscillations with frequencies between 30 kHz and 1 MHz were most attenuated and become damped as a function of downstream location as observed in Fig. 26.

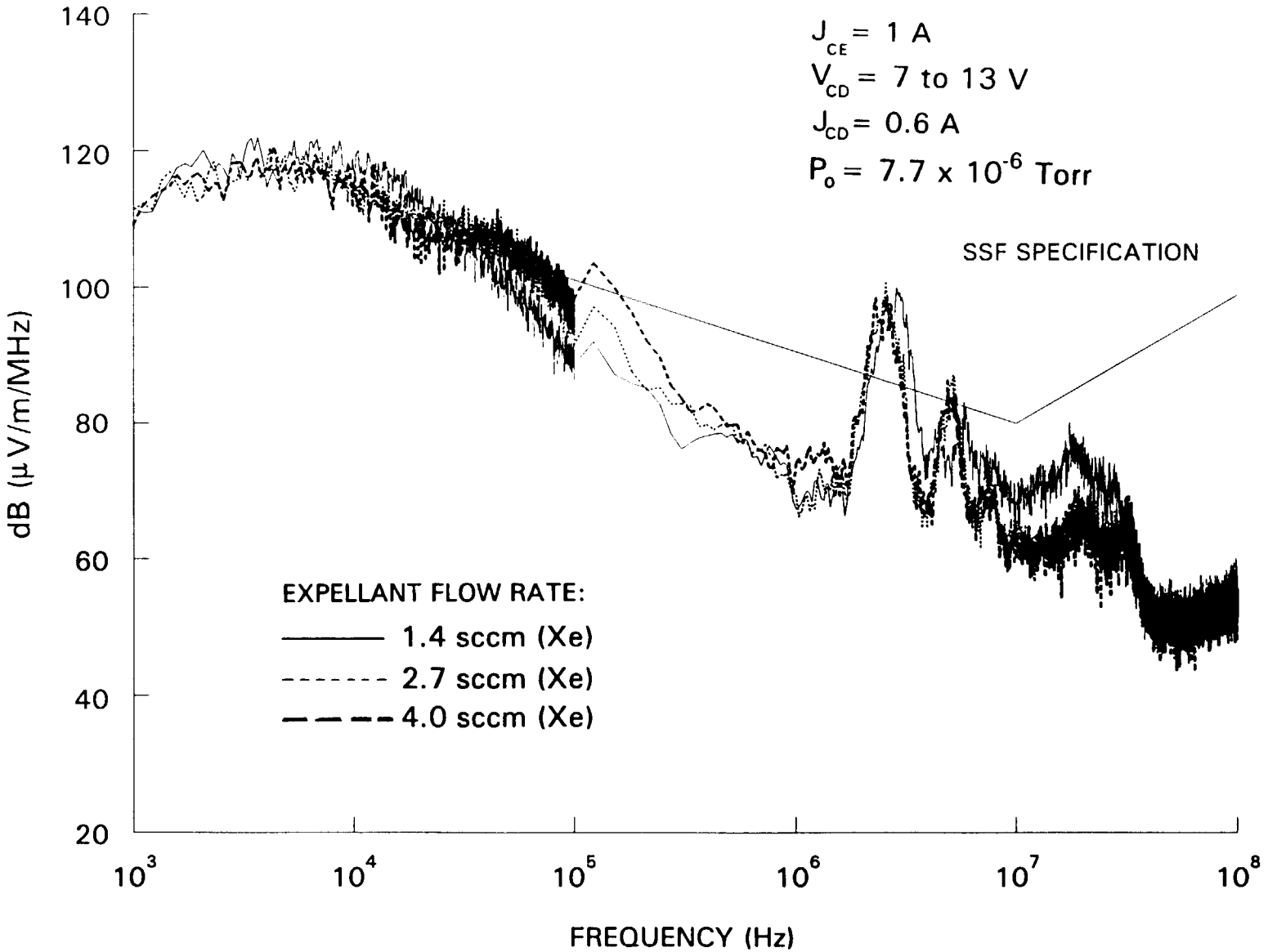

Fig. 24 The Effect of $\dot{m}_c$ on the Radiated Emissions

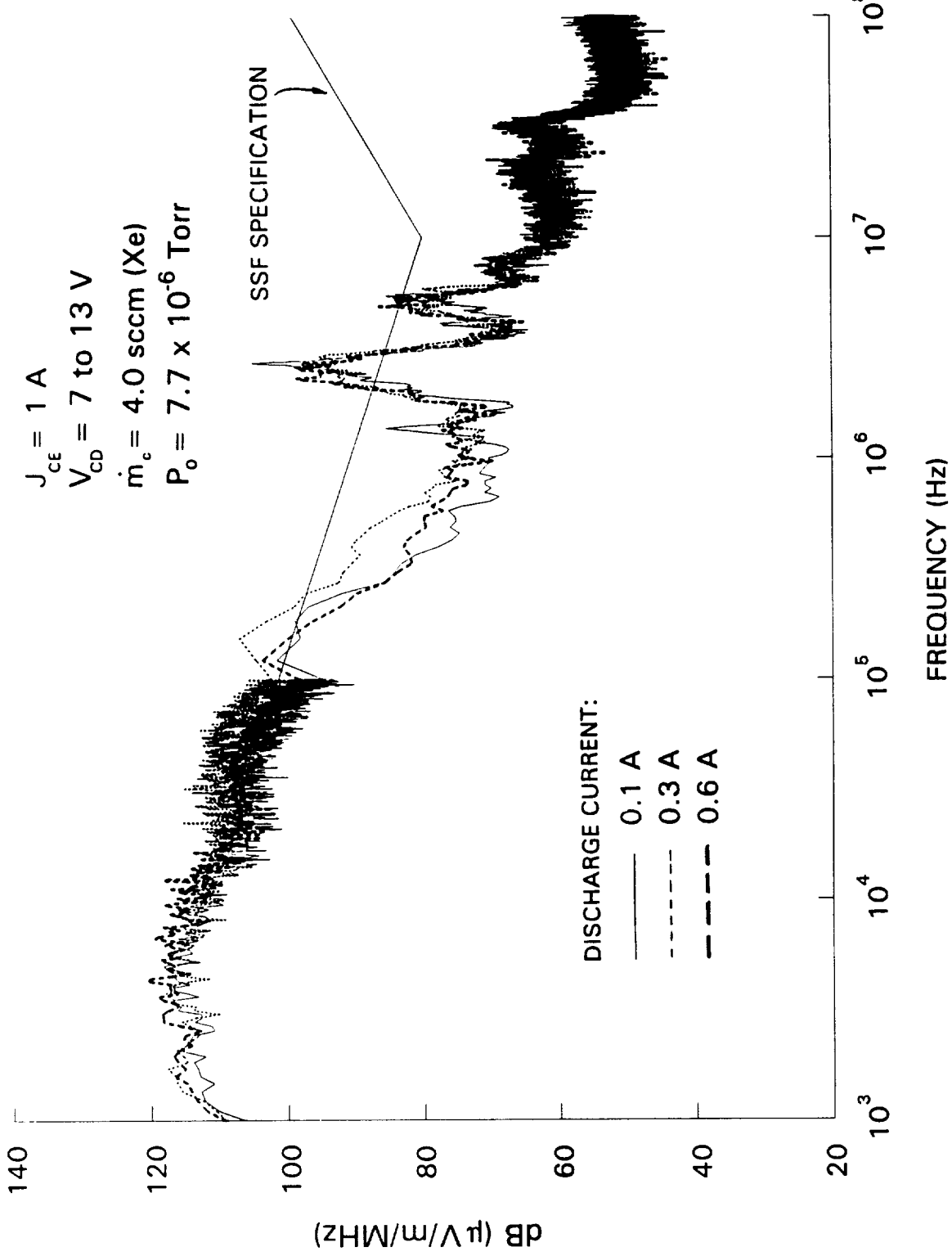

Fig. 25 The Effect of J_{CD} on the Radiated Emissions

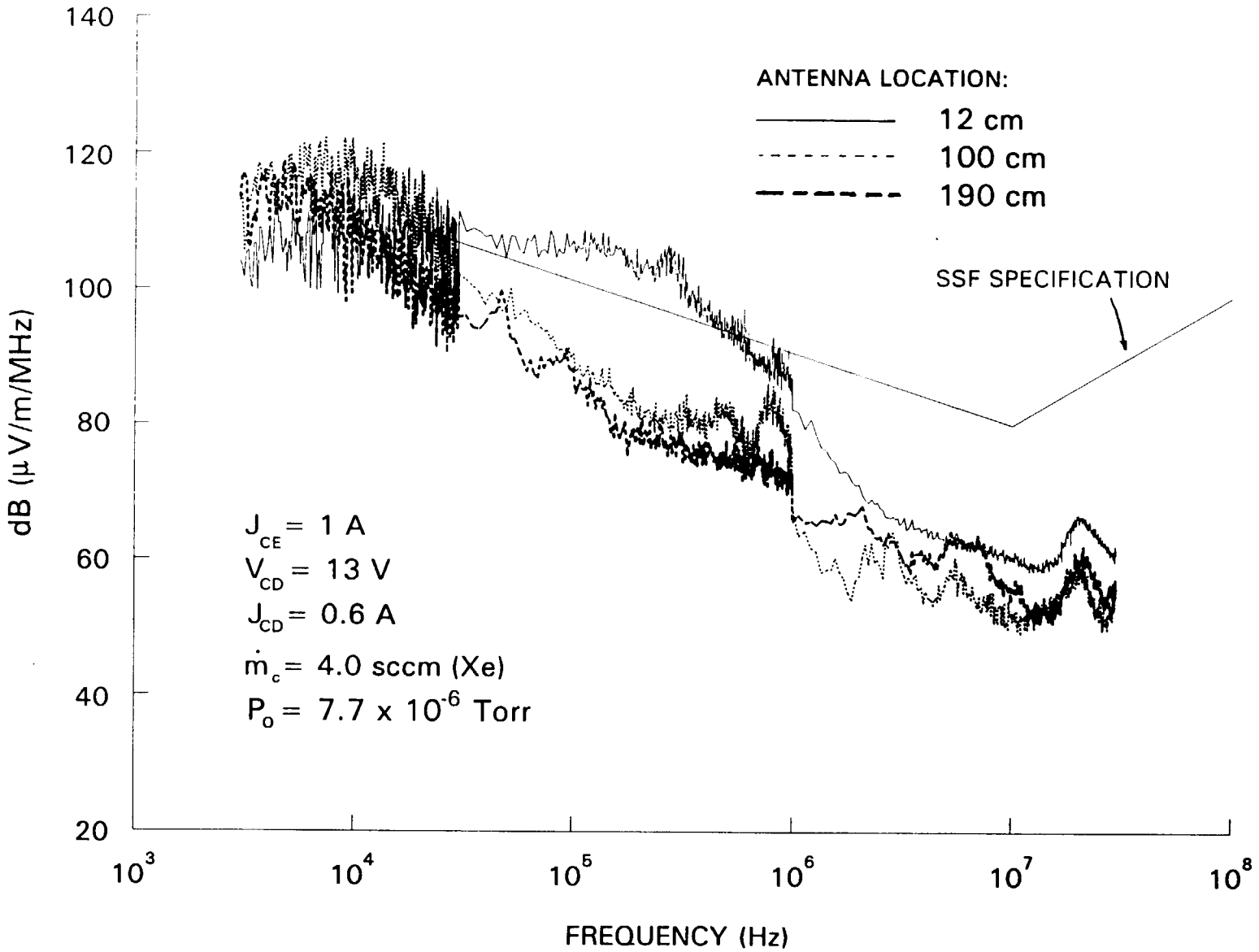

Fig. 26 The Effect of the Antenna Position on the Radiated Emissions

Another experiment was conducted to determine if the orientation of the antenna produced a significant difference in the measured RE. For this test, the antenna was shortened slightly (66 cm) and then attached to the cart vertically as depicted in Fig. 27. The plasma contactor was then operated at standard conditions and RE were measured with the antenna positioned 140 cm downstream of the contactor. The results are plotted in Fig. 28 as the dashed line and can be compared to those measured with the antenna oriented horizontally and located 100 cm downstream (solid line). These data indicate that a different antenna orientation causes some variation in the detected emissions which could be attributed to the orientation of the electric fields oscillations in the vacuum tank. As with tests conducted with the antenna oriented horizontally, spectral data obtained with the antenna vertical exhibited the same trends (i.e. variation in the radiated emission levels as a function of emission currents).

Plasma Noise Detected by Langmuir Probes

For this investigation, the conventional or capacitive Langmuir probes provide a means of detecting plasma potential and density fluctuations which reflect the effects of plasma turbulence. It is expected that plasma turbulence induces transients in the effective plasma impedance which in turn affects the conducted and radiated emissions. The magnitude and spectral composition of the measured turbulence sensed by a Langmuir probe can be expected to vary from one location to another because both standing and transient waves can be expected. For this preliminary study, however, probes were placed only 18 cm downstream from the plasma contactor along the contactor-simulator centerline. At this location, it was believed the probe should experience representative but not overwhelming plasma noise induced near the contactor.

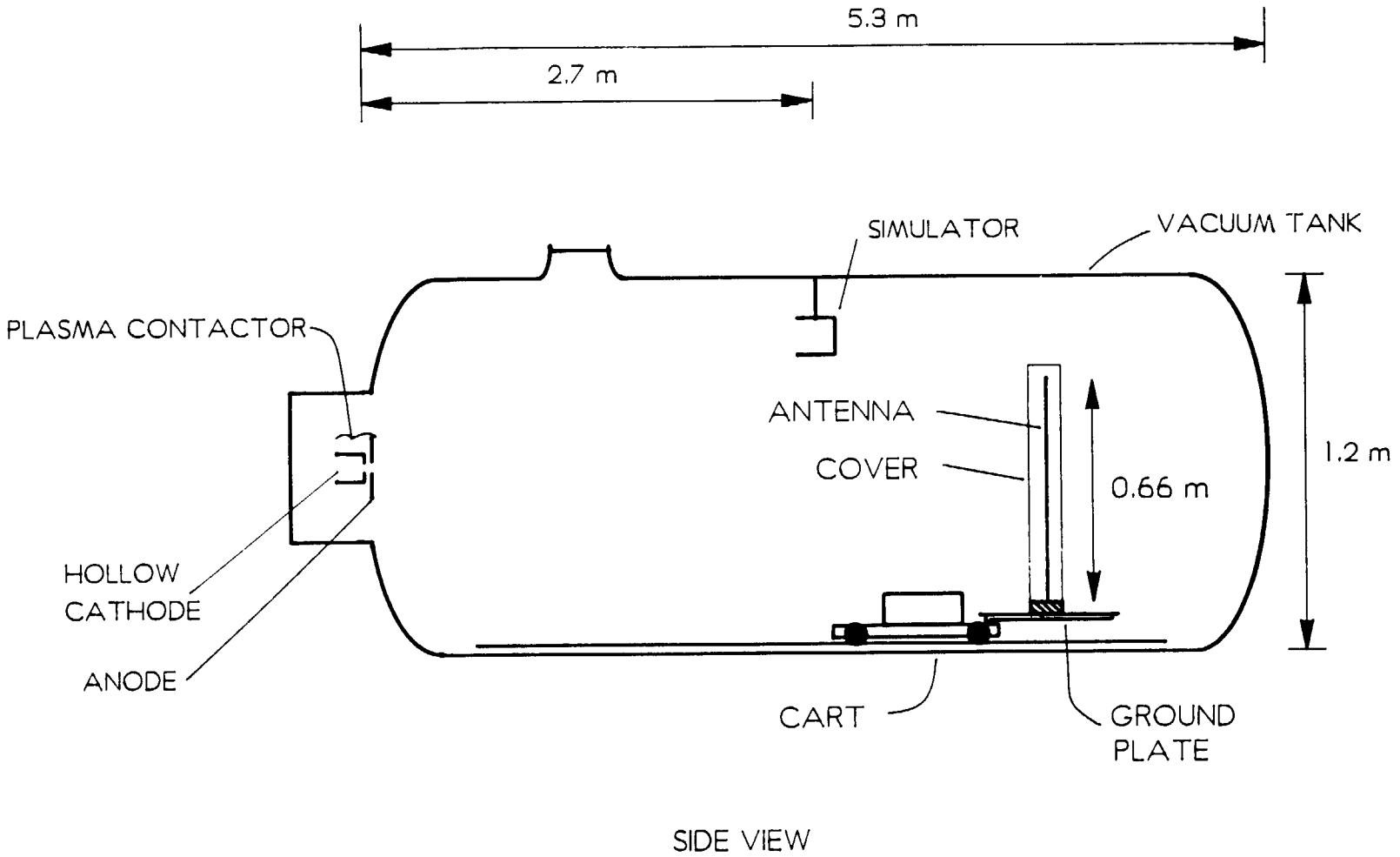

Fig. 27 **Vertical Antenna Configuration**

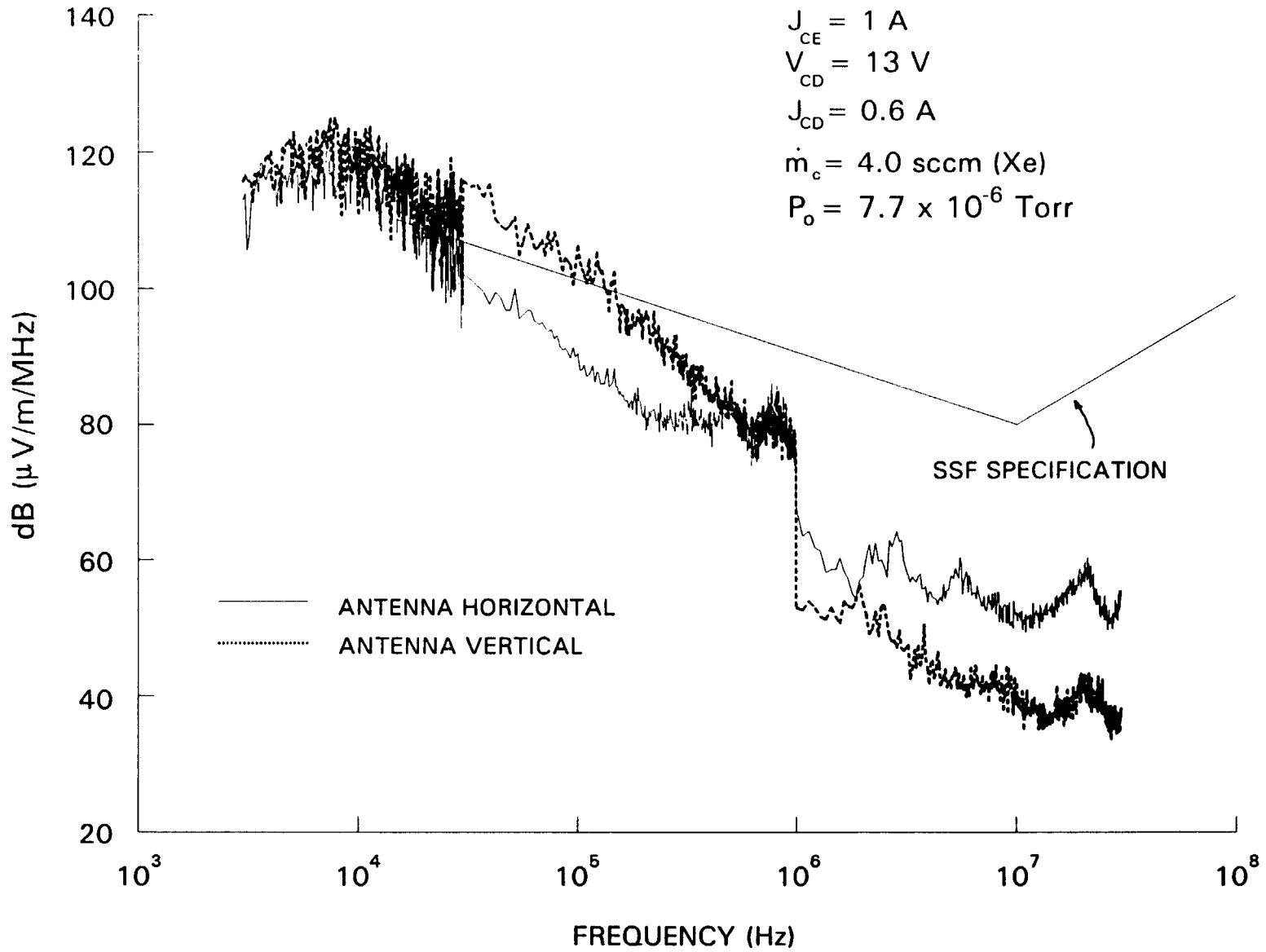

Fig. 28 The Effect of Antenna Orientation on the Radiated Emissions

An experiment was conducted to determine changes in the character of the fluctuations in the plasma as the emission current was varied. While the contactor was operated at standard conditions, plasma noise was first measured with a Langmuir probe (LP). The resulting power spectral density data (PSD) obtained when J_{CE} = 1, 5, and 10 A are plotted in Fig. 29 as the solid, dotted, and dashed lines, respectively. These results show the PSD levels increase with emission current. This effect can be expected because the electron density also increases with J_{CE} and this in turn causes the Langmuir probe to collect more current and thus amplifies the signal when it is biased at about the same potential.

This same procedure was repeated with the capacitive Langmuir probe (CLP) and typical results are graphed in Fig. 30. These noise data do not vary in direct proportion to emission current in the same manner as those obtained with the Langmuir probe (Fig. 29). The CLP system has lower inductance and is therefore, also able to detect higher frequency plasma noise than the LP. For these reasons, plasma noise data obtained with the CLP will be used when conducted and radiated emission data are compared in the following section.

Correlation between Conducted and Radiated Emissions

In order to gain insight into the correlation between conducted and radiated emissions, one can compare their spectra measured with the same resolution bandwidths (see Appendix A). Power-spectral-density results were computed from the measurements made with the current monitor, antenna, and CLP while the plasma contactor emitted 1 A (J_{CE} = 1 A). For comparison purposes, these are plotted in Fig. 31 where it appears all of the PSD data follow the same general trend (i.e. similar variations in power per unit frequency with frequency). A closer examination of these data reveals that similar signals are detected at certain frequencies by the different instruments. For example, the spectral data associated with the antenna and the current monitor both exhibit an increase in PSD at frequencies near 2 MHz. Likewise,

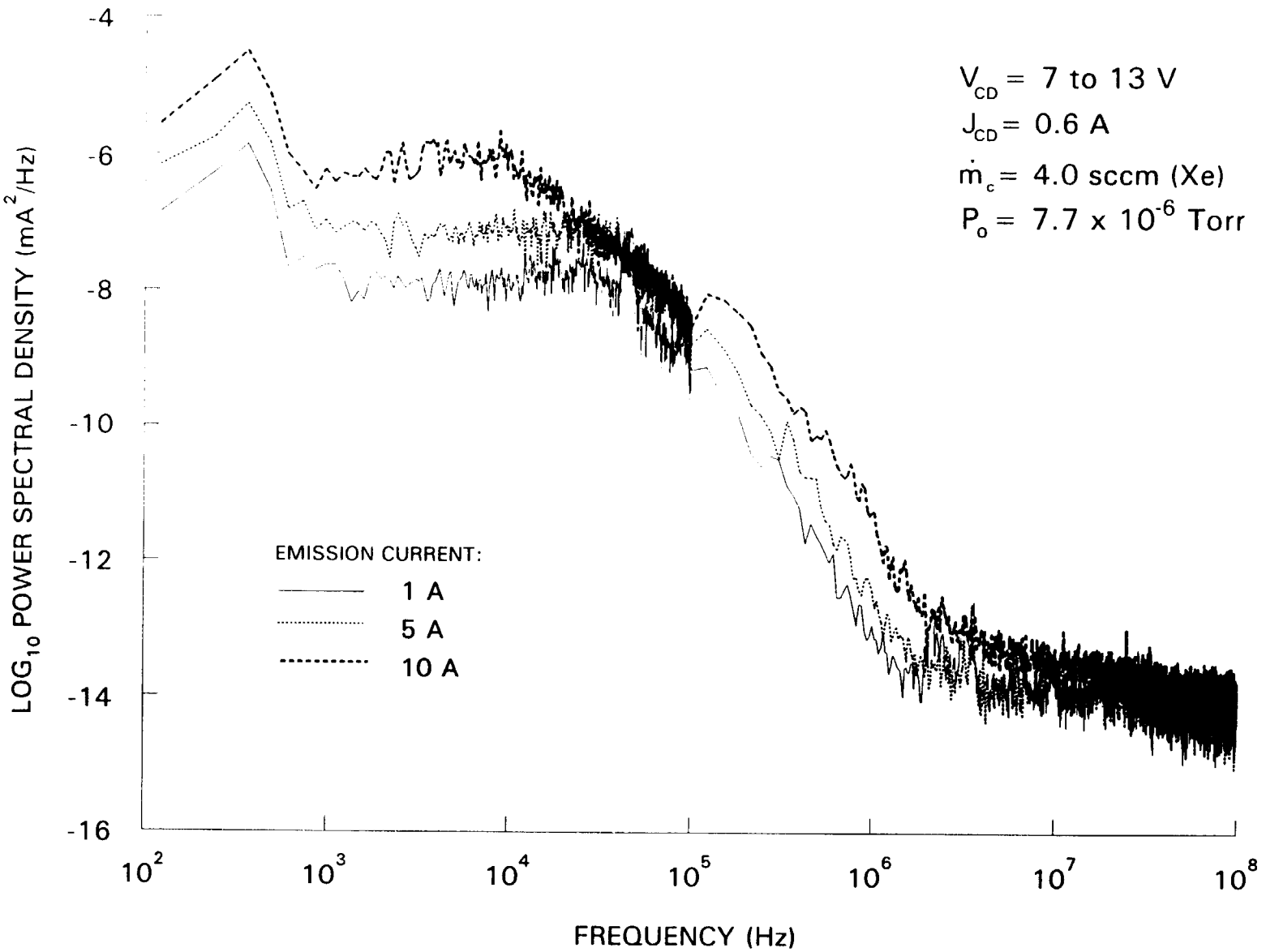

Fig. 29 The Effect of J_{CE} on Plasma Fluctuations (Langmuir Probe)

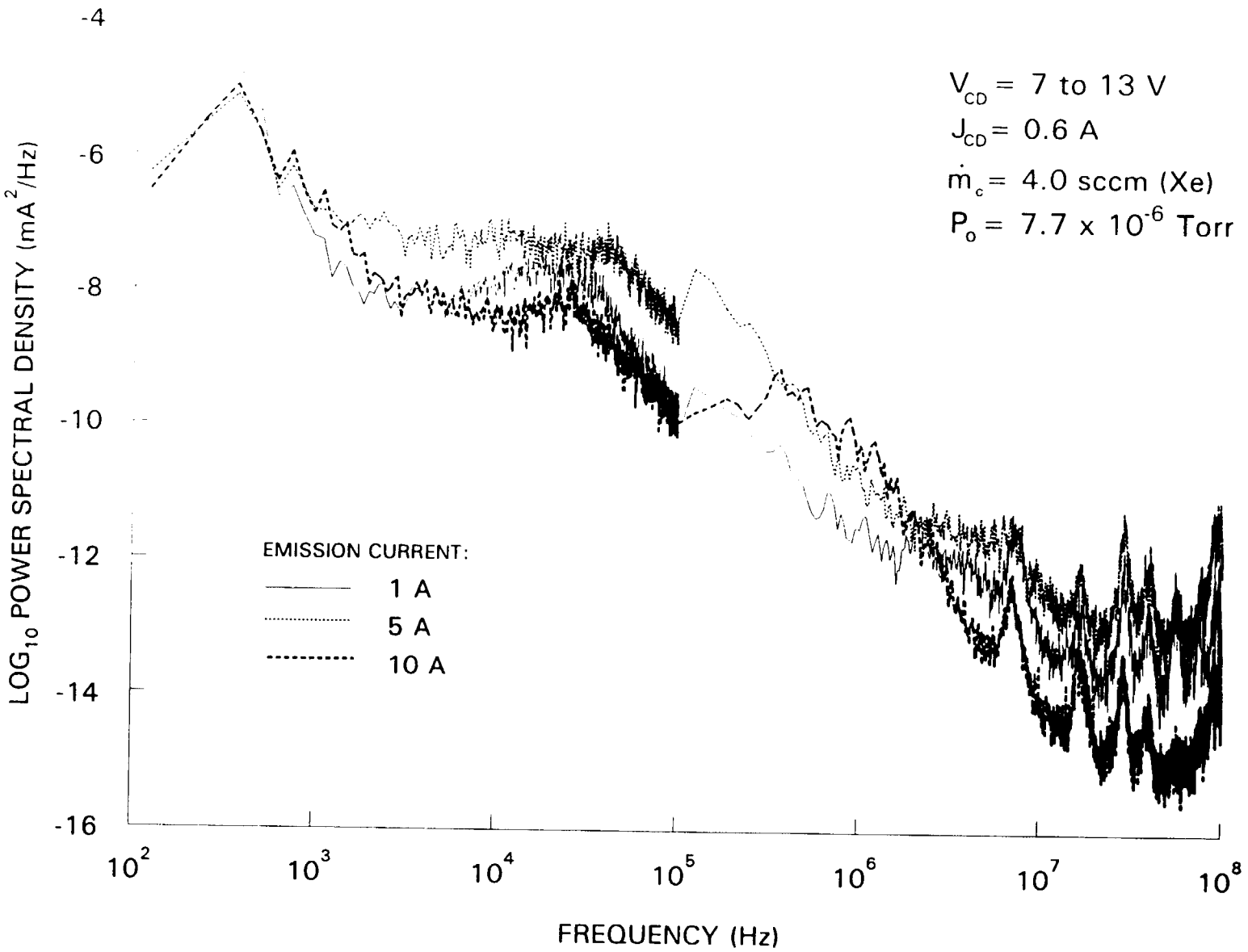

Fig. 30 The Effect of J_{CE} on Plasma Fluctuations (Capacitive Langmuir Probe)

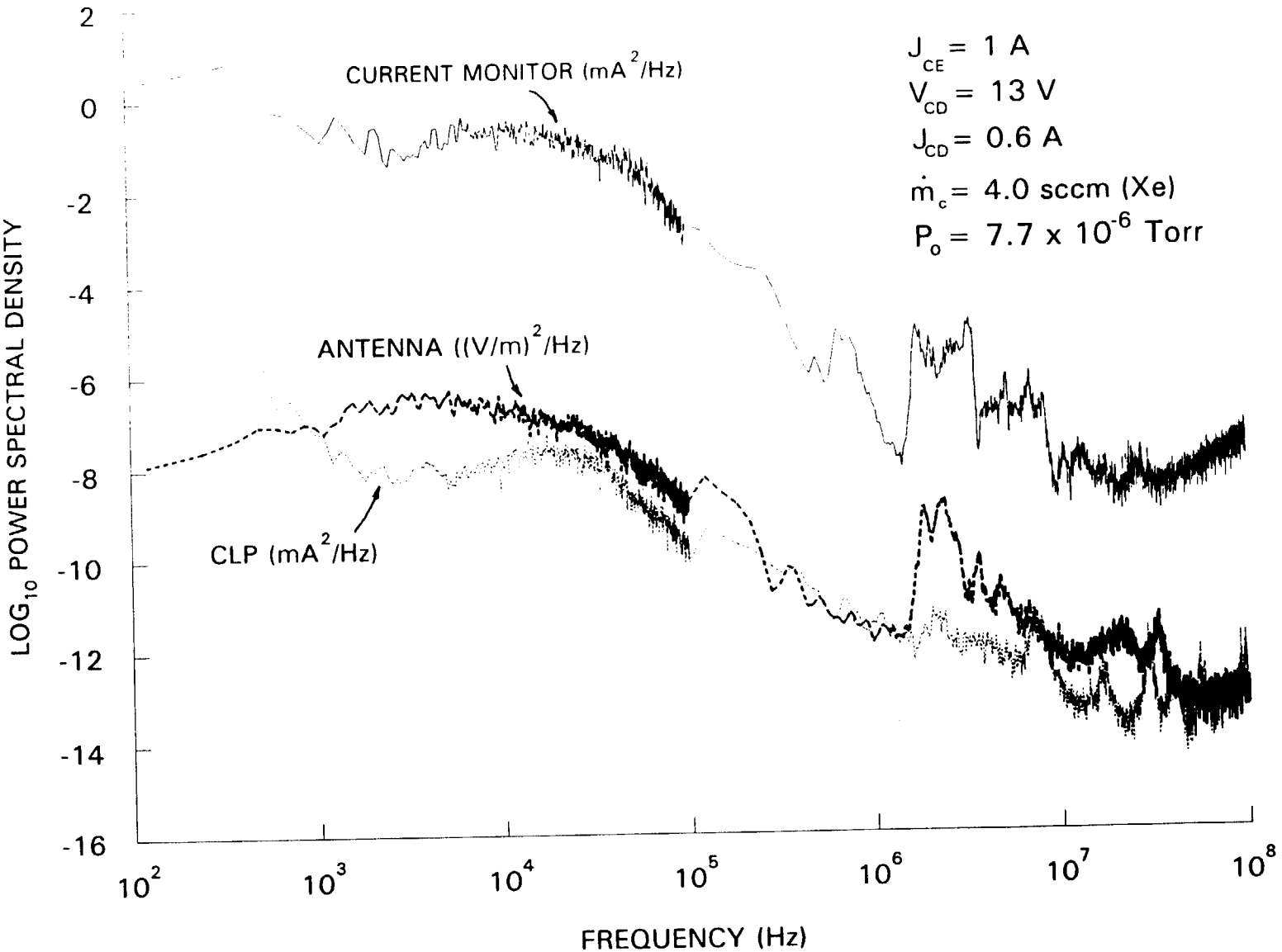

Fig. 31 A Spectral Comparison Between the Various Instruments

small signals around 20 MHz are sensed by the antenna and CLP whereas the current monitor and CLP detect a signal at ~360 Hz. These correlations are considered typical and it is anticipated that if the CLP were placed closer to the contactor, stronger correlations between its output and the other two might occur.

Stronger correlations between these instruments are expected because of how fluctuations in current and electric field affect the other. For example, current fluctuations in the return line (Figs. 4 and 5) can be expected to induce both electric field oscillations (electromagnetic radiation) and perturbations in plasma electron density and potential. The process whereby oscillating electric fields are driven by current fluctuations associated with the contactor has been modelled numerically by Katz *et al* [18]. Frequency-dependant current fluctuations from the contactor are used as input to a model and electric field amplitudes are determined as a function of frequency. Maxwell's equations coupled with Ohm's law are solved to describe electric field fluctuations in a plasma environment as a function of current fluctuations through the plasma so field intensities can be determined as a function of position and frequency [18]. This two-dimensional, preliminary model includes plasma properties measured in a ground-based facility and describes the vacuum tank walls as perfect conductors. The final result is the development of a transfer function that is used to compute radiated emissions from conducted emissions.

Using the model and experimentally measured conducted emissions (J_{CE} = 1 A), RE have been computed 1 m downstream of the contactor in the vacuum chamber with the geometry described in Fig. 2. These results are compared to the experimentally measured radiated emissions in Fig. 32 and they appear to be in good agreement with each other. This agreement leads to the conclusion that the model accurately describes the physical relationship between the current fluctuations from the contactor and the detected electric-field fluctuations in a plasma.

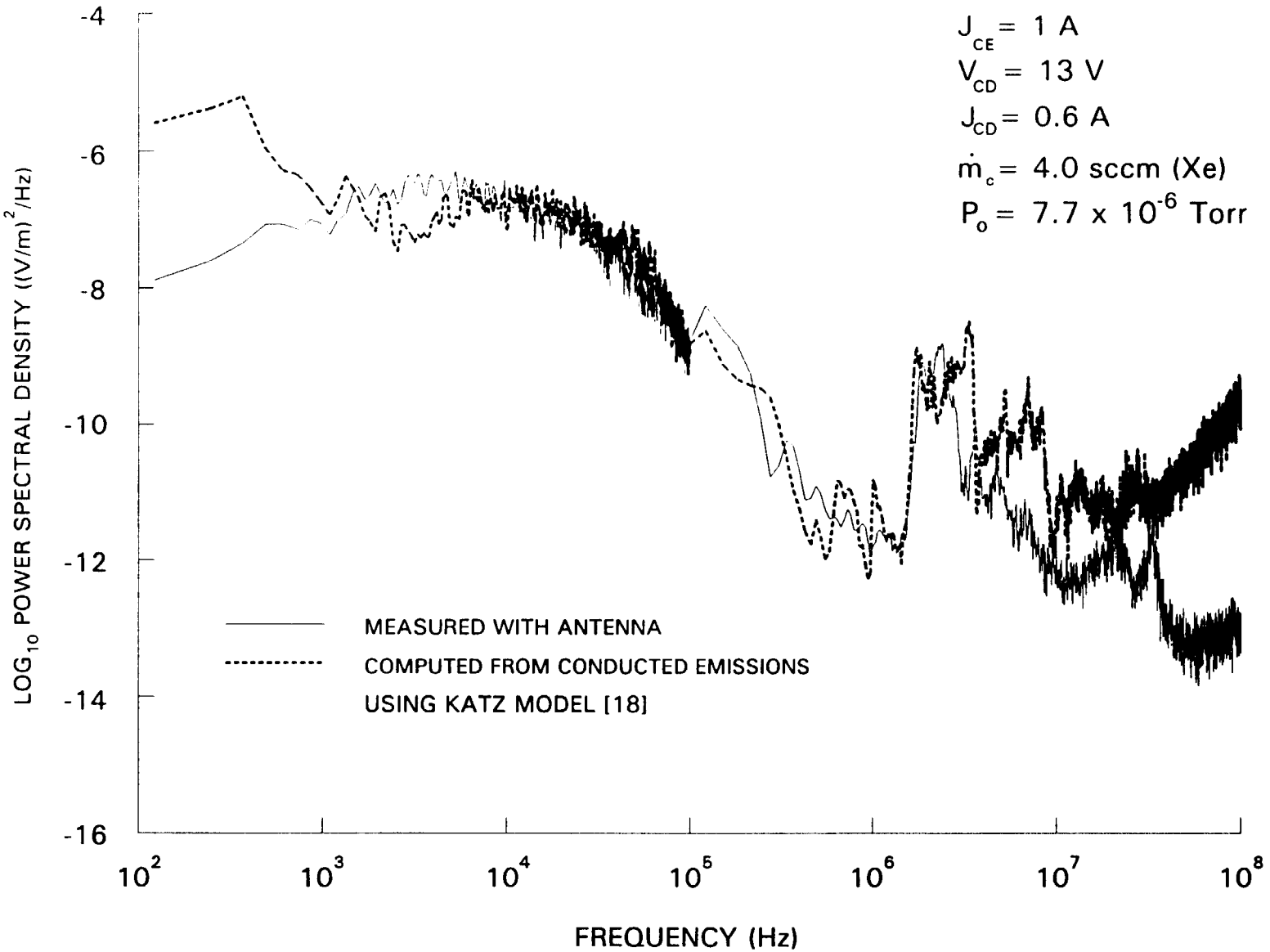

Fig. 32 Radiated Emissions, Measured and Calculated

V. CONCLUSION

For a plasma contactor to operate successfully on Space Station Freedom, it must emit electrons to space at the rate they are being collected thereby controlling the potential of the spacecraft relative to that of the space plasma. In addition, the contactor must neither emit conducted noise nor electromagnetic radiation at levels which could interfere with the operation of other equipment or instrumentation on the station. Ground-based experiments and tests provide a means to determine if the contactor might cause such electrical interference problems. It is therefore important that 1) the proper techniques for noise emission measurements be defined, 2) sufficient tests be conducted and 3) analysis be carried out to establish the mechanisms by which the noise is produced. Using this information, models can be developed that may make it possible to determine the noise levels that can be expected in space. This report has addressed the first two issues and has given a description of the steps and precautions which must be taken to make accurate noise-emission measurements. Brief, preliminary attention has been given to the third issue, however, it is clear that more work is required in this area.

From the experimental data presented in this report on conducted emissions, it is apparent that these emissions are mainly influenced by the contactor flow rate ($\dot{m}_c$), discharge current (J_{CD}), and the plasma environment. The CE spectral data do not follow any particular, predictable trend, however the spectral data presented do indicate that by operating the contactor at a selected flow rate ($\dot{m}_c$ = 4.0 sccm) and discharge current (J_{CD} = 0.6 A) the conducted emissions can be reduced. Also, as J_{CE}

is varied, the frequency-dependent magnitudes of the CE vary possibly because of transitional phenomena associated with plasma-wave production. In addition to these operating parameters, the ac ripple associated with the bias power supply appeared to be responsible for the low frequency CE. These low frequency signals will not be present with the contactor on the space station because a bias power supply is not required (i.e. the potential that forces electrons to be emitted will be induced by the solar cells). In addition, it is anticipated that properly designed (quiet) discharge power supplies may also facilitate decreased conducted emissions.

It is evident from the initial investigation into the radiated emissions produced by the contactor that the plasma interferes with antennae used to sense electric fields when the plasma is in contact with both the antenna and its ground plate (i.e. when the antenna is immersed in the plasma). This interference occurs because the plasma conducts current thereby reducing the voltage signal sensed between the antenna and ground plate as it attempts to sense electric fields. Consequently, it is believed more accurate measurements of RE are obtained when an insulating cover, such as a plexiglas tube, is placed over the antenna.

From the investigation of RE made with the covered antenna, it appears RE magnitudes are mainly influenced by contactor emission current and not other operating parameters such as flow rate and discharge current. Although this influence is slight and unpredictable, it is expected because fluctuations in emission current establish electric field fluctuations (i.e. plasma waves) in the plasma which in turn are sensed by the antenna. It is argued that as the emission current is varied, the transitions between mechanisms of plasma-wave production may occur and cause the radiated emissions to vary unpredictably. It is believed these transitional effects are a result of the coupling between the bias power supply and the plasma and consequently

will not be observed on the space station. The covered antenna was also able to detect spatial attenuation of the electric-field fluctuations. It is believed this attenuation is a consequence of a greater plasma-wave intensity close to the contactor which decreases as a function of downstream position.

A comparison of the conducted- and radiated-emission spectral data, obtained with the same resolution bandwidths, reveals that the variations in the amplitudes correlate reasonably well with each other. Additionally, a model developed by Katz, *et al.* [18] suggests CE and RE are directly related (i.e. RE can be predicted from CE) and this is consistent with the fact that CE and RE spectral data exhibit frequency correlation with each other. This model describes how current fluctuations from the contactor establish electric-field oscillations in a plasma. Experimental data from this investigation assisted in the verification of this model. These results suggest it may be possible to reduce the RE by decreasing the CE which, for example, might be achieved by operating the contactor at an appropriate flow rate and/or discharge current. The capacitive Langmuir probe serves as another method to measure the noise emitted from a contactor and provides a means gaining improved understanding of noise-generation mechanisms.

Finally, the conducted- and radiated-emission characteristics presented throughout this investigation describe the behavior of a hollow cathode contactor which has not been optimized to reduce these emissions. In fact, the contactor used for these tests is probably very different from the final flight unit. The purpose of this report was, therefore, not to determine if the plasma contactor which will be used on SSF satisfies the relevant specifications (although the contactor used in this study satisfied these requirements for the most part). It remains useful to present these specifications in order to examine the relative noise levels which were detected at a

ground facility. Several factors should be taken into consideration before judgement is passed on the acceptability of the contactor. For example, the background noise at the facility in which measurements were performed may contribute to the noise emissions detected. It was shown that power supplies influence the CE but other electrical equipment, such as lights and computer equipment, could contribute to the measured noise levels. Also, the vacuum tank is likely to have a significant influence on the detected noise emissions. Plasma wave reflections and/or propagation from sheaths in the vacuum tank could contribute to the measured noise levels. This "tank effect" might also explain the various transitions in noise levels which were observed for both conducted- and radiated-emission measurements. Therefore, more research is required to determine the significance these variables have on the observed noise levels.

VI. FUTURE WORK

The results presented in this report are considered preliminary because the majority of this work was conducted to demonstrate that these types of measurements could be performed at a ground based facility and to identify the equipment necessary to make them. Additional research into electromagnetic noise produced by a plasma contactor is required to determine the generation mechanisms. For example, a further investigation should be conducted on the plasma interaction with the antenna and its cover. It is suggested that antenna covers with different dimensions be examined to determine the influence they might have on the radiated emissions detected. Also, plasma fluctuations should be examined more carefully in order to understand the evolution of plasma waves [19]. For instance, if two capacitive Langmuir probes are positioned apart a known distance and then placed in the contactor plume, the propagation characteristics of plasma fluctuations can be studied. Other work could be done to determine a more precise description of the trends in the CE as contactor operating parameters, such as flow rate and discharge current, are varied. Finally, means by which conducted and radiated emissions could be reduced should be investigated. The CE and RE appear to be correlated at some frequencies but additional work is required to explain these emissions in terms of plasma stability phenomena.

VII. REFERENCES

1. Parks, D. E., Ira Katz, and V. A. Davis, "Spacecraft Environment Interactions Modeling III," Monthly Progress Report, Aug. 13, 1992, Maxwell Laboratories Inc., S-Cubed Division, La Jolla, California

2. Katz, I. et al, "Preliminary Plasma Contactor Requirements," Progress Report, Dec. 17, 1992, Maxwell Laboratories Inc., S-Cubed Division, La Jolla, California

3. "Space Station Electromagnetic Techniques - SSP 30238," NASA Space Station Freedom Program Office, Reston, Virginia, March 15,1991

4. "Space Station Electromagnetic Emission and Susceptibility Requirements for Electromagnetic Compatibility - SSP 30237 Revision A," NASA Space Station Freedom Program Office, Reston, Virginia, Sept. 1991

5. Williams, J. D., and P. J. Wilbur, "Experimental Study of Plasma Contactor Phenomena," Journal of Spacecraft and Rockets, V. 27, N. 6, Nov. 1990, pp. 634-641

6. Williams, John D., "An Experimental Investigation of Hollow Cathode-Based Plasma Contactors," NASA CR-187120, May 1991

7. Williams, John D., "Plasma Contactor Research - 1990," P. J. Wilbur, ed., NASA CR-187097, Jan. 1991

8. Buchholtz, Brett "Plasma Contactor Research - 1991," P. J. Wilbur, ed., NASA CR-189140, April 1992

9. Horowitz, Paul and Winfield Hill, The Art of Electronics, Cambridge University Press, New York, 1965, Chap. 7

10. Stix, Thomas Howard, The Theory of Plasma Waves, McGraw-Hill, New York, 1962, Chaps. 1, 6 , & 7

11. Chen, Francis F., Introduction to Plasma Physics and Controlled Fusion, 2nd Ed., Vol. 1, Plenum Press, New York, 1984, Chap. 4

12. Book, D. L., "Naval Research Laboratory Plasma Formulary," Office of Naval Research, Washington D.C., 1978, pp. 40

13. Roadstrum, William H. and Dan H. Wolaver, Electrical Engineering for All Engineers, John Wiley & Sons, 1987, pp. 269-270

14. Roth, J. Reece, and Walter M. Krawczonek, "Paired Comparison Tests of the Relative Signal Detected by Capacitive and Floating Langmuir Probes in a Turbulent Plasma from 0.2 to 10 MHz," The Review of Scientific Instruments, V. 42, N. 5, May 1971, pp. 589-594

15. Wang, En Yao, et al, "Direct Indication Plasma Potential Diagnostic Based on Secondary Electron Emission," The Review of Scientific Instruments, V. 56, N. 6, June 1986, pp 1085-1089

16. Wang, En Yao, et al, "Secondary Electron Emission-Capacitive Probes for Plasma Potential Measurements in Plasmas with Hot Electrons," Journal of Applied Physics, V. 61, N. 10, May 1987, pp. 4786-4790

17. Ramo, Simon, et al, Fields and Waves in Communication Electronics, John Wiley and Sons, New York, 1965, Chaps. 1, 6, 9, & 12

18. Katz, I., Myron Mandell, and Gary Jongeward, *Private Communications*, Feb. - March 1993, Maxwell Laboratories Inc., S-Cubed Division, La Jolla, California

19. Hollenstein, Ch. and M. Guyot, "Experiments on Potential Gradients in a Current-Carrying Plasma. I and II," Physics of Fluids, V. 26, N 6, June 1983, pp. 1596-1615

20. Chapra, Steven C. and Raymond P. Canale, Numerical Methods for Engineers, 2nd Ed., McGraw-Hill, New York, 1985, Chaps. 13 & 14

21. Bendat, Julius S. and Allen G. Piersol, Random Data: Analysis and Measurement Procedures, 2nd Ed., John Wiley and Sons, New York, 1986, Chaps. 1, 8, 10, & 11

22. Press, William H., et al Numerical Recipes: The Art of Scientific Computing, Fortran Version, Cambridge University Press, New York, 1989, Chap. 12

23. Ramirez, Robert W., "The Fast Fourier Transform's Errors Are Predictable, Therefore Manageable," Electronics, June 13, 1974

APPENDIX A

Acquiring and Interpreting Conducted and Radiated Emissions Data

Emitted noise, whether it is conducted or radiated, can be described as the fluctuations-in-time of a particular variable of interest. For example, the time varying electric field fluctuations generated by a plasma contactor (i.e. radiated emissions). It is useful to examine the spectral composition (amplitudes of the signal v. frequency) of these fluctuations in order to determine the source(s) and/or production mechanism(s) of the noise. Such spectra can be obtained from experimental data by employing Fourier transforms which take a continuous function, or signal, in the time domain and convert it into a function in the frequency domain. This article describes how noise spectra can be obtained when experimental data are recorded (digitized) with an oscilloscope and then analyzed using a computer algorithm.

Figure A1a illustrates a fluctuating signal, in this case a sine wave in the time domain, which has amplitude A_1, frequency f_n, and period τ, where $\tau = 1/f_n$. The sine wave also has a phase shift ϕ, but this parameter will generally be unimportant for the applications being considered in this report. The sine wave of Fig. A1a can also be represented in the frequency domain which is illustrated in Fig. A1b as a function of amplitude verses frequency. The integral Fourier transform provides a method to convert a function in time (e.g. x[t]) into a function in frequency (e.g. X[f]) and an expression for this is given by Eq. A1. In order to use Eq. A1, x(t) must be defined as a piece-wise continuous function over an infinite time interval. In this report,

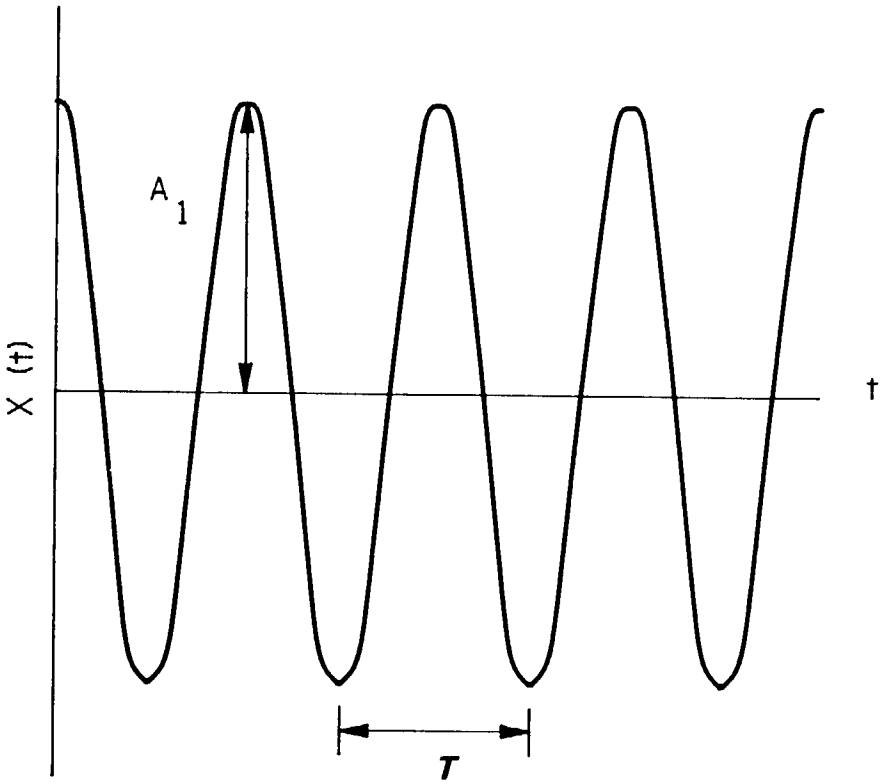

a) Time Domain: $X(t) = A_1 \sin(\omega_n t + \phi)$

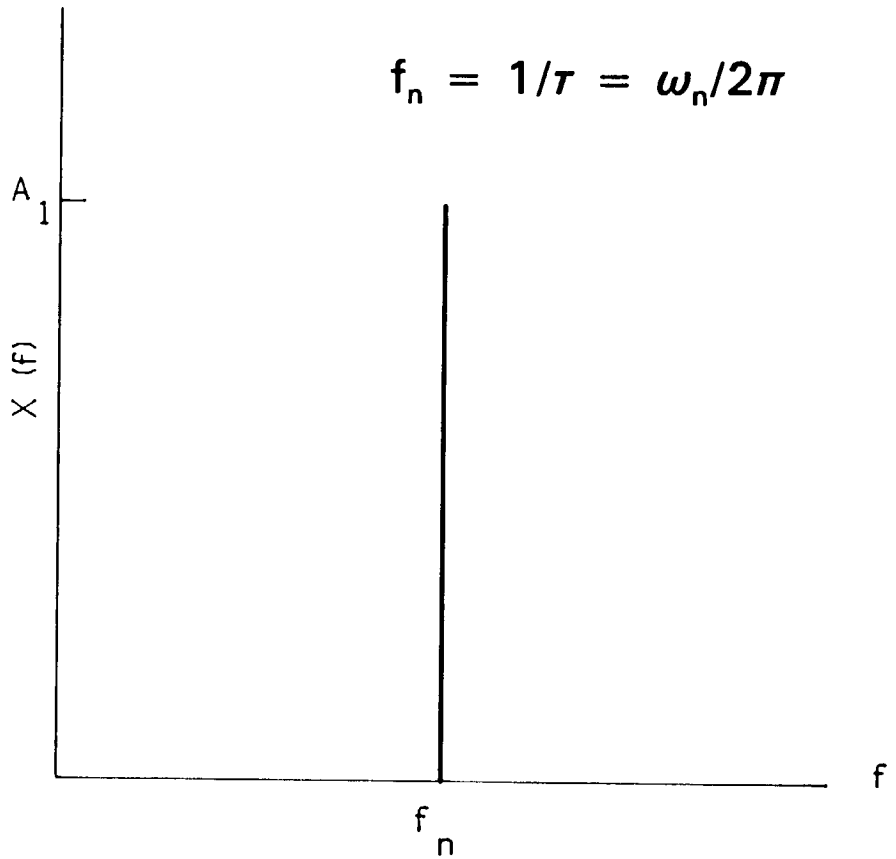

b) Frequency Domain Characteristics (Spectrum)

Fig. A1 Sinusoidal Function Example

$$X(f) = \int_{-\infty}^{\infty} x(t)\, e^{2\pi i f t} dt \qquad (A1)$$

experimental data are only collected over a finite time period using a digital oscilloscope. A discrete Fourier transform, which is given by,

$$X(f_n) = \sum_{k=0}^{N-1} x_k e^{2\pi i k n/N} \Delta t \qquad (A2)$$

facilitates the conversion of a signal in a finite-time domain (x_k), represented by a discrete number of data points (N), into the frequency domain. There have been computer algorithms developed to estimate the discrete Fourier transform, however, depending upon the number of data points involved, they can require excessive amounts of computational time [20]. The fast Fourier transform (FFT) is an algorithm designed to compute the discrete Fourier transform more efficiently (i.e. in less time) [20,21]. Therefore, the FFT can be used to convert noise data, represented by discrete data points, collected over a finite-time interval into its frequency components (amplitudes) rapidly. A FFT computer code similar to that used for data analysis in this report can be found in Ref. [22].

The FFT requires an integer-power-of-2 data points (N) which were evenly sampled over a certain time interval which is referred to as the window time (T) [20,22]. Equation A3 is the relationship between this window time and the smallest frequency (Δf) that can be detected by the FFT; it is also known as the resolution bandwidth. An expression for the sampling rate is given by Eq. A4 and is defined as the number of data points acquired divided by the window time. There are two features of the FFT, namely windowing and aliasing, which can introduce errors into the results and should, therefore, be understood before one attempts to use the FFT.

$$\Delta f = \frac{1}{T} \qquad (A3)$$

$$f_s = \frac{N}{T} \qquad (A4)$$

Windowing

The concept of windowing is illustrated by the various plots shown in Fig. A2. First, consider the continuous signal shown in Fig. A2a and the window (a unit step function of duration T), shown in Fig. A2c, through which the data are to be collected. The result of multiplying the continuous signal and the window is pictured in Fig. A2e. The window passes the full amplitude of the original signal for a finite duration and it is this portion of the signal which the FFT algorithm uses. Fast-Fourier-transform analysis assumes the input signal being used is continuous in the time domain so for the present case, the windowed signal is assumed to repeat. The ideal Fourier transform of the sine wave (Fig. A2a) is represented by the spike shown in Fig. A2b. The Fourier transform of the unit step function, on the other hand, exhibits a peak at zero frequency coupled with some roll off into higher frequencies (Fig A2d). When the two transforms (Fig. A2b and A2d) are convoluted in the frequency domain, the fast Fourier transform of the non-continuous signal is obtained (Fig. A2f). This transform contains extraneous noise, known as side-lobe leakage, which occurs as a consequence of the abrupt boundaries imposed on the windowed signal. Side-lobe leakage is not present in the ideal transform, hence, it is erroneous and should be removed.

In order to reduce side-lobe leakage, other types of windows can be used. For example, Fig. A3a shows the same continuous signal (i.e. the one of Fig. A2a) which will be convoluted with another window known as the Hanning, or cosine-squared

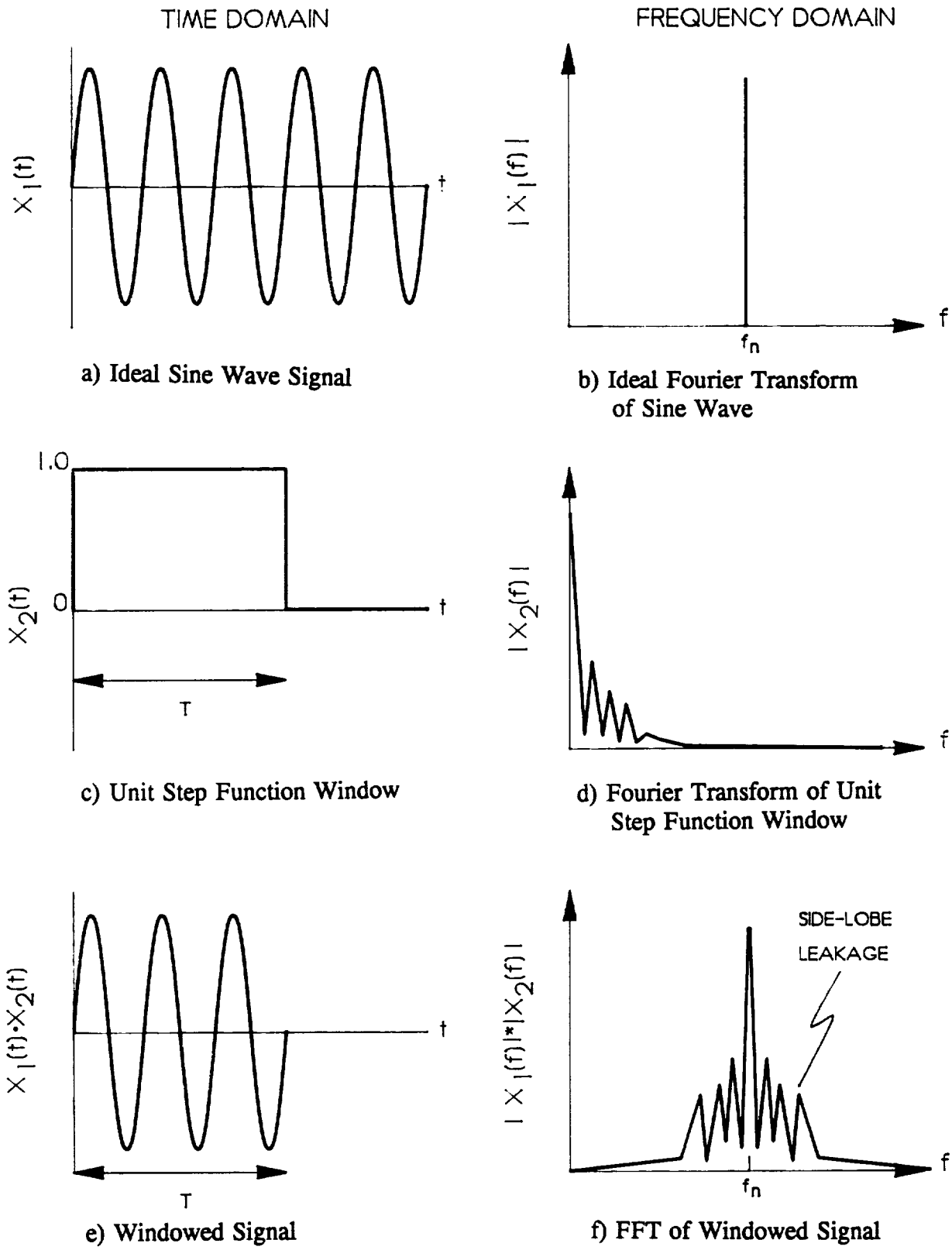

Fig. A2 The Effect of a Unit Step Function Window on the FFT

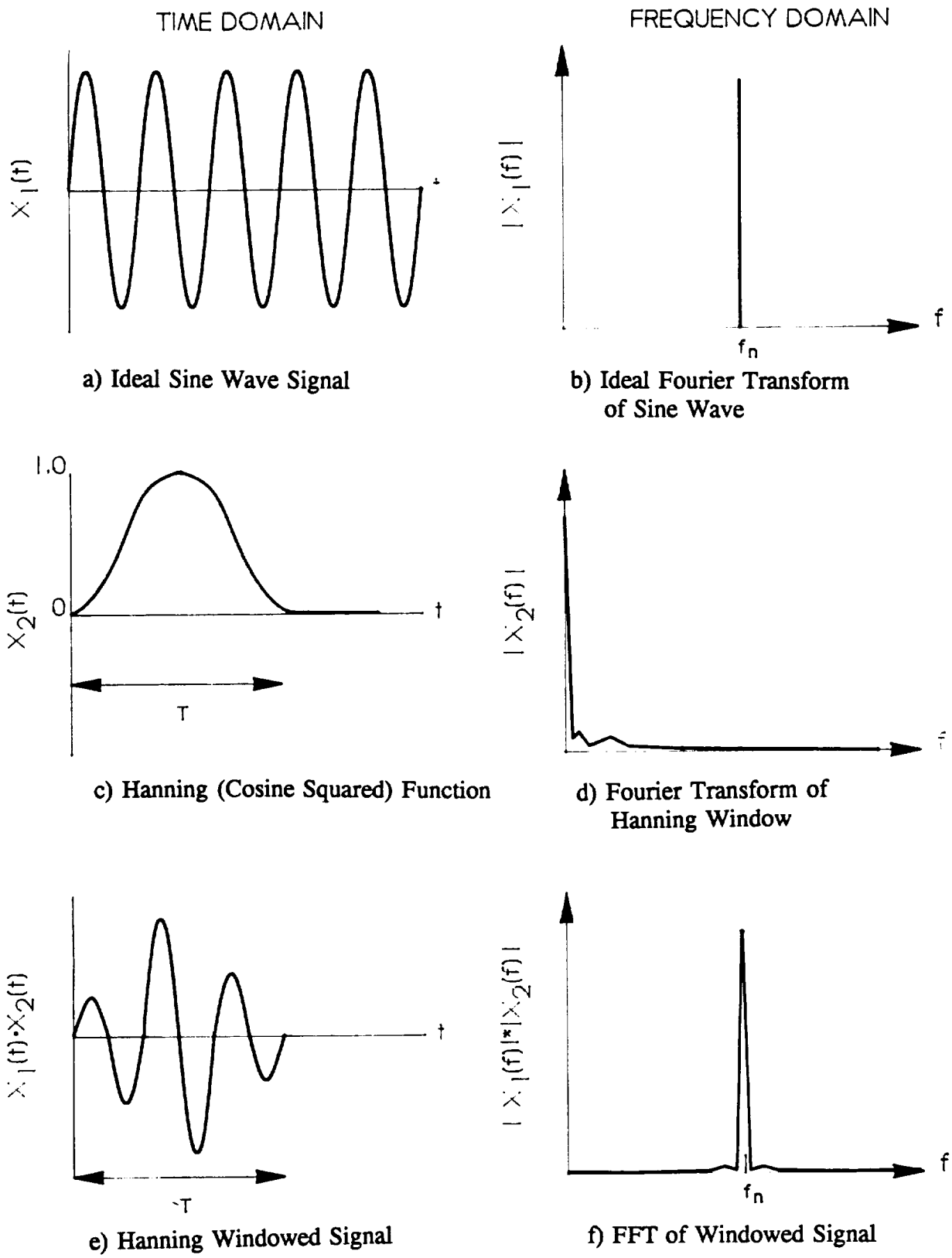

Fig. A3 The Effect of a Hanning Window on the FFT

window (Fig. A3c). This type of window does not have the abrupt changes at the window edges like the unit-step-function window (Fig. A2c) and, as a consequence, the product of these two signals (Fig. A3e) is tapered. In the frequency domain, the Fourier transform of the continuous (ideal) signal is again represented by a spike (Fig. A3b) and the transform of the Hanning window (Fig. A3d) has less roll off than the unit step function transform (Fig. A2d). Most importantly, the fast Fourier transform of the non-continuous, windowed signal, depicted in Fig. A3f, exhibits reduced side-lobe leakage. The Hanning window does produce overall amplitude attenuation in the FFT results but this loss is predictable and, therefore, correctable [21].

Proper windowing reduces side-lobe leakage into other frequencies thereby yielding a high-resolution spectral plot (i.e. one in which amplitudes associated with two similar frequency components close together, can be resolved). Larger amplitudes near the window edges induce greater side-lobe leakage. There are many different windows [23] and the preferred one depends on the resolution required. The Hanning window is commonly used for the FFT because it yields adequate resolution and, therefore, is used in the analyses presented in this report.

Aliasing

Aliasing, like windowing, yields false amplitudes in a spectrum but, unlike windowing, these false amplitudes tend to appear at frequencies far from the true frequency rather than as adjacent, roll-off signals. Hence, these false amplitudes are more difficult to identify and eliminate. Errors due to aliasing are generally prevented by using both mathematical (transform-related) and physical (raw data collection-related) procedures. The mathematical procedures exploit the fact that the FFT uses discrete data points which are sampled from the input signal. Aliasing can occur when

an insufficient number of data points are collected (sampled). For example, Fig. A4a depicts a sine wave, with frequency, f_n, being sampled at a rate which yields the five solid points indicated. When these are the only data analyzed, a false frequency is detected in the frequency domain (Fig. A4b). This error can be prevented by sampling at a higher rate. In fact, the minimum sampling rate required to prevent aliasing is determined by the Nyquist criterion and is equal to $2f_n$ where f_n is the maximum frequency to be sensed [21,22]. When this condition is invoked, the data points in Fig. A4c are obtained and the proper spectral plot (Fig. A4d) is realized.

If a signal contains more than one frequency component, aliasing is prevented by sampling the data at a rate greater than or equal to twice the cutoff frequency ($2f_c$), where f_c is the highest frequency component in the signal (the cutoff frequency for the FFT is 1/2 of Eq. A4). For example, Fig. A5a shows the spectrum of a signal which contains two frequency components, f_a and f_b. If this signal is sampled at a rate $2f_c$, where $f_a < f_c < f_b$, the frequency, f_b, will be improperly detected or aliased because the sampling rate is too low (Fig. A5b).

In many cases the highest frequency of the signal is unknown so physical means must also be used to minimize errors due to aliasing. Physical prevention of aliasing makes use of signal filters which attenuate the high frequency components of the signal and thereby establish a physical cutoff frequency (the cutoff frequency of the filter). Figure A6a illustrates a fictitious Fourier transform of a signal containing two groups of frequency components which lie reasonably close together. If this signal is sampled at a rate $2f_c$ and a filter is not installed to eliminate high frequencies, aliasing will occur when the Fourier transform has been applied (Fig. A6b). The extent to which this problem can be corrected depends upon the attenuation characteristics of the physical filter through which the data are collected. Attenuation characteristics for

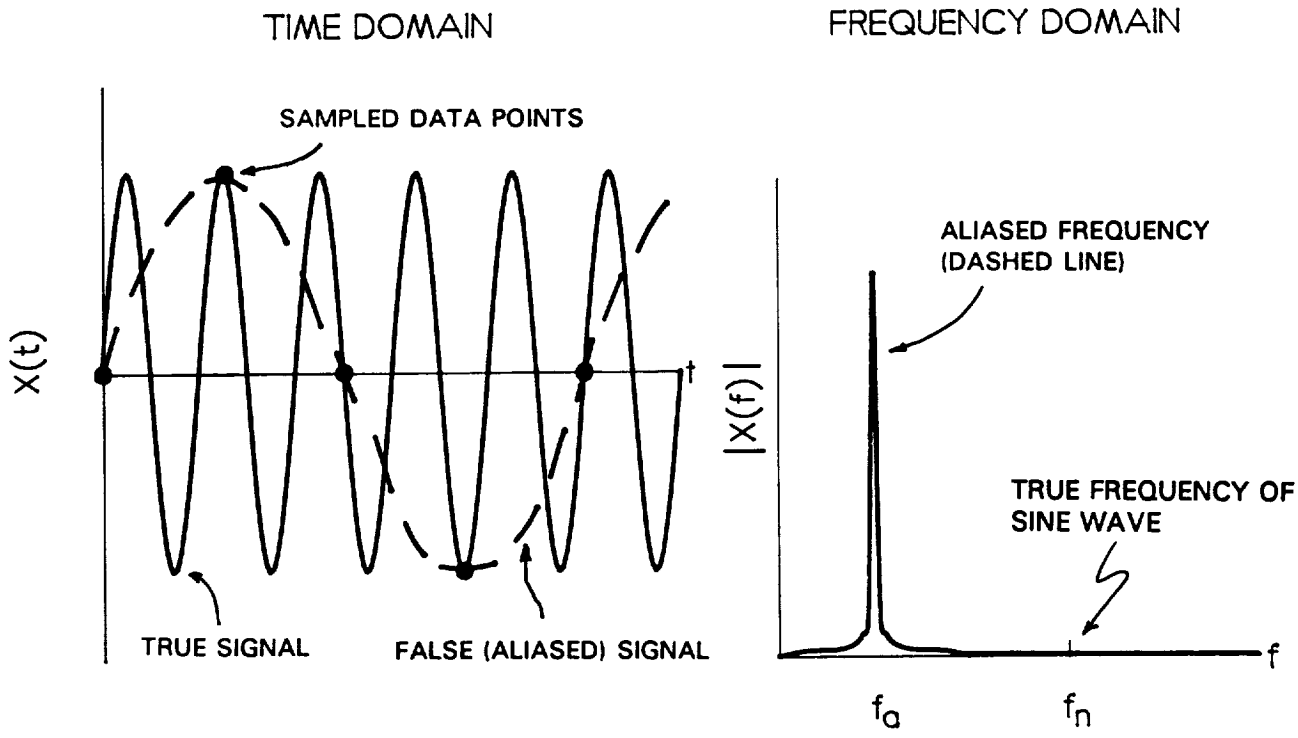

a) Ideal Sine Wave Sampled at a Low Rate

b) FFT at a Low Sampling Rate

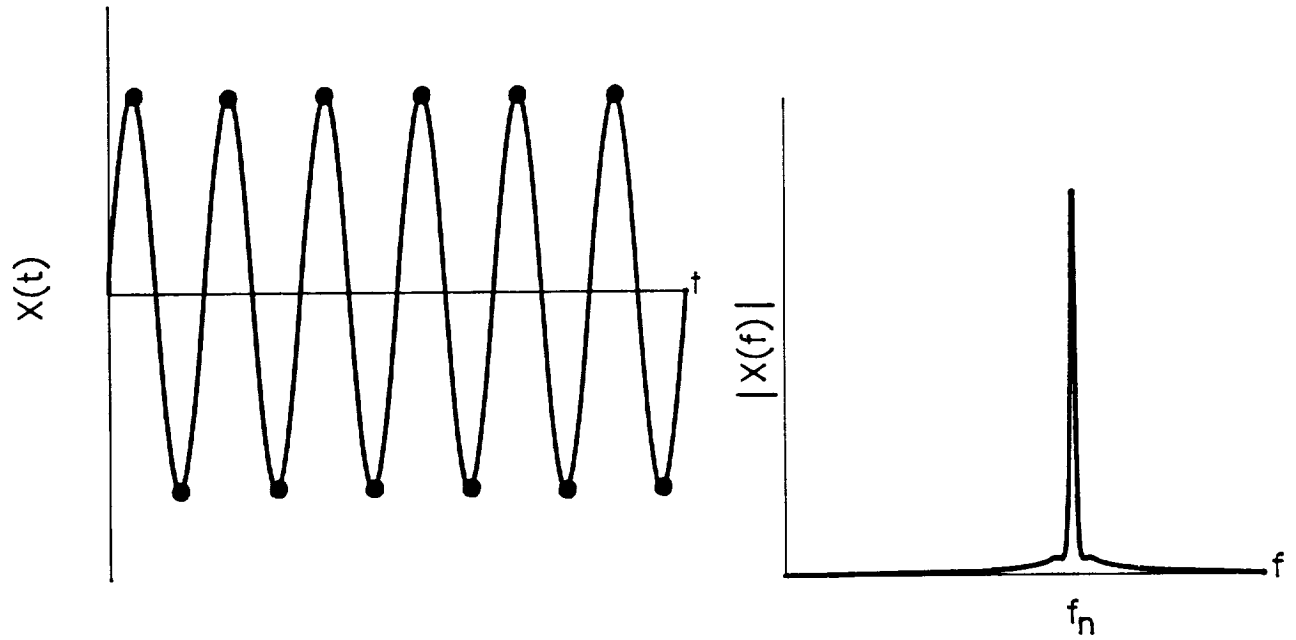

c) Ideal Sine Wave Sampled at a Sufficient Sampling Rate

d) FFT at a Sufficient Sampling Rate

Fig. A4 Aliasing of an Ideal Sine Wave

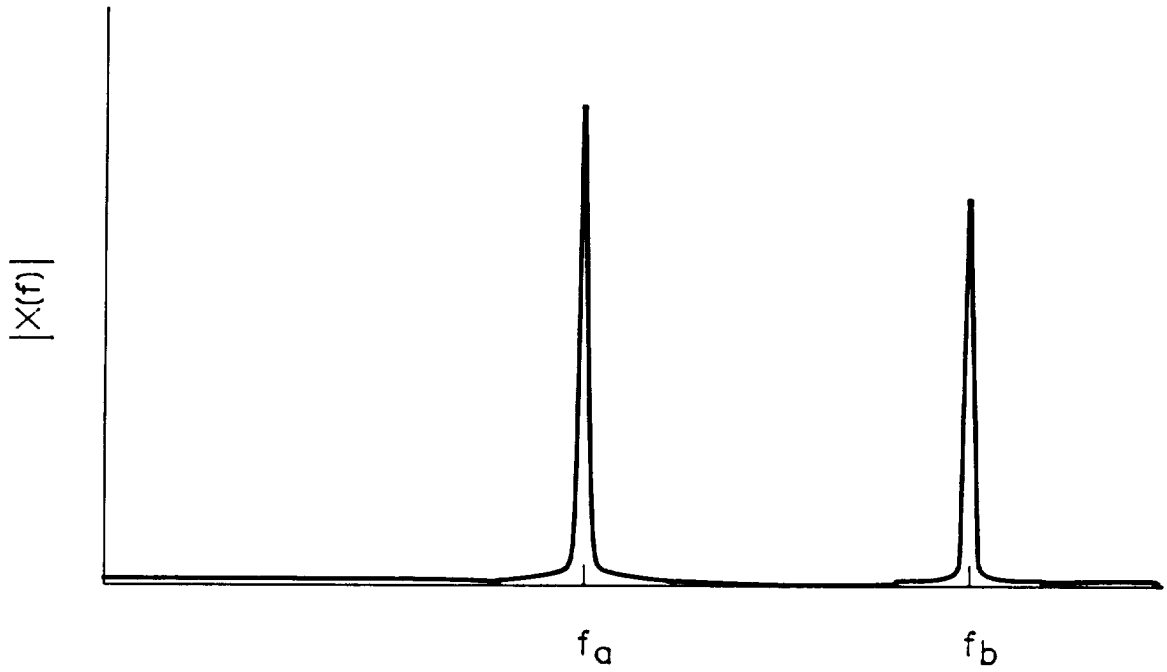

a) True Spectrum With a Signal Containing Two Frequency Components (f_a, f_b)

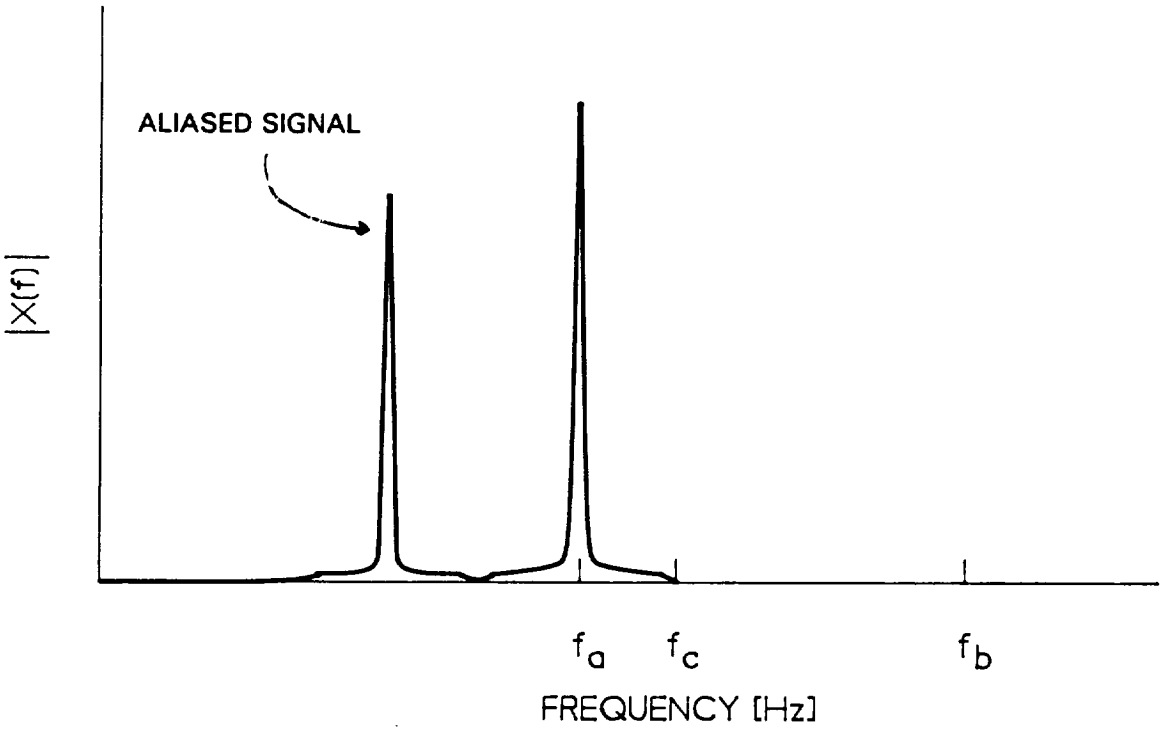

b) Observed Spectrum When Cutoff Frequency is Below f_b

Fig. A5 Aliasing when Multiple Frequencies are Involved

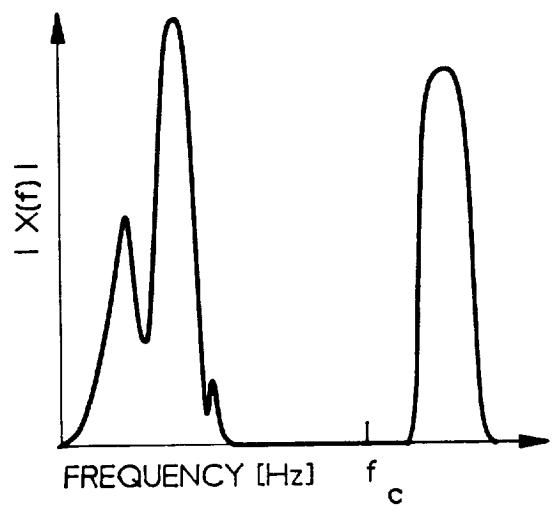

a) True Spectrum

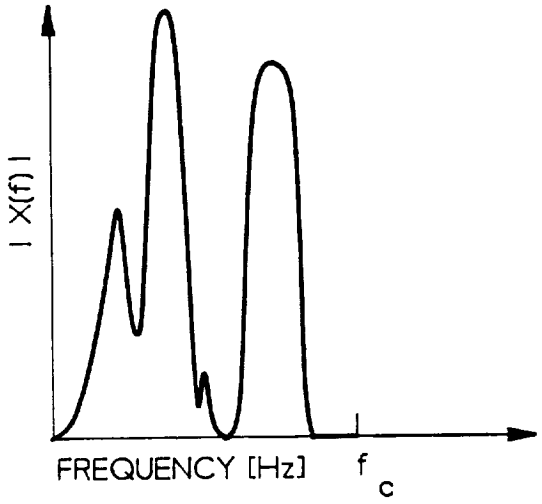

b) Aliased Spectrum

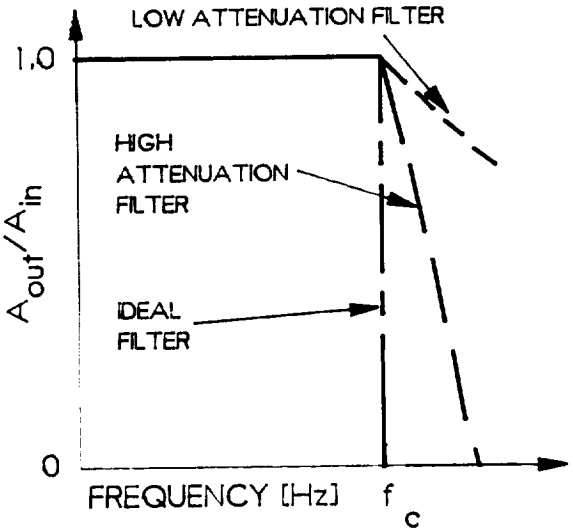

c) Filter Characteristics

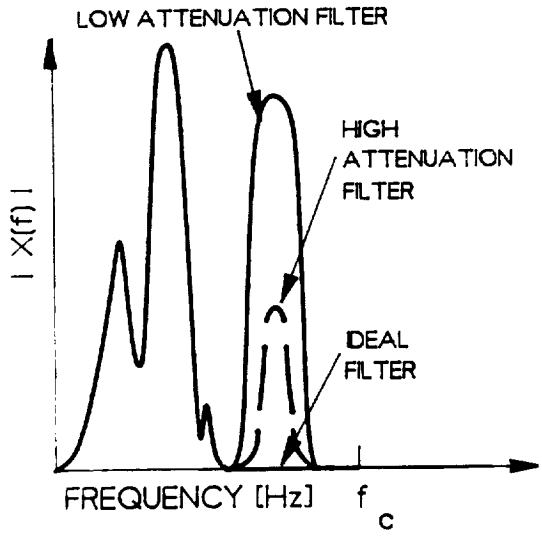

d) Filtered Spectrum

Fig. A6 Filter Effects on Aliasing

various filters are illustrated qualitatively in Fig. A6c. When an ideal filter with a cutoff frequency, f_c, is used to filter the signal (Fig. A6a) and the sampling rate is adequate ($>2f_c$), only frequencies below f_c are passed and the aliased portion is completely removed (Fig. A6d). With real filters, aliased signals are present to a lesser extent as the low and high attenuation filtered curves in Fig. A6d suggest. Therefore, if a filter is used to eliminate frequency components above the frequency determined by the sampling rate, the effects of aliasing can be reduced to acceptable levels in the Fourier transform.

A summary of the appropriate steps necessary to ensure accurate FFT results is illustrated in Fig. A7 along with a schematic of the data acquisition system. First, a noise signal is passed through a low-pass (or bandpass), high-attenuation filter providing a physical cut-off frequency. Second, the data are sampled, or digitized on the oscilloscope at a sample rate greater than or equal to twice the cut-off frequency to prevent aliasing. Next, using a computer with the appropriate software, the digitized signal is windowed (a Hanning window is used for the analyses in this report) and the fast Fourier transform is computed. In order to acquire a representative portion of the emission signal, it was decided that this process should be repeated 8 times for a given frequency range.

The oscilloscope used in this investigation would typically record 8000 points. Before these digitized data were analyzed, 192 zeros were amended to each data set so that the FFT could analyze 8192 points (i.e. an integer power of 2). This inclusion of zeros is known as zero padding and, for this analysis, it introduces ~2% error in the resulting spectrum. In addition, the data were typically collected in 2 or 3 frequency bands to cover the full frequency range. The data corresponding to high frequencies were not filtered because, typically the power level of the signal for these frequency

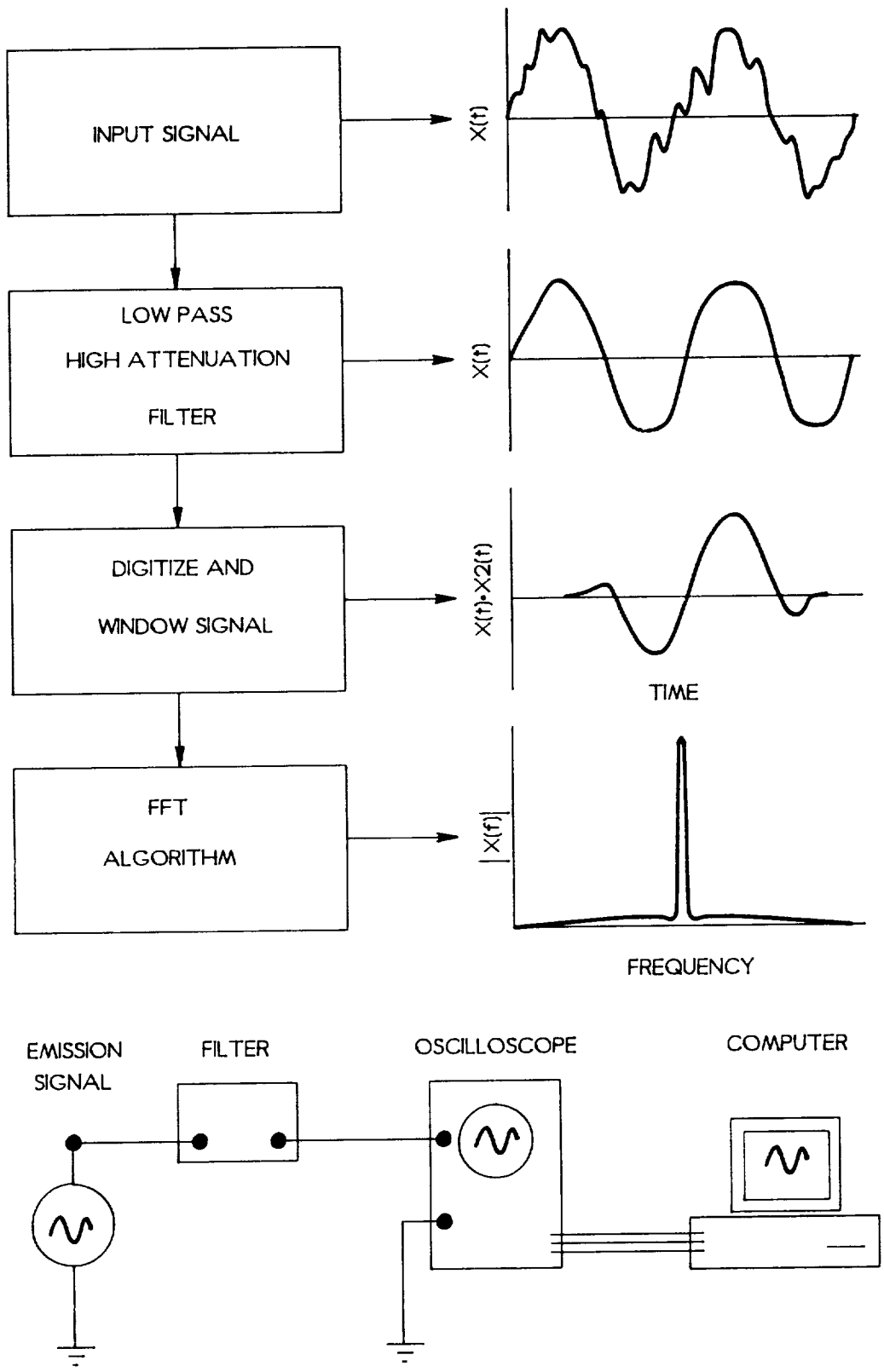

Fig. A7 The Steps and Instrumentation Required for Signal Analysis

ranges was low so that aliasing was not considered to give substantial error. The standard oscilloscope and filter settings are tabulated below in Table A1.

Frequency Range	Sample Rate of Oscilloscope (samples/sec.)	Filter Cutoff Frequency	Resolution Bandwidth (Δf)
Typical Broadband Settings:			
300 Hz - 30 kHz	2.5 MSa/s	100 kHz	313 Hz
30 kHz - 1 MHz	25 MSa/s	not used	3.13 kHz
1 MHz - 30 MHz	1 GSa/s	not used	125 kHz
Typical Narrowband Settings:			
300 Hz - 30 kHz	250 kSa/s	100 kHz	31.3 Hz
30 kHz - 1 MHz	2.5 MSa/s	not used	313 Hz
1 MHz - 30 MHz	100 MSa/s	not used	12.5 kHz

Table A1. Data Acquisition Settings

Interpreting Power Spectral Density Plots

Once the FFT has been computed with acceptably small errors using the steps mentioned above, results are often presented as autospectral, or power spectral, density plots (PSD). These plots are useful tools for studying noise because 1) dominant frequencies can be determined and 2) the rms value of a noise-related amplitude (e.g. electric field) over certain frequency ranges can be estimated. The PSD is defined as the mean-squared amplitude of a signal at a given frequency divided by the resolution bandwidth associated with the measurement [21]. The PSD is estimated by squaring the amplitude corresponding to a particular frequency (computed from the FFT) and then dividing by this resolution bandwidth. By acquiring 8 signals of 8000 points each, as mentioned previously, a normalized rms

error of ~35% was achieved for the power spectral data presented in this report [21]. A fictitious PSD is plotted as a function of frequency in Fig. A8 where a Log-Log scale is used and the units (for this case) are mean-squared current per unit bandwidth (mA^2/Hz). Power-spectral-density plots are frequently integrated over a prescribed frequency range to obtain a mean-squared value of the amplitude for that frequency range. For example, in Fig. A8, the area between frequencies f_a and f_b is 900 mA^2. Therefore, the root-mean-square (rms) current for Fig. A8 in the frequency range 100 to 1000 Hz is 30 mA. The rms current for an entire PSD plot (Fig. A8, for example) is determined by integrating over the full frequency range (0 to ∞).

Output Comparison

Another, more straight forward means by which spectral data can be obtained with less concern about the problems of windowing and aliasing, is to use a spectrum analyzer. Tests were conducted to insure that spectral data obtained with either instrument were similar. One test consisted of applying a known signal of ~50 kHz into both instruments. The signal acquired on the oscilloscope and then analyzed using the FFT algorithm is plotted in Fig. A9 (dB [μV] v. frequency) as the solid line. The resolution bandwidth of the spectrum analyzer was set to match that of the oscilloscope and the signal it detected is plotted in Fig. A9 as the dashed line. The difference in the data plotted Fig. A9 indicate the spectrum analyzer has a larger dynamic range than the oscilloscope. However, the data suggest that amplitudes of a known signal are accurately detected using either instrument.

Another test was to collect and compare radiated emission data from an operating plasma contactor sensed by an antenna. Using the broadband settings in Table A1, the resulting radiated emissions spectra obtained are plotted in Fig. A10. The spectral data are slightly different for frequencies greater than 30 kHz possibly because of aliasing errors in the data recorded using the oscilloscope (i.e. a filter was not used for this frequency range). Regardless, it is believed there is fairly good

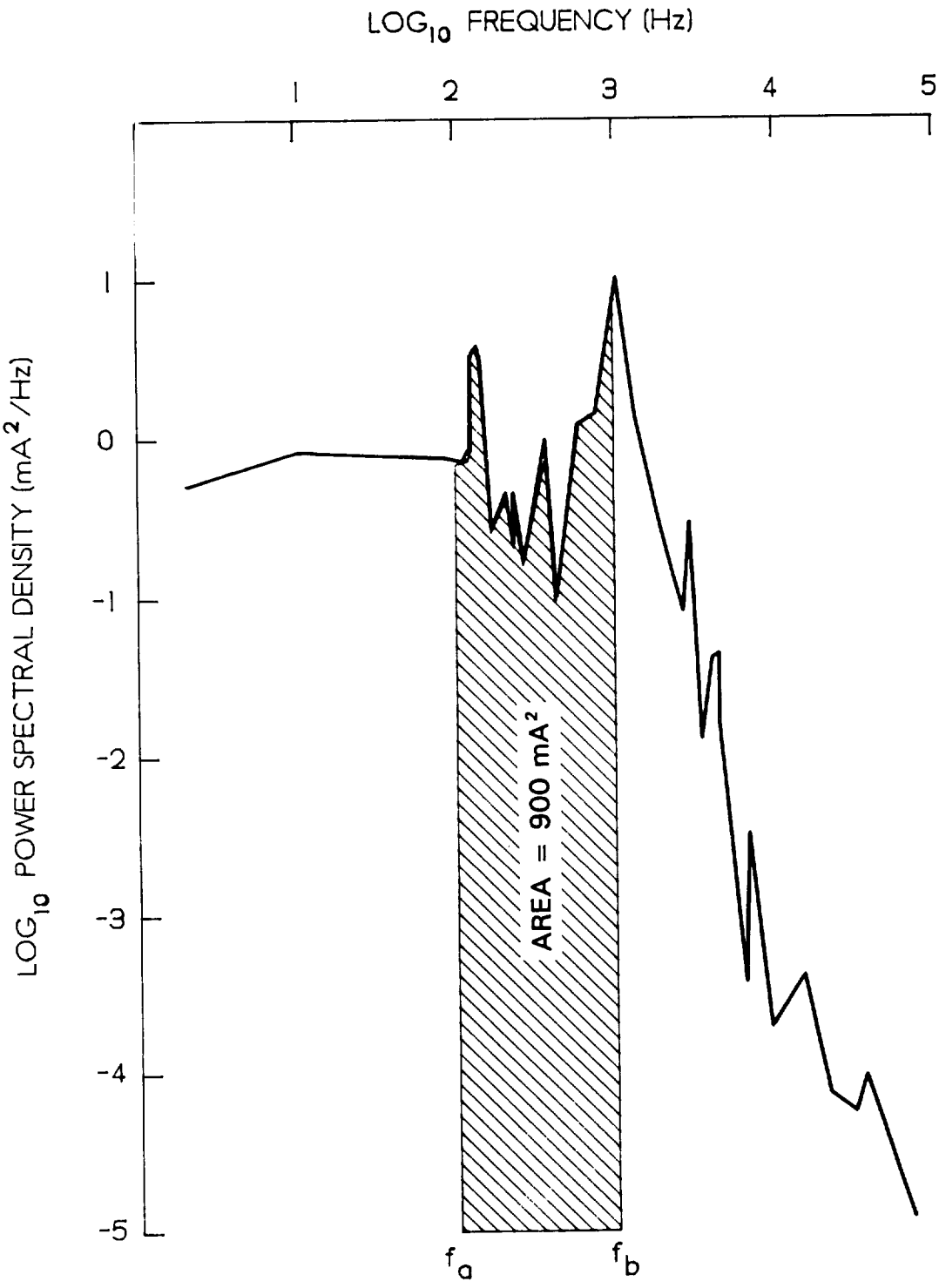

Fig. A8 Finding the RMS in a Frequency Range f_a to f_b

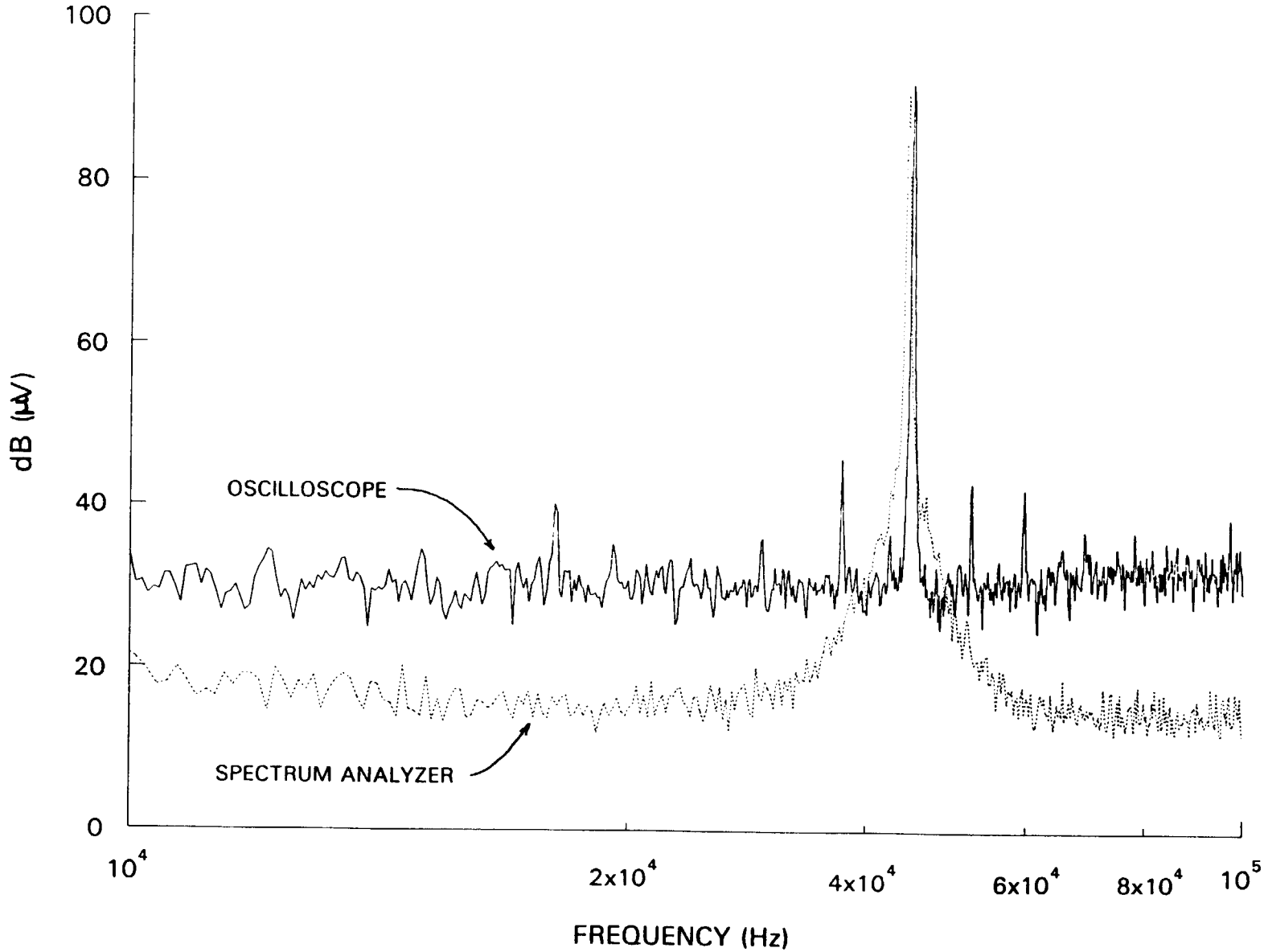

Fig. A9 A Comparison Between Signal Analysis Using the Oscilloscope and Spectrum Analyzer

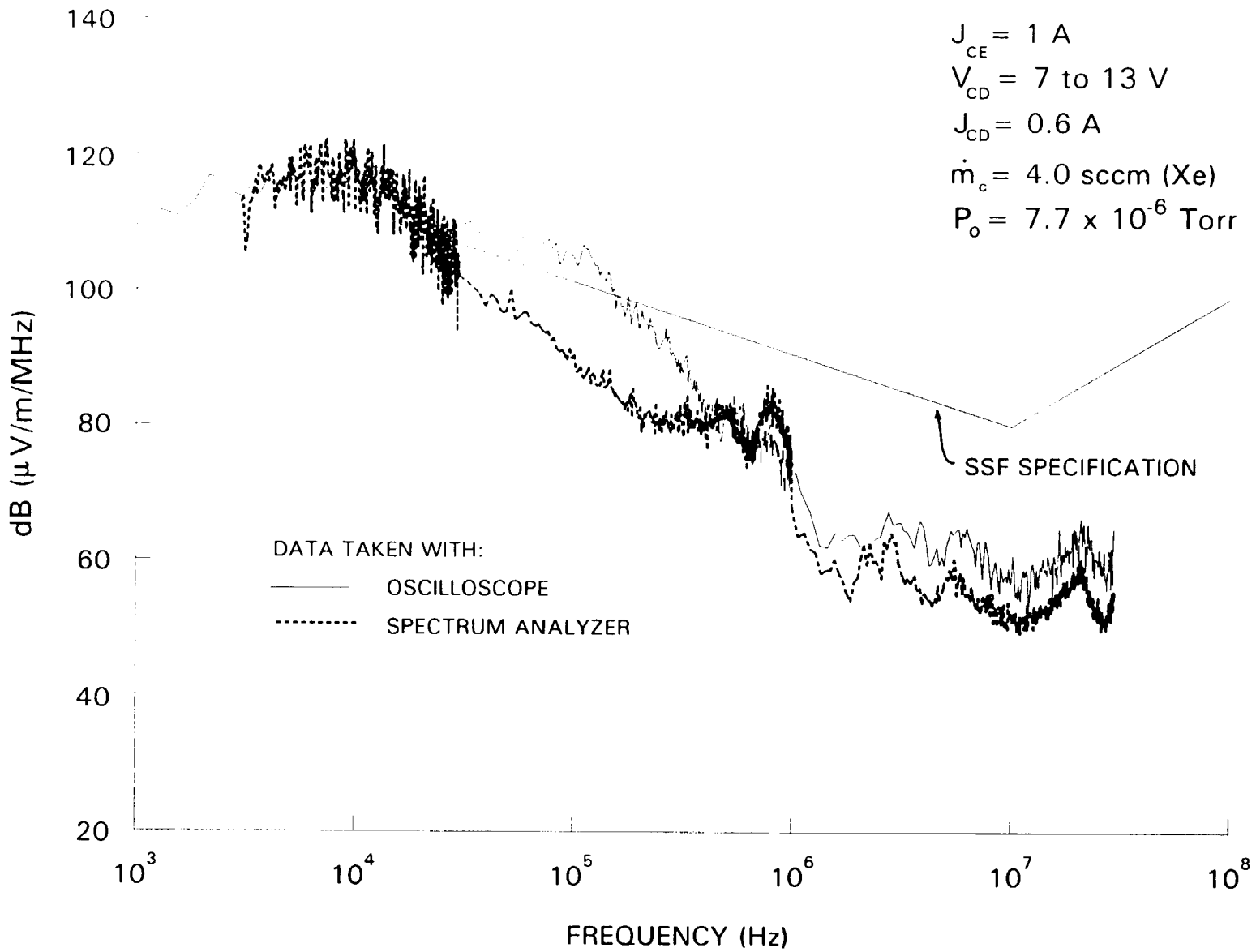

Fig. A10 Typical Radiated Emissions Measured Using Oscilloscope and Spectrum Analyzer

agreement between these data. In addition, spectrum presented in this report that were compared against other spectra, were taken using just the oscilloscope/filter or spectrum analyzer. Therefore, differences between spectrum presented are believed to be genuine.

APPENDIX B

Instrumentation Calibration

Most of the emission noise data presented in this report are spectral data and because of this, the frequency response (also known as the transfer function) was determined for the various instruments used to make conducted and radiated emission measurements. It was crucial to calibrate the instrument to insure it would respond adequately in a frequency range of interest and to measure its transfer function. The transfer function was then used to obtain, for example, true currents from the ones measured by the current monitor.

In general, the frequency response of the instrumentation was determined by using a signal generator and applying a sine wave, at a particular frequency, with an amplitude A_{in}. The output, A_{out}, of the instrument would be measured using an oscilloscope and the ratio A_{out}/A_{in} could then be calculated. The frequency of the input signal was then varied incrementally to cover the desired frequency range of 100 Hz to 100 MHz. After the frequency response for a particular instrument was determined, a polynomial fit to this transfer function was computed using a least squares method [20]. The polynomial approximation could then be used to recalibrate spectral data determined by the fast Fourier transform computer algorithm described in Appendix A. The following describes the frequency response measured for the various instruments, in addition to other tests conducted to ensure accurate data collection.

Current Monitor:

The frequency response of the current monitor (illustrated in Fig. 6a) was determined by connecting the signal generator (A_{in}) to its primary windings and measuring the output signal at the secondary windings (A_{out}). The results obtained from this test are plotted in Fig. B1a (A_{out}/A_{in} v. frequency) where three different values of A_{in} (i.e. A_{in} = 1, 3, or 5 V) were used to determine whether or not input amplitudes affected the frequency response. It appears from the data that the frequency response is non-linear and differences caused by varying A_{in} are apparent in the low frequency range (0.1 to 10 kHz). The signals associated with A_{in} = 1 V were difficult to detect because they were very small, however, when large amplitude signals are applied, the output signals are more easily detectable. Therefore, it is believed a more accurate frequency response of the current monitor is represented by the large-amplitude (5 V) input signals.

A concern with the current monitor is the magnetic saturation of the core created by the steady emission current (J_{CE}) passed through the primary winding. A test was conducted to determine if this DC current would change the frequency response of the current monitor. To simulate a DC current, another primary winding was attached to the current monitor and currents of 0, 1, and 2 A were passed through the wire. The frequency response was determined for each current level and the results are plotted in Fig. B1b where it is apparent that the DC current does not change the frequency response of the current monitor significantly. A similar test was conducted to see if a 10 A current effected the current monitor. For this test, another primary wire was wrapped 20 times around the core and 0.5 amps was passed through (to simulate a magnetic field created by 10 A). The results from this test did not show any significant changes in the frequency response (similar to the 1 or 2 A cases) and

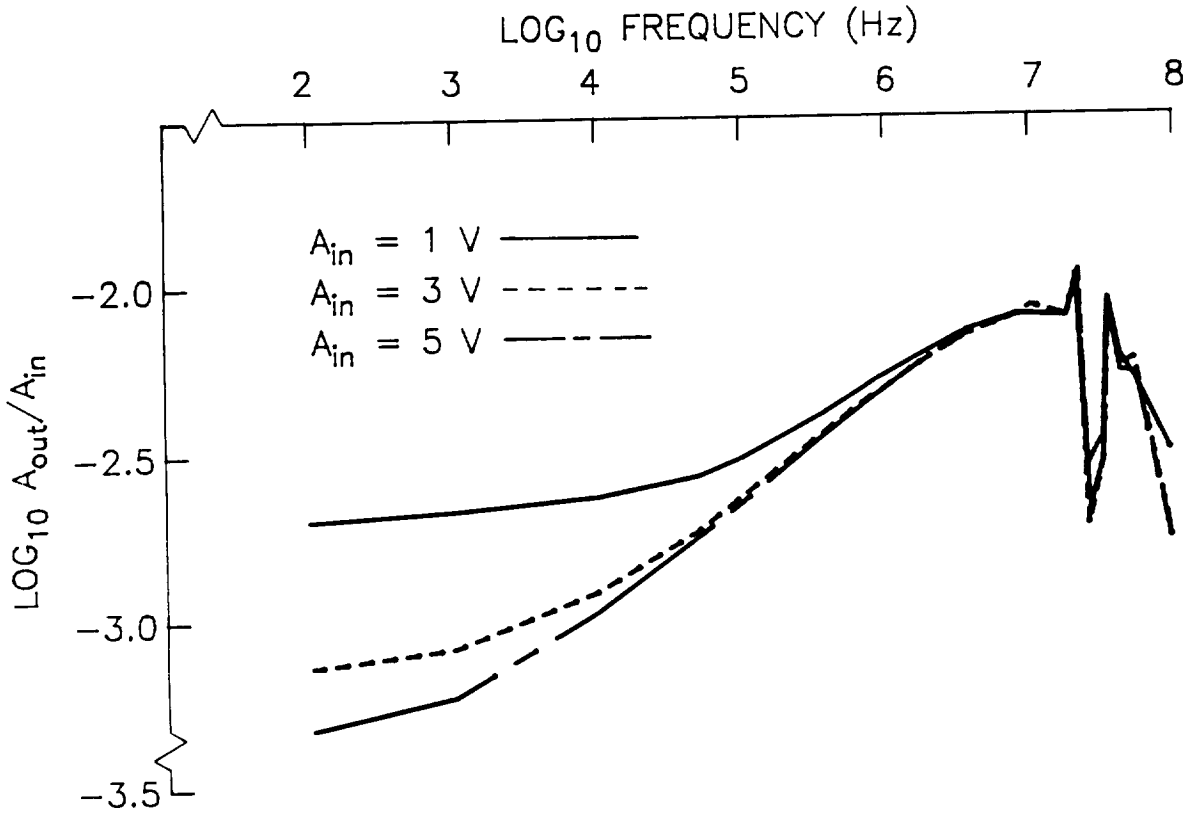

a) Variations in frequency response due to changes in amplitude of the input signal

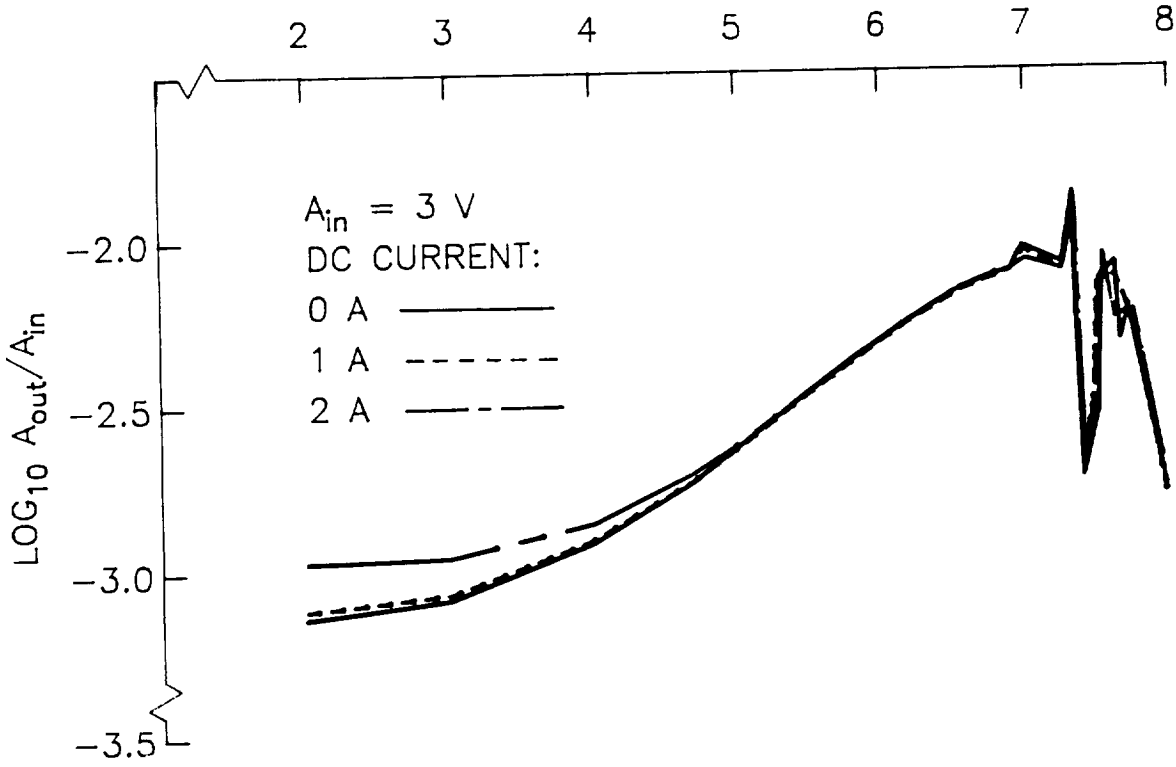

b) Variations in frequency response due to different steady magnetic fields

Fig. B1 Frequency Response of the Current Monitor

the data are not presented. Therefore, the current monitor has a predictable frequency response for emission current levels between 0 and 10 A.

A final test for the current monitor was to examine if it could accurately detect a known signal input to the primary winding (A_{in} = 5 V, f = 50 kHz). For this test, both the input and output signals were measured using the oscilloscope and the fast Fourier transform of each was computed. The data acquired from the secondary windings were then recalibrated in the frequency domain using the calibration data presented in Fig. B1 and the resulting power spectral density (PSD) for both signals are plotted as a function of frequency in Fig. B2 on a Log-Log scale. From Fig. B2 it is apparent that the current monitor is able to detect and reproduce the original 50 kHz signal fairly accurately.

Antenna:

The frequency response of the antenna was not determined because calibration information provided by the manufacturer stated that the response was linear up to 60 MHz.

Langmuir Probe:

The frequency response of the Langmuir probe was described in Ref. [8] and was linear from 100 Hz to 1 MHz.

Capacitive Langmuir Probe:

In order to determine the frequency response of the capacitive Langmuir probe, a metal foil was wrapped to the outside of the probe and the signal generator was connected between this foil and ground (A_{in}). For this test, the probe was installed in its standard mounting and with the wiring used to make plasma measurements. The amplitude of the fluctuating potential difference induced by the interior electrode of the probe and ground (A_{out}) was measured using the oscilloscope. Using the standard

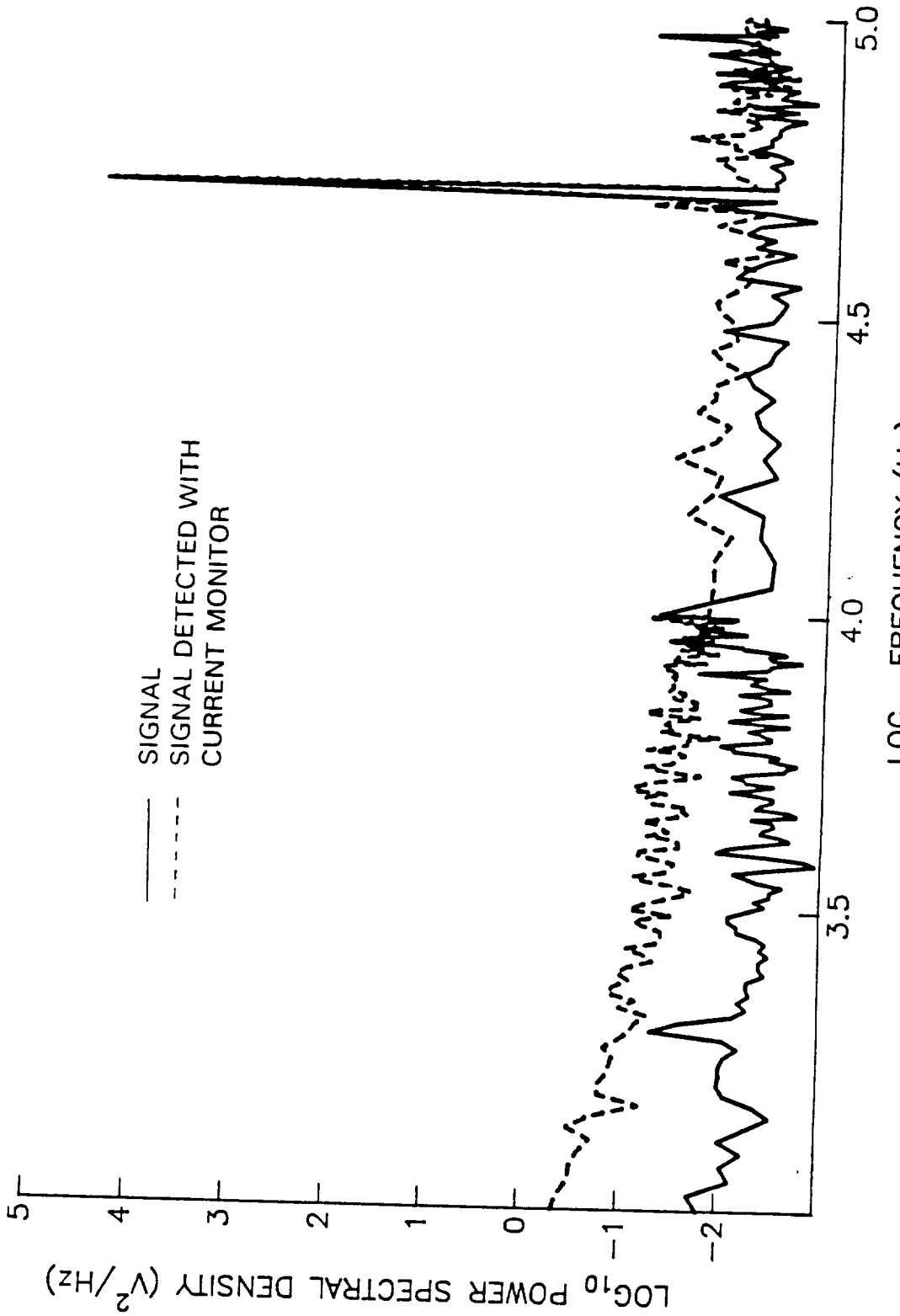

Fig. B2 A Signal Detection Test with the Current Monitor

techniques described above in addition to varying the applied voltages (A_{in} = 0.5, 1.1, and 1.8 V_{rms}), the frequency response of the capacitive Langmuir probe was measured. The results, which are plotted in Fig. B3, indicate a gain that is approximately constant up to ~10 MHz and then increases dramatically. In addition, these data also suggest the frequency response of the probe is not significantly affected by changes in the input signal amplitude. The results from this calibration suggest the capacitive probe should be able to operate in the frequency range 100 Hz to 100 MHz with predictable behavior.

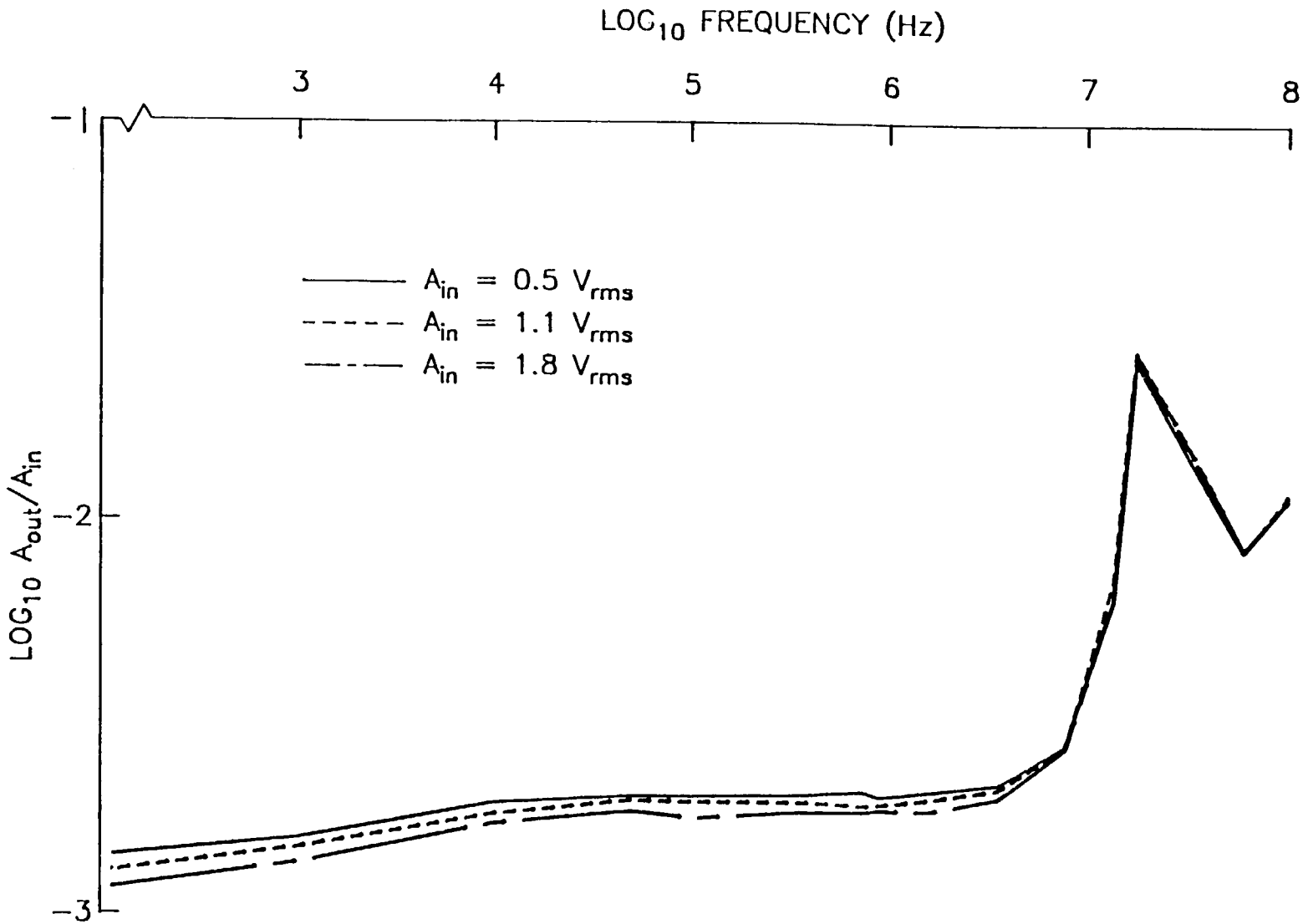

Fig. B3 The Frequency Response of the Capacitive Langmuir Probe